



8-2012

SURFACE STRUCTURING STRATEGIES FOR MICRO-CANTILEVER SENSING PLATFORMS AND APPLICATIONS FOR HYDROGEN RELATED ISSUES

James F. Patton
jpatton5@ion.chem.utk.edu

Recommended Citation

Patton, James F., "SURFACE STRUCTURING STRATEGIES FOR MICRO-CANTILEVER SENSING PLATFORMS AND APPLICATIONS FOR HYDROGEN RELATED ISSUES." PhD diss., University of Tennessee, 2012.
https://trace.tennessee.edu/utk_graddiss/1405

This Dissertation is brought to you for free and open access by the Graduate School at Trace: Tennessee Research and Creative Exchange. It has been accepted for inclusion in Doctoral Dissertations by an authorized administrator of Trace: Tennessee Research and Creative Exchange. For more information, please contact trace@utk.edu.

To the Graduate Council:

I am submitting herewith a dissertation written by James F. Patton entitled "SURFACE STRUCTURING STRATEGIES FOR MICRO-CANTILEVER SENSING PLATFORMS AND APPLICATIONS FOR HYDROGEN RELATED ISSUES." I have examined the final electronic copy of this dissertation for form and content and recommend that it be accepted in partial fulfillment of the requirements for the degree of Doctor of Philosophy, with a major in Chemistry.

Michael J. Sepaniak, Major Professor

We have read this dissertation and recommend its acceptance:

David C. Joy, Bin Zhao, Ziling Xue

Accepted for the Council:

Dixie L. Thompson

Vice Provost and Dean of the Graduate School

(Original signatures are on file with official student records.)

**SURFACE STRUCTURING STRATEGIES FOR MICRO-
CANTILEVER SENSING PLATFORMS AND APPLICATIONS
FOR HYDROGEN RELATED ISSUES**

**A Dissertation
Presented for the
Doctor of Philosophy Degree
The University of Tennessee, Knoxville**

**James F. Patton
August 2012**

DEDICATION

This dissertation is dedicated to my family. Especially my grandmother Elizabeth Gorman, mother Connie Patton, my aunt Cathy Gorman, and my uncle Paul Gorman. Each of these people have influenced my life and encouraged me through their love and support.

ACKNOWLEDGMENTS

First and foremost I would like to thank Dr. Michael J. Sepaniak for his help and guidance. He has served as a role model that I will strive to emulate in my future endeavors. I would like to thank the members of the Sepaniak group for their help with my development as a member of the scientific community. In particular our past members including; Deepak Bhandari for sharing his knowledge and input into my work, Lisa Taylor for helping me with the Labram Instrument, and Sabrina Wells for assistance using the PVD apparatus. More recently I would like to thank Tess Kirchner for being a great TA in the Chemistry 319 lab that we taught together. Some newer members in our group that I wish to thank include Hector Areizaga, Nahla Abu Hatab, Nicole Crane, Jennifer Charlton, and Chris Frye. I wish to thank my collaborators at ORNL including, Dr. Scott Hunter, Dr. Bart Smith, Dr. Nickolay Lavrik, and Dr. Panos Datskos. The support staff at both the University of Tennessee and CNMS has also been extremely helpful I especially want to thank Gary Wynn, Tim Free, Dale Hensley, Dr. Joe Spruielle and all of the staff in the stock room. Finally, I wish to thank all the members of my committee Dr. David Joy, Dr. Ziling Xue and Dr. Bin Zhao. I wish to sincerely thank all of you for taking time to serve on my committee.

Finally, I wish to extend my appreciation for the support of my family over the past several years.

ABSTRACT

Recent developments in microelectro-mechanical systems have enabled the exploration of transduction modes that involve mechanical energy and are based primarily on mechanical phenomena. As a result an innovative family of chemical and biological sensors has emerged which utilize a transducer in the form of microcantilevers (MCs). MCs offer greater sensitivity than comparable mass-responding sensors due in large part to their small dimension. These low cost devices can be deployed for remote testing, providing real-time information for the analyst. An additional advantage is the ability to employ MCs in an arrayed fashion adding a unique selectivity not available to many sensing platforms. The goal of this research is to explore improvements and advances in surface modification strategies for MC design. A practical application has been demonstrated for H₂ related detection.

The initial research (Chapter 2) focused on a novel surface structuring technique for introducing a molecular recognition phase (MRP) onto a MC transducer. The MRP in this study was introduced via spontaneous galvanic displacement reaction (SGDR) and has been implemented for H₂ detection. Combining the advantages of a MC sensing platform with a high active surface area of nano-porous (np-Pd) created by a SGDR, a fast, selective, and sensitive means to detect hydrogen gas has been achieved.

A second study (Chapter 3) investigates the nature of np-Pd systems created by the SGDR process. Experimental evidence is provided to support a mechanistic model which allowed a better understanding of both processing and material properties related to this strategy to create np-Pd films. This study has provided information for H₂ related issues including catalysis, storage, and sensing applications.

A final study (Chapter 4) explores improvements in the properties of materials used for MC design. A nano-laminate composite (NLC) surface composed of alternating layers of $\text{SiN}_x/\text{SiO}_2$ has shown advantages for MC design in comparison to conventional materials used for MCs. The NLC-MCs fabricated using this method exhibit superior reflectivity for optical read-out. The NLC materials experience less thermal induced drift compared to MCs that use metalized surfaces. The asymmetric layering of the NLC material used for MC design show promise for flexible functionalization strategies.

PREFACE

Chapter 1 is intended to introduce the reader to the fundamentals of chemical sensors. Particular attention is paid to Micro-cantilever (MC) based chemical sensors which encompasses the work presented in this dissertation. The advantages of a MC sensing platform and how improvements to these advantages can be achieved by exploring surface structuring strategies will be discussed. First, a Spontaneous Galvanic Displacement Reaction (SGDR) has been used to chemically functionalize MCs for H₂ sensing offering near ideal performance characteristics. A second strategy using a physical means to tailor materials for MC design has been demonstrated. A Nano-Laminate Composite material for MC design provides several advantages for an MC platform including, superior reflectivity, thermal stability, and flexible functionalization strategies.

Chapter 2 presents a chemical sensor that has been created using an SGDR approach. The major focus of this study is to present a novel method of surface structuring using an SGDR to create a nano-porous palladium (np-Pd) based MC H₂ sensor which shows optimal performance characteristics. The figures of merit that have been achieved using this new method will be the focus of this section.

Chapter 3 will present a detailed study on the mechanism that governs the optimal sensing characteristics of the np-Pd MCs for H₂ related sensing applications. This will include a description of the processing requirements that were needed to achieve these optimal figures of merit. The information gained by this study may be extended to such areas as H₂ storage and catalysis.

Chapter 4 will introduce another surface structuring strategy for improving MC design. In this section a Nano-Laminate Composite material has been fashioned using standard

photolithography to create a MC material with improved reflectivity, hence no need for a reflective metalized surface. The absence of metallization results in a more thermally stable sensing device. The native asymmetry of these materials may also provide a flexible and efficient means of surface functionalization.

Chapter 5 will summarize the conclusions of each of the preceding chapters. A discussion on the possible future of MC sensing platforms with respect to these conclusions will also be presented.

TABLE OF CONTENTS

Chapter 1: INTRODUCTION TO CHEMICAL SENSORS, MICROCANTILEVERS, AND HYDROGEN DETECTION.....	1
1.1 CHEMICAL SENSORS.....	1
1.1.1 Properties of Chemical Sensors.....	1
1.1.2 Comparative Mass Sensors.....	2
1.2 MICROANTILEVERS (MCs).....	3
1.2.1 Microcantilever Background.....	3
1.2.2 Microcantilever Measurement Modes.....	7
1.2.3 Figures of Merit for Sensing	14
1.3 INFLUENCES OF MC DESIGN ON PERFORMANCE CHARACTERISTICS.....	17
1.3.1 Geometry.....	17
1.3.2 Surface Modification of MCs.....	18
1.4 HYDROGEN AND ENERGY RELATED CONCERNS.....	22
1.4.1 Current Demands.....	22
1.4.2 Theory of Palladium Hydrogen Systems.....	22
1.4.3 Hydrogen Sensing/Detection Methods.....	24
1.4.4 Pd Films vs np-Pd.....	26
1.4.5 Deposition of np-Pd Using SGDR.....	27
1.5 MICROCANTILEVER MATERIALS AND PROCESS DESIGN.....	28
1.5.1 Nano-Laminate Composites.....	28

CHAPTER 2: RAPID RESPONSE MICROSENSOR FOR HYDROGEN DETECTION USING NANOSTRUCTURED PALLADIUM FILMS.....	29
2.1 INTRODUCTION.....	29
2.1.1 Background.....	29
2.1.2 Hydrogen sensing techniques.....	30
2.1.3 Microcantilever Based Hydrogen Sensors.....	33
2.2 EXPERIMENTAL SECTION.....	34
2.2.1 Microcantilever Surface Modification.....	34
2.2.2 Testing protocol.....	35
2.3 RESULTS AND DISCUSSION.....	37
2.3.1 Mechanistic Considerations.....	38
2.3.2 Novel Wet Chemical Processing.....	39
2.3.3 Optimization/Gas Phase Composition.....	39
2.3.4 Conditioning and Regeneration.....	42
2.3.5 Performance Evaluation.....	45
2.4 CONCLUSIONS.....	50
CHAPTER 3: CHARACTERIZATION OF HYDROGEN RESPONSIVE NANOPOROUS PALLADIUM FILMS SYNTHESIZED VIA SPONTANEOUS GALVANIC DISPLACEMENT REACTION.....	51
3.1 INTRODUCTION.....	51
3.1.1 Background.....	51
3.2 EXPERIMENTAL SECTION.....	54
3.2.1 Surface Preparation.....	54

3.2.2 Instrumental.....	55
3.3 RESULTS AND DISCUSSION.....	57
3.3.1 Chemical Effects Oxide.....	57
3.3.2 Morphological Effects: SGDR Composition and Processing Time.....	66
3.3.3 Effects of O ₂ and H ₂	73
3.4 CONCLUSIONS.....	77
CHAPTER 4: EXPLORING NANOLAMINATE COMPOSITES AS MATERIALS FOR MICROCANTILEVER DESIGN.....	80
4.1 INTRODUCTION.....	80
4.2 EXPERIMENTAL.....	82
4.2.1 NLC-MC Processing.....	82
4.2.2 NLC-MC Testing.....	82
4.2.3 Instrumentation.....	84
4.3 RESULTS AND DISCUSSION.....	85
4.3.1 Characterization of Nano Laminate Composite Materials.....	85
4.3.2 Advantages of Nano Laminate Composite Materials.....	95
4.3.3 Future Directions.....	103
4.4 CONCLUSIONS.....	105
CHAPTER 5: CONCLUDING REMARKS.....	106
REFERENCES.....	109
VITA.....	116

LIST OF FIGURES

Figure	Page
Figure 1.1 MC geometry and nomenclature.....	4
Figure 1.2 MC appearance and static mode of detection.....	6
Figure 1.3 MC surface stress methods.....	10
Figure 1.4 Stoney response mechanism.....	12
Figure 1.5 MC instrumental design.....	13
Figure 1.6 Arrayed MC optical beam bending technique.....	15
Figure 1.7 Surface modification of MCs.....	19
Figure 1.8 SGDR process flow.....	21
Figure 2.1 Experimental Set-up static bending mode of detection.....	36
Figure 2.2 MC Response characteristics to H ₂ in O ₂ and N ₂ environments.....	41
Figure 2.3 Effects of carrier gas and flow rate.....	43
Figure 2.4 Calibration, linear response to hydrogen np-Pd MCs.....	46
Figure 2.5 Selectivity studies of H ₂ responsive np-Pd MCs.....	47
Figure 2.6 Lifetime studies of H ₂ responsive np-Pd MCs.....	49
Figure 3.1 Processing of np-Pd MCs using an SGDR strategy.....	58
Figure 3.2 Raman/PdO band and corresponding nano-mechanical response/H ₂	60
Figure 3.3 Pd nanoparticle/oxide layer and H ₂ /O ₂ interaction process.....	62
Figure 3.4 Effects of O ₂	64
Figure 3.5 Effects of filtering SGDR bath and procesing time.....	68

Figure 3.6 Sacrificial silver and regression data/limiting reagent studies.....	69
Figure 3.7 Nano-structure comparison of np-Pd films.....	72
Figure 3.8 XRD of np-Pd films.....	75
Figure 3.9 np-Pd MCs response profiles and immunity to H₂S.....	78
Figure 4.1 Process flow for silicon dioxide/silicon nitride microcantilevers.....	83
Figure 4.2 XPS survey spectrum for NLC surfaces.....	86
Figure 4.3 HF etch experiment and NLC response.....	89
Figure 4.4 NLC-MC native state pH response.....	92
Figure 4.5 Resonance frequency profiles of NLC-MCs.....	94
Figure 4.6 Reflectivity of NLC materials.....	96
Figure 4.7 Comparative reflectivity studies.....	98
Figure 4.8 NLC-MC thermal stability profiles.....	100
Figure 4.9 FTIR of Octa-decyl trimethoxysiloxane.....	102
Figure 4.10 Protein immobilization strategies.....	104

LIST OF TABLES

Table 2.1 Important performance requirements for H₂ sensing.....	31
Table 4.1 Effects of HF Etch and Surface wettability for NLCs.....	88

ABBREVIATIONS AND SYMBOLS

AET	2-aminoethanethiol
AFM	atomic force microscopy
ANNs	Artificial Neural Networks
D	Diffusion Coefficient
Δf	resonance peak at half amplitude
Δm	mass change
$\Delta\sigma$	surface stress change
ΔV	volume change
DA	dealloyed
DNA	deoxyribonucleic acid
DOE	Department of Energy
E	Youngs Modulus
EDC	Endocrine disrupting chemical
EPA	Environmental Protection Agency
F	filtered
f	resonance frequency
FIB	Focused Ion Beam Milling
FITC	fluorescein isothiocyanate
FTIR	Fourier Transform Infra-Red
GA	glutaraldehyde
GC	Gas Chromatography
HRSEM	high resolution scanning electron microscopy
ICP-OES	inductively coupled optical emission sepectrometry
K	spring constant
l	MC length
LOD	limit of detection
m^*	effective MC mass

m_b	beam mass
MC	microcantilever
MCA	microcantilever array
MEMS	micro-electromechanical system
MRP	molecular recognition phase
n	MC geometric factor
N-F	non-filtered
NLC	nano laminate composite
np-Pd	nano-porous Palladium
NREL	National Renewable Energy Laboratory
ODTMS	octadecyltrimethoxysilane
PSD	position sensitive detector
PVD	physical vapor deposition
PXHSP	Panalytical X'Pert High Score Plus
Q	MC quality factor
QCM	quartz crystal microbalance
RIE	reactive ion etching
SAM	self-assembled monolayer
SAW	surface acoustic wave
SEM	scanning electron microscopy
SGDR	spontaneous galvanic displacement reaction
t	MC thickness
VCSEL	vertical cavity surface emitting laser
VOC	volatile organic compound
XPS	X-ray Photoelectron Spectroscopy
XRD	X-ray Diffraction
z_{max}	MC tip deflection
ν	Poisson Ratio

CHAPTER 1: INTRODUCTION TO CHEMICAL SENSORS, MICROCANTILEVERS, AND HYDROGEN DETECTION

1.1 CHEMICAL SENSORS

1.1.1 Properties of Chemical Sensors

A chemical sensor is a transducer which provides direct information about the chemical composition of its environment. It is composed of both a physical transducer and a chemically selective layer.¹ The chemically selective layer differentiates a sensor from a simple transducer such as a thermocouple or photodiode by offering specificity to a desired analyte. There are several fundamental properties that an ideal chemical sensor should possess. It is paramount that a sensor displays linear response to analyte concentration over a fairly wide dynamic range. This ensures a means of quantitatively comparing samples and providing meaningful data about the sample. These responses must be reversible such that the sensor returns to its initial state after being exposed to analyte. Response time must be fast, which is important for real-time analysis. The sensor must perform with high sensitivity and low intrinsic noise levels that afford an ability to distinguish differences in low-levels of analyte concentration. Selectivity is also a vital feature of an ideal sensor, such that measured responses are due to only the targeted analyte.

Chemical sensors are differentiated by the class in which they are placed. These classes include thermal, electrochemical, optical, and mass sensitive devices. The focus of

this study will explore the attributes of mass sensitive chemical sensors, specifically micro-cantilever (MC) systems.

1.1.2 Comparative Mass Sensors

A few mass sensing devices that will be compared include the quartz crystal microbalance (QCM), surface acoustic wave (SAW) and the micro-cantilever (MC) that is the subject of this work. A QCM sensor utilizes the change in frequency of the quartz crystal resonator when material is deposited on the surface² taking advantage of the piezoelectric characteristics of quartz. While used in sensing^{3,4} these devices are used in our work as a reference source for thin film depositions. SAWs are also mass sensors⁵⁻⁷ that employ alternating voltage on two interdigital transducers. This creates a surface wave on the piezoelectric substrate such that the amount of material deposited between the transducers can be measured due to the change in the surface wave velocity and therefore frequency of the measuring device.⁸ Limitations to QCM and SAW sensors include inability to operate at temperature extremes and frequency dampening within a viscous liquid environment. Thus, both QCM and SAW sensors have limited application for aqueous phase real-time analysis and generally do not meet biological testing needs.

MCs are an example of a microelectro-mechanical system (MEMS) sensing platform; a detailed description of these devices follows in the next section. A molecular recognition phase (MRP) on the MC provides selectivity that is not inherent to a MC device. The MRP is a surface feature which creates a favorable absorption equilibrium for distribution of a desired analyte within this phase. Signal transduction occurs due to mass loading, surface induced stresses, or a combination of both of these phenomena and will be discussed in more

detail in section 1.2.2. MCs outperform both QCMs and SAWs in terms of sensitivity, while offering real-time information. The ability to create an array of MCs adds a distinct advantage for remote testing in both gaseous and aqueous phase environments. MCs can also be utilized in a more flexible sensing strategy based upon either dynamic or static mode of measurement as will be discussed later in this chapter.

1.2 MICROCANTILEVERS (MCs)

1.2.1 Microcantilever Background

The use of MCs as a chemical and biological sensor has been explored for nearly three decades. Atomic force microscopy (AFM) cantilever probes provided motivation for the production and use of MCs as a sensing platform. Conventional use of AFM involves a flexible cantilever tip which is scanned or rastered over a surface. The force between the tip and the surface causes a deflection of the cantilever; this deflection is measured and the topography of the surface can be mapped.⁹ AFM cantilever probes can also vary with physical changes in local environment which include humidity, pressure, temperature, and acoustic noise.¹⁰ Recognition of variations in AFM probes due to such environmental phenomena sparked interest to evaluate the feasibility of employing these devices for uses beyond surface characterization.

By 1995 the diminutive AFM cantilever became recognized as a sensitive analytical tool for quantitative applications¹¹⁻¹⁴ MCs are tiny plates or leaf springs, typically 0.2–1 μm thick, 20–100 μm wide, and 100–500 μm long, which are connected on one end to an appropriate support for convenient handling (Figure 1.1). A sharp tip on the

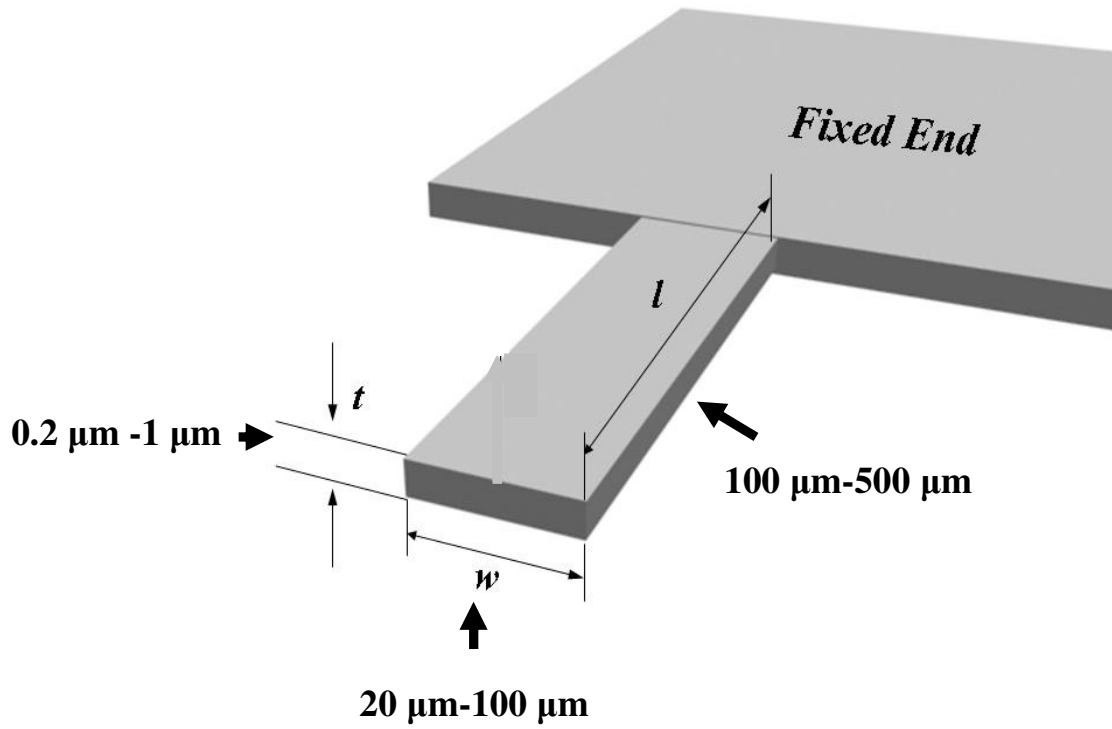


Figure 1.1. MC geometry and nomenclature.

underside of the microscopic leaf spring makes it useful as a probe for mapping localized surface topology in AFM, much like the stylus of an old-fashioned record player probing the grooves on vinyl records. However, a tip-less version is commonly used for sensing applications.

Advantages of MCs as a sensor are in part to the devices small size, relatively low cost, disposable platform, easy integration or coupling with other methodologies including chromatographic separations¹⁵ and Raman spectroscopy,¹⁶ and real-time information. In terms of performance characteristics MC platforms provide excellent sensitivity with a reported dynamic range typically spanning nearly three orders of magnitude.¹⁷

Micromechanical transduction in MC devices can be affected by physical, chemical, or biological stimuli that can induce changes, which can be measured electronically, optically, or by other means.¹⁸ The stimuli effectively measured on MCs include surface stress, small mechanical forces, charges, temperature, and infra-red photons.¹⁸ Because of MCs role in AFM, these devices can be bulk fabricated in an arrayed fashion using routine photolithographic patterning and a combination of surface and bulk micromachining.¹⁹ MC shapes and geometries can be patterned by photolithography followed by reactive ion etching (RIE) using a silicon or silicon nitride film.²⁰ For example in Figure 1.2a an SEM image of a triangular MC is shown in comparison to a schematic of a rectangular MC Figure 1.2b operating in the static detection mode as discussed in the next section.

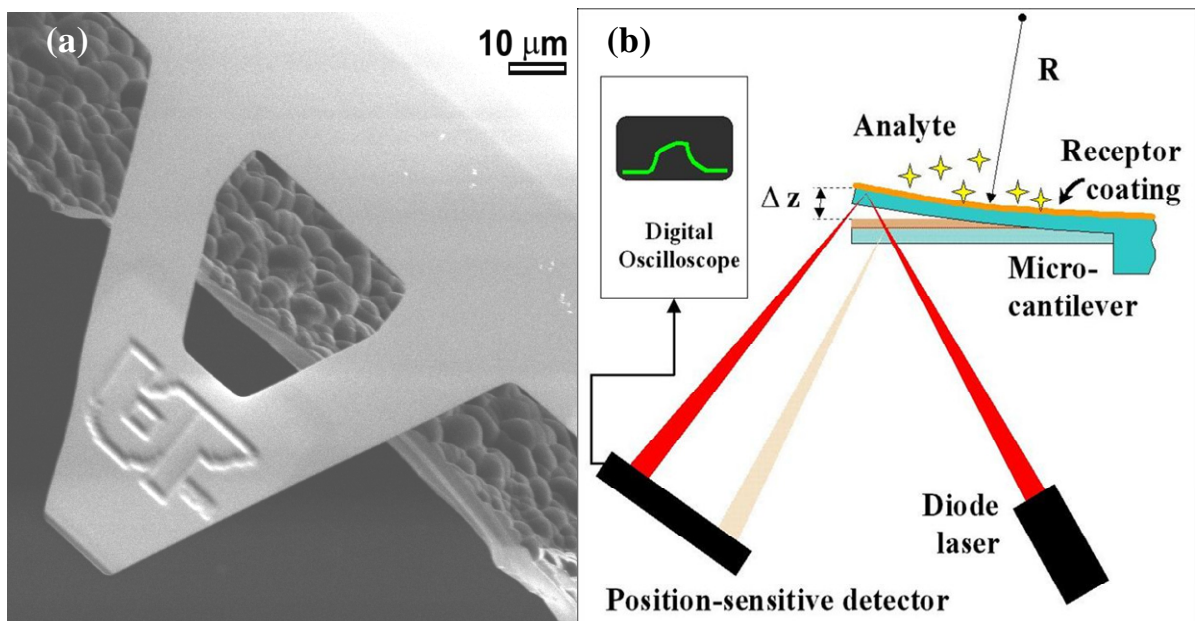


Figure 1.2 (a) Triangular micro cantilever. (b) Rectangular micro cantilever operating in the static mode of measurement.

1.2.2 Microcantilever Measurement Modes

The two modes of MC sensing that will be presented in this dissertation are dynamic and static. The choice of mode is dictated by application need, the medium it will be used in, and what transduction mechanism is responsible for sensor response. Resonant or dynamic mode can use changes in resonance frequency (f_0) of MC oscillations to evaluate mass changes on the MC surface.¹⁸ Resonance is the tendency of a system, such as a suspended beam to oscillate at greater amplitudes at certain frequencies. The change in f_0 can be measured and may indicate analyte binding to an MRP on the MC surface. This can be understood by considering the f_0 of an oscillating cantilever and the dependence of this parameter on mass as defined by equation 1.1:²¹

$$f_0 = 1/(2\pi) \times \sqrt{(K/m^*)} \quad (1.1)$$

where K is the MC spring constant, m^* is the effective MC mass. Effective MC mass is related to the beam or lever mass, m_b , through equation 1.2.²¹

$$m^* = nm_b \quad (1.2)$$

For rectangular cantilevers n , a geometric parameter; has a value of 0.24.¹⁸ It is known that changes in measured f_0 are related to changes in mass, Δm , and changes in spring constant (K) and can be expressed through equation 1.3¹⁹

$$1/f_1^2 - 1/f_0^2 = \Delta m / (4\pi^2 K) \quad (1.3)$$

Dynamic or resonant mode provides analysis with excellent sensitivity in some applications. Indeed, it has been reported that single E.Coli organisms have been measured by MCs operated in the dynamic mode.^{22,23} A reduction in MC size plays a vital role in improving the sensitivity using the dynamic mode of detection. However readout of the MC frequency can be difficult with reduction in MC size.

Signal transduction in the dynamic mode of MCs consists of three mechanisms, adsorbate-induced mass-loading, chemical changes of cantilever stiffness, and dampening by the viscous medium.¹⁸ As discussed above adsorbate-induced mass-loading is responsible for changes in f_0 as a measurement parameter in dynamic mode for sensing applications. However, changes in K (spring constant) may also accompany adsorbate-induced mass-loading. In this case an increase in f_0 may result in direct opposition to the reduced f_0 expected by analyte interaction as predicted by equation 1.3. To avoid this adverse effect coating of MRP on the MC apex has been reported.²⁴ This method however reduces the availability of MRP binding sites for targeted analyte on the MC active surface and hinders sensitivity. Another obstacle for the dynamic mode is the dampening that can occur in liquid media, which may also inhibit sensitivity.²¹ Dynamic mode is still used in liquid or aqueous media depending on the mechanism being studied. It has been reported in studies conducted by Dareing that the frequency shift due to dampening is small compared to the frequency shift induced by effective mass.²⁵ In another report a system has been designed using magnetic or acoustic energy to drive f_0 to an appreciable value (10-15 kHz)²⁶ thus reducing the effects of dampening in an aqueous medium.

Static mode measures the deflection of the MC tip due to the bending of the MC. These measurable tip deflections may be caused by either external forces on the surface or stresses generated on or in the lever.¹⁸ The static bending mode can utilize the optical beam deflection technique in which a laser spot is reflected off the tip of the lever and focused on a position sensitive detector (PSD). A single lever system is shown in Figure 1.2b, in a later section an arrayed arrangement will be presented exploiting the distributed response advantage available to this platform. Calibration of electrical response (milli-volts) to tip deflection (nano-meter or micro-meter) based upon instrument geometry is useful for comparing responses of analytes on different instrumental settings and facilitates comparing sensor reproducibility.

To take advantage of static mode measurements one must establish a MC with asymmetric surfaces, ie. an active and passive side. An MRP is fashioned on the active side of the MC and shows some degree of affinity for the analyte, whereas the passive side does not have affinity for the analyte molecule. The MRP on the active, functionalized side of the lever will interact with the analyte molecule in one of three surface stress methods as shown in Figure 1.3. In the first method, the analyte molecules adsorb to the functionalized surface, resulting in expansion of the surface. Figure 1.3a is an example of the first method depicting thiolization of a gold surface resulting in expansion of the active surface. The second method (Figure 1.3b) occurs when the functionalized surface is an analyte-permeable layer that swells when the analyte disperses through the coating. The third method (Figure 1.3c), utilizes nanostructured surfaces for MRPs that increases the number of analyte binding sites on a MC. With an increase in active surface a resultant increase of sensitivity may be observed. We have also observed that reversibility is improved with nano-structured MCs.¹⁹

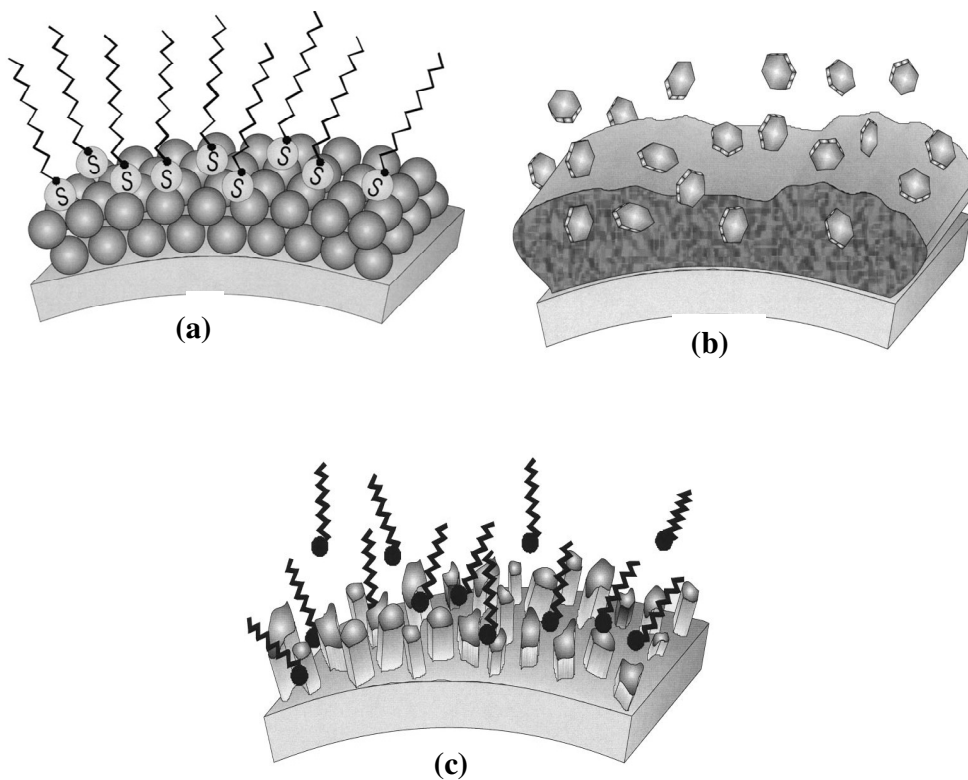


Figure 1.3. Schematic depiction of (a) immobilization of thiol monolayer on a gold coated MC surface, (b) analyte-induced deformation of MC coated with an analyte-permeable thick film, (c) analyte-induced deformation of MC coated with a nanostructured modifying phase.

The static bending or tip deflection, z_{\max} , of the MC varies depending on the preferential binding of analyte molecules to the active, functionalized side of the lever and is governed by Stoney's equation (equation 1.4):²⁷

$$z_{\max} = 3l^2(1-\nu)\Delta\sigma/Et^2 \quad (1.4)$$

where ν and E are, respectively, the Poisson ratio and Young's modulus for the cantilever, t is the MC thickness, l is the MC effective length, and $\Delta\sigma$ is the analyte-induced differential surface stress ($\Delta\sigma_{\text{active side}} - \Delta\sigma_{\text{passive side}}$). Figure 1.4 illustrates the mechanism involved in MCs and the relationship to several parameters presented in the Stoney Equation upon analyte interaction. The MC static bending mode functions well in both liquid and gas media, since it has no dependence on the resonant frequency of the MC, and is the method most commonly used in AFM. Herein, the static bending mode is used with functionalized MCs for sensing applications unless otherwise noted.

The MC static bending mode or tip deflection instrumental setup consists of the following parts: a laser, lenses, a PSD, a microfluidic cell, the MC chip and an output device or recorder, as seen earlier in Figure 1.2 b and the photograph in Figure 1.5. The microfluidic cell is designed to flow background and analyte solutions (either aqueous phase or gas phase) past the MCs. A well designed flow cell requires low volumes and has a thorough, quick washout of analyte solution and can be utilized with pump, regulated gas flow or gravity flow in aqueous applications for analyte and background delivery.

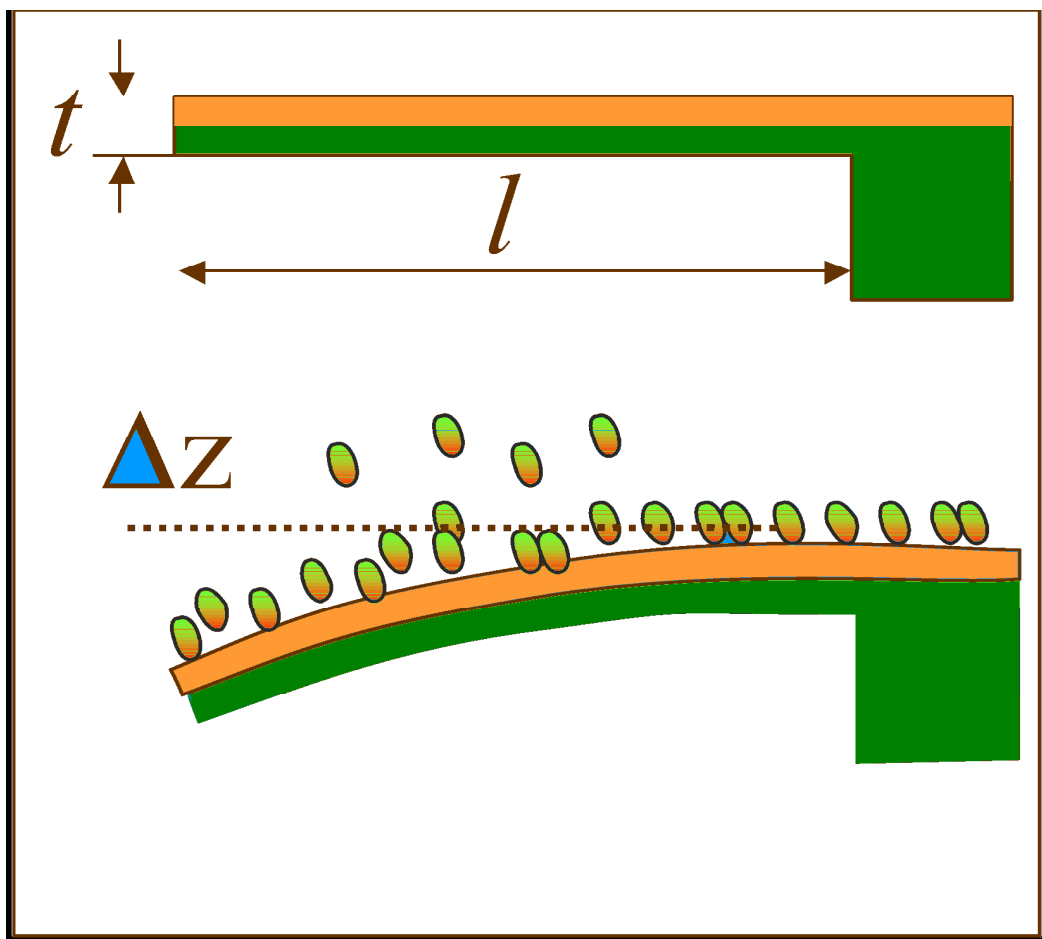


Figure 1.4. Stoney response mechanism. A thin beam of length l , and thickness t undergoing tip displacement Δz upon analyte interaction on active yellow surface opposed to non-active green surface.

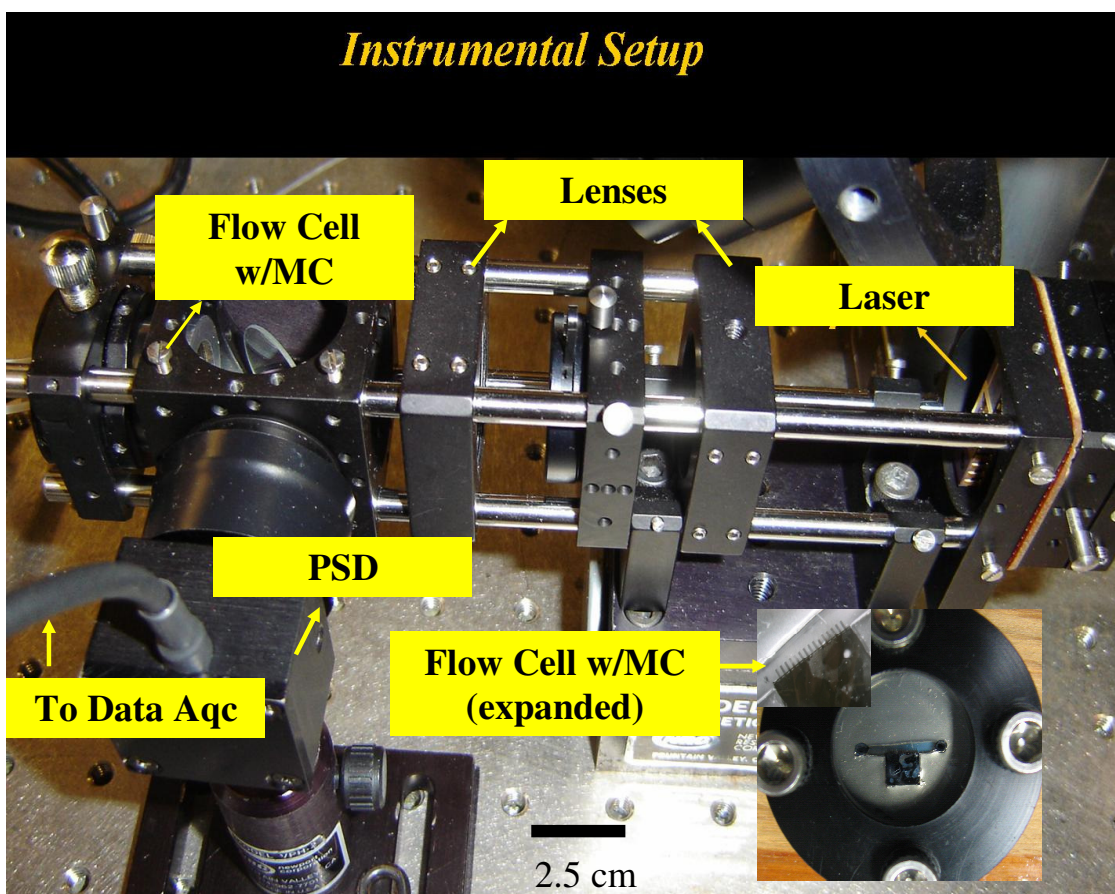


Figure 1.5. MC instrumental design. Illustration of a typical instrumental set-up for an MC platform using the optical beam bending method (static mode). The diminutive nature of this apparatus is easily adaptable for remote applications.

1.2.3 Figures of Merit for Sensing

Figures of merit are quantitative performance criteria that can be used to decide whether a given instrument or method is suitable for solving an analytical problem.²⁸ As discussed in section 1.1 several important figures of merit for an ideal sensing platform include selectivity, reversibility and sensitivity. Each of these criteria will be described with respect to MC sensing platforms in terms of advantages and limitations.

Selectivity of an active surface can be achieved by judicious choice of an MRP. MRPs can be fashioned by a variety of compounds such as, polymers, proteins, macrocyclic receptors, and sol-gels.^{18,19,21,29-31} Two methods for utilizing MRPs to impart selectivity include moderately selective phases for distributed selectivity and bioaffinity or other high affinity phases. Moderately selective phases rely upon weaker interactions, such as Van der Waals forces (eg, induced dipole), electrostatic interactions and in some cases hydrogen-bonding ability. The highly selective bio-affinity phases experience stronger concerted interactive forces.

MRPs which show distributed selectivity have been studied using an arrayed platform providing response patterns for specific analytes, or classes of analytes. Figure 1.6 shows an arrayed arrangement in which a vertical cavity surface emitting laser can be employed in conjunction with a single PSD. In one study it was reported that components of a complex matrix can be identified using artificial neural networks (ANNs).³² Specifically, it was demonstrated that selectivity was accomplished by using a large number of moderately

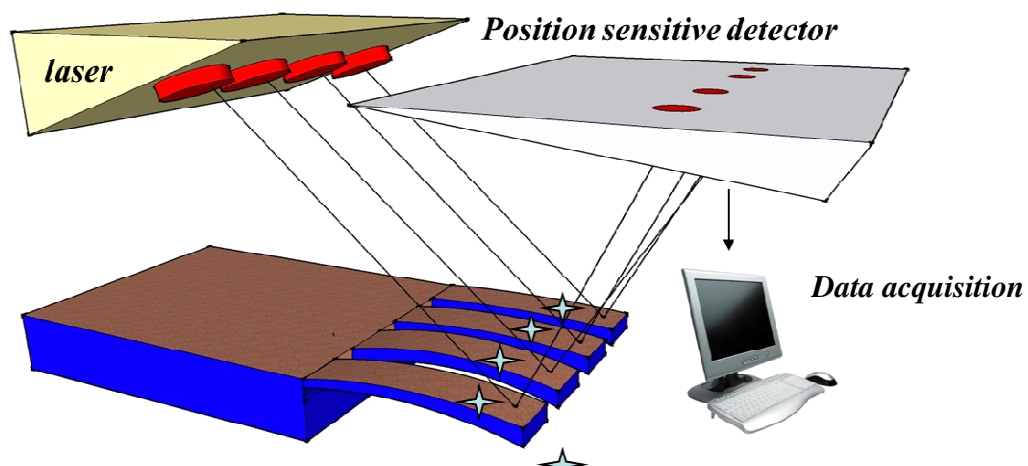


Figure 1.6. Beam bending optical read-out method. The position sensitive detector measures laser spot movement as analyte preferentially interacts with the molecular recognition phase (top surface)

selective MRPs and pattern recognition algorithms to examine the unique analyte responses. Disadvantages of the distributed selectivity method may arise with complicated data sets if there is not enough contrast between the response profiles or the amount of time and difficulty that surrounds creating arrays with many MRPs. In this dissertation an arrayed system was not incorporated.

Bioaffinity MRPs (biosensors) provides selectivity by exploiting the interaction or binding that is inherent to many biological receptors to specific analytes.^{30,31} Examples have included the ability to detect a single DNA mismatch³³ and screening of prostate specific antigen.³⁴ Disadvantages of the bioaffinity method may include reversibility issues and the robustness of the immobilized bioreceptor.

Gas phase analysis incorporates an MRP that undergoes analyte induced swelling and/or changes in surface stress. Unlike liquid phase sensing regimes the effects of noise related issues due to medium viscosity are minimal. The diffusion of analyte in and out of the MRP results in a much faster sensing system in comparison to liquid phase methods, thus minimizing kinetic issues in terms of both response and recovery times. Fast wash-out in gas-phase testing has approached diffusion limited response kinetics in many respects. MC's have been used in gas phase analysis as a detector for GC,¹⁵ landfill siloxane contaminant detection,³⁵ and as selective sensing device for H₂ fuel infrastructure.¹⁷

Sensitivity is a measure of an instrument or methods ability to discriminate between small differences in analyte concentration.²⁸ A common metric for measuring sensitivity is a methods limit of detection, generally taken as the analyte concentration/amount that yields a signal that is three times the standard deviation of the blank. The sensitivity afforded by MC devices depends upon the mechanism of analyte/MRP affinity either through mass loading,

surface induced adsorption or contributions from both (Figure 1.3). Mass loading results from swelling of the receptive MRP phase. In this mode the magnitude of the apparent stress scales up in proportion with the thickness of the MRP.¹⁸ Hence a thicker MRP results in a more sensitive measuring device at the expense of response speed and recovery. Surface induced adsorption is improved by increasing the active surface area of the MRP. In this mechanism responses are usually faster, combining effects of bulk, surface and inter-surface interactions.¹⁸ Methods of increasing the active surface area of the MC include de-alloying (DA),^{29,36} surface machining (trenches),³⁷ and the use of a chemical pathway involving a spontaneous galvanic displacement reaction¹⁷ each of these approaches will be discussed in the next section.

1.3 INFLUENCES OF MC DESIGN ON PERFORMANCE CHARACTERISTICS

1.3.1 Geometry

The geometry of the MC can take on several forms; optimization of the desired design relies upon factors that influence energy dissipation or dampening effects on the nature of response in these devices. A parameter which is used for design optimization is the mechanical quality factor (Q factor), and is defined by equation 1.5.³⁸

$$Q = f_0 / \Delta f \quad (1.5)$$

Here f_0 is the resonant frequency, and Δf is the resonance peak at half-amplitude. MC applications include use in microscopy and force measurements, and in the current discussion

chemical and biological sensing. Of the two common modes of measuring MC responses (dynamic and static) discussed previously, the optical beam bending technique (static) will be the focus in this dissertation. The static mode measurement method requires focusing a laser spot off of the MC tip and reflected onto a PSD. A single laser arrangement is shown in Figure 1.2b, and as discussed previously when distributed selectivity is desired arrays can be probed as depicted in Figure 1.6. Stoney's equation (equation 1.4) shows that tip deflection Δz is proportional to (MC length)² hence; rectangular MCs provide an optimal sensing device with a high aspect ratio (length/width).

Material properties of the MC itself are also an important design parameter. Commercially available MCs are typically composed of either silicon or silicon nitride, however a new design of a composite of these materials will be presented in Chapter 4.

1.3.2 Surface Modification of MCs

Focused Ion Beam Milling (FIB)³⁷ methods have been used to increase the surface area of MEMS devices by physically creating features in the active surface Figure 1.7a shows trenches created using this surface structuring method. De-alloying uses a chemical means to etch silver out of a co-deposited silver-gold substrate. The procedure begins with deposition of a chromium adhesion layer followed by a gold barrier layer with a final co-deposition of a silver-gold composite. The MC is then immersed in a H₂AuCl₄ solution resulting in a de-alloying of silver and yielding a roughened surface. Figure 1.7b shows the steps in this procedure and an SEM of the roughened surface created using this strategy. Analyte induced deflections of MCs using a DA surface which has been functionalized with

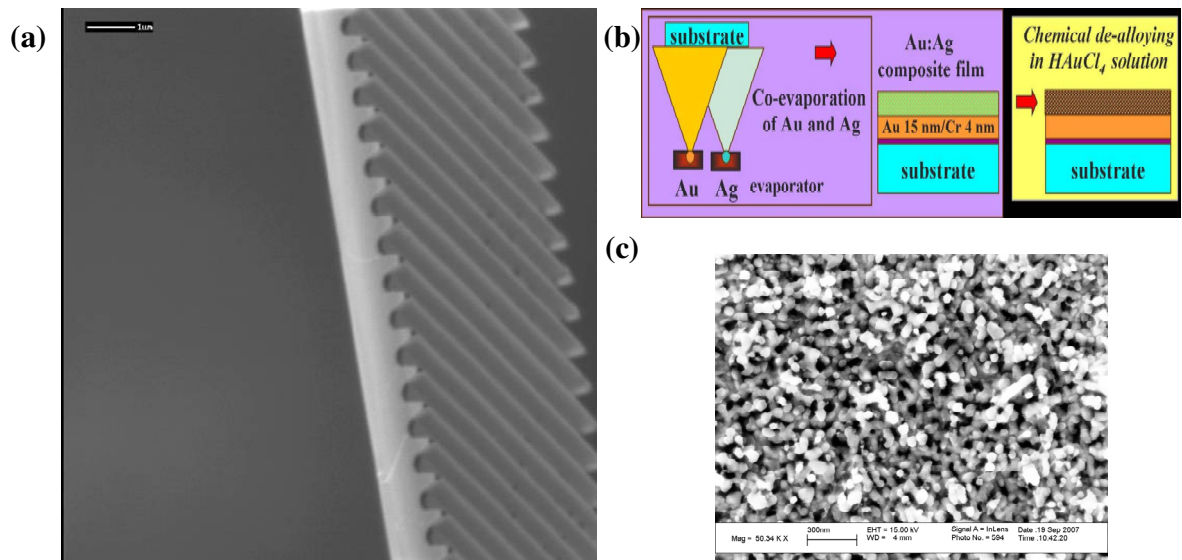


Figure 1.7(a) Trenches created on a micro-cantilever surface using Focused Ion Beam milling. **(b)** De-alloying procedure. **(c)** Resulting dealloyed surface.

a MRP enjoy a response mechanism due to bulk, surface and inter surface effects (Figure 1.3c). The increased surface area results in a greater number of possible analyte binding sites yielding better sensitivity. Studies in which DA surfaces functionalized with a self-assembled monolayer as a MRP have reported a nearly two order of magnitude increase in MC response.^{29,36} Additionally the FIB and DA methods create a roughened surface, improving adhesion of thin film MRPs. An effective strategy for H₂ sensing based upon a spontaneous galvanic displacement reaction (SGDR) has been demonstrated.¹⁷ np-Pd films have been functionalized onto an active MC surface following the process flow depicted in Figure 1.8 only four layers are shown for clarity. Briefly, a chromium adhesive layer is first deposited on a native silicon MC chip (Figure 1.8a), followed by a gold barrier layer and finally a sacrificial silver layer, resulting in a multi-layered metal composite (Figure 1.8b). The MC is then placed in a warm, aqueous, saturated bath of PdCl₂. A spontaneous exchange between palladium and silver ensues (Figure 1.8c). The surface created by this process (Figure 1.8d) is a nano-porous-palladium(np-Pd) MRP. This novel method of simultaneously functionalizing and nano-structuring a MC surface further reduces issues related to poor adhesion, providing an active surface which is selective for H₂ gas. A discussion on the figures of merit, processing conditions and theory of mechanism will be discussed in later chapters.

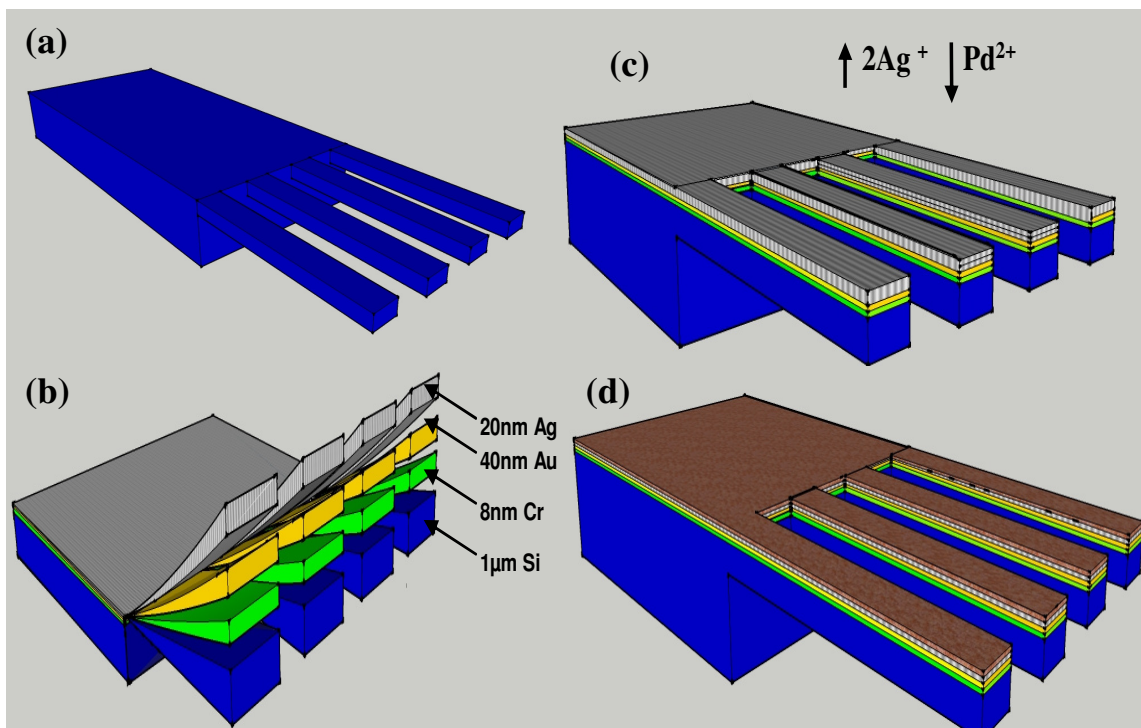


Figure 1.8. SGDR process flow. (a) Silicon MC as received. (b) Physically vapor deposited composite metal surface. (c) SGDR of sacrificial silver for palladium. (d) Nanostructured/functionalized np-Pd film.

1.4 HYDROGEN AND ENERGY RELATED CONCERNS

1.4.1 Current Demands

The current need for alternative energy resources has led to consideration of developing a hydrogen fuel infrastructure. Along with use and storage the ability to detect hydrogen is imperative considering its explosive nature above 4%. Hence; safety outlines (2009) mandated by the U.S. Department of Energy (DOE) impose the following requirements for optimal sensor design:

- 1) Response time of 1 second at 4% H₂
- 2) Response time of 60 seconds at 1% H₂
- 3) Recovery time of 60 seconds independent of concentration.
- 4) Dynamic range between 0.4% H₂ -4% H₂

No current technology meets these requirements while satisfying analyte specificity at a cost < \$40/sensing node.³⁹ However it is demonstrated herein that a np-Pd MC sensing platform approaches these requirements.

1.4.2 Theory of Palladium Hydrogen Systems

The unique characteristics of the palladium/hydrogen system have been studied for over a century dating back to the early work of Graham.⁴⁰ It was discovered that transition metals show exceptional hydrogen uptake, and have been classified as endothermic and exothermic absorbers of hydrogen. This classification is based on the contributions of the enthalpy of hydrogen dissociation (104 kCal/mol), which is independent of the nature of the metal; and enthalpy of hydrogen solvation. The enthalpy of hydrogen solvation depends upon the interactions of dissolved hydrogen atoms and between hydrogen and the metal⁴¹ of

choice. In particular palladium, an exothermic absorber of hydrogen has been studied extensively for sensing, storage and catalytic applications.^{17,42-45} A major focus in this dissertation is creating a better understanding of palladium/hydrogen systems and the use of this system in hydrogen sensing. Hence, a discussion on the thermodynamic, geometric and kinetic properties of palladium interactions with hydrogen will be presented here and continued in Chapters 2 and 3.

Palladium exceeds all group VIII elements for H₂ absorption.⁴⁶ This unique distinction is related to the exothermic nature of hydrogen adsorption on palladium (9.5kCal/mole) in contrast to the other members of Group VIII. Hydrogen insertion into palladium results in phase transitions. These phases are referred as α for H/Pd < .04, and β for H/Pd > 0.5, with co-existence of these phases between these two regions. Once in the β phase a lattice expansion of up to 4% for palladium has been reported. This large expansion is a consequence of hydrogen insertion into palladium lattice in non-stoichiometric ratio. Interstitial site occupancy occurs in the energetically favored octahedral position of the face centred cubic structure of palladium. Nakatsuji et al have reported that single palladium atoms show affinity for molecular hydrogen,⁴⁷ explaining that palladium 4d orbitals are a major contributing factor to this effect while the 5s orbital is less influential. This report describes a re-hybridization of the 4s/5d atomic orbitals in terms of creating “dangling” bonds on the metal surface, where the H-H bond is elongated and weakened as the Pd-H bond is formed. Insertion of hydrogen weakens the Pd-Pd bond by decreasing electron density between the two atoms⁴⁷ leading up to lattice expansion. This symmetry allowed process results in a stabilization of ~ 2 kcal/mol for dissociated hydrogen in comparison to the molecular form of hydrogen.

Hydrogen insertion within palladium results in contributions related to electronic, morphological and thermodynamic advantages. An electronic advantage has been discussed by Messmer et al.⁴⁸ The high solubility of hydrogen into palladium has been attributed to near zero orbital electronegativity difference between the Pd(4d) and H(1s) overlap. Louie et al.⁴⁹ reported that atomic hydrogen lies in the 3-fold hollow site of Pd(111), which favors the Pd(4d)-H(1s) interaction. An even more advantageous system will be discussed later involving the effects of palladium oxide. Briefly, Nakatsuji has suggested that hydrogen dissociation on palladium is encouraged by the presence of electro-negative ligands attached to the palladium atom.⁴⁷ Hakanagalou et al.⁵⁰ have provided a model describing the unique influence of oxide with respect to electronegativity and morphological advantages that will be discussed in a later chapter.

1.4.3 Hydrogen Sensing/Detection Methods

Electrochemical

Several reports have been published in which electro-chemical properties of metals including catalytically active metal oxides,⁵¹ palladium,⁵²⁻⁵⁵ and palladium oxide⁵⁶ undergo measurable electrochemical changes in the presence of hydrogen gas. Typically, sensors composed of palladium undergo a change in material resistance upon exposure to hydrogen gas. Depending upon the regime of operation the resistance may increase⁵⁴ or decrease.⁵² In the former regime increased resistance is associated with incorporation of dissociated hydrogen into the fcc lattice positions within palladium resulting in increased electron scattering centers. In the latter regime the $\alpha \rightarrow \beta$ phase transition occurs providing more pathways for electron conduction hence a reduction in resistance. Advantages of

electrochemical sensors include; low power consumption, portability and fast response. Disadvantages of this platform include; lifetime dependence on operating environment (ruggedness),⁵³ hysteresis, slow recovery and surface fracture due to phase transition dependence of response characteristic.^{53,54,56} Additionally, high temperatures (>200°C) are required for fast response.⁵⁵

Optical

Optical methods for hydrogen safety sensing devices have also been reported.^{57,58} These methods have been used to evaluate optical changes that occur due to the presence of hydrogen. Reports have been published which include the use of a chemochromic pigment composed of PdO/TiO₂.⁵⁷ In this report a reversible color change occurs due to the reduction of PdO to Pd in the presence of H₂. Another report on the use of palladium nano-particles deposited on tungsten oxide⁵⁸ has also described a chemochromic response/measurement mechanism useful for hydrogen based sensing applications. Advantages of these methods include short-term fast response (~1 second) and minimal effects from local environment (robust). However, operating temperatures over 80°C⁵⁷ are required for fast response which diminishes over long term use. These reports^{57,58} have provided no information on effects of interfering agents. Another report explores increases in optical transmission due to lattice expansion of thin palladium films.⁵⁹

MEMs

The mechanical stresses generated in thin palladium films have been exploited in MEMs sensing strategies. Lattice expansion has been described by Oriani⁴¹ using a “ball-in-

hole” model to provide a semi-quantitative understanding of this process. A hydrogen atom is taken as an incompressible sphere, which is inserted into a cavity of smaller dimension within the metal lattice. Upon insertion the volume of the body increases (ΔV_2) by an amount larger than that required for accommodating the solute atom.

$$\Delta V_2 = [3(1-\nu)/1+\nu]\Delta V_1 \quad (6)$$

Where ΔV_1 is the volume change associated with insertion of a hydrogen atom alone and ν is the Poisson ratio. Oriani describes this as the origin of the increase in lattice parameter due to insertion of hydrogen. MC designs⁶⁰⁻⁶³ have exploited this compressive stress generated during palladium lattice expansion, however in those studies slow response and poor selectivity were limitations. Improvements to MC devices focused on structuring the MC surface to improve adhesion and increase surface area using FIB milled trenches.⁶¹ A more recent study¹⁷ has focused on a creative means to introduce a nano-porous palladium (np-Pd) film.

1.4.4 Pd Films vs np-Pd

Early attempts at utilizing palladium-based hydrogen sensors relied on the use of palladium films. The uptake in thicker films (~1mm) has been reported to obey diffusion-limited kinetics.^{64,65} Technological advances in processing and thin-film deposition ultimately lead to the ability to use thinner films (μm). No reports on the use of these thinner films have shown diffusion limited kinetics for hydrogen uptake, which would place sensing responsiveness much faster. Still two major drawbacks were presented which included hydrogen induced embrittlement⁵⁶ and an inherent slow response time.⁶⁶ These shortcomings

encouraged continued research in the area of palladium nano-particles as an alternative to thin films. Nano-particles are materials or ensembles whose radii are <100 nm. Advantages of using such material are related to increased surface to volume ratio, extensive network of grain boundaries and often-superior mechanical properties (hardness and tensile strength) and reported reduction in phase transition related obstacles.^{43,67,68}

1.4.5 Deposition of np-Pd Using SGDR

Galvanic displacement, also referred to as immersion plating is a technique of substituting a base material of lower oxidation potential to that of an ion in solution of higher oxidation potential.^{69,70} An advantage of this method is that it does not require a reducing agent, as the base material serves this purpose. A disadvantage of this method is control of reaction rates due to fast exchange of charges between oxidizing and reducing species. A convenient system to consider for this exchange is the silver/palladium pair. Silver has a red-ox potential of 0.779V, whereas palladium has a red-ox potential of 0.915V. Hence, an overall spontaneous displacement can be written as equation 1.7.



Recently it has been demonstrated that MCs decorated using this route for surface functionalization offer near ideal H₂ sensing performance characteristics.¹⁷ It was later reported¹⁶ that these surfaces rely on palladium oxide for improved response kinetics. It has also been hypothesized that the effects of oxide may also play an important role in relationship to immunity of common interfering agents. In ensuing chapters the details of this

unique material will be elaborated. This brief introduction to Pd/H₂ systems and the uses of nano-porous features to enhance the Pd/H₂ interaction will brief our audience on innovations in material design and a better understanding of these properties related to palladium/hydrogen based systems. Chapter 2 will address figures of merit for H₂ sensing applications that have been made using nano porous palladium based MC devices. In Chapter 3 a discussion on material properties and processing will be presented providing information which may be relevant for catalysis and H₂ storage.

1.5 MICROCANTILEVER MATERIALS AND PROCESS DESIGN

1.5.1 Nano-Laminate Composites

It is often the physical transducer which imposes both practical and fundamental limitations on many classes of chemical sensors. Overcoming these obstacles are important contributions to further advancing chemical sensing technology. The final section of this dissertation will focus on the advantages of introducing a nano-laminate composite (NLC) material composed of alternating layers of SiN_x/SiO₂ for MC design. Several advantages using NLC materials for MC design are presented which include improved reflectivity, thermal stability and flexible functionalization strategies. The ability to mechanically structure these surfaces may also offer an alternative means to introduce a greater active surface area in comparison to chemical options such as DA and SGDR. The advantages and disadvantages of employing “top-down” approaches will be introduced while comparing and contrasting this with “bottom-up” strategies both as competing and complementary techniques.

CHAPTER 2: RAPID RESPONSE MICROSENSOR FOR HYDROGEN DETECTION USING NANOSTRUCTURED PALLADIUM FILMS

Chapter 2 is an adaptation of a research article published in *Sensors and Actuators A*, 163, 2010, 464-470. This article demonstrates the near ideal H₂ sensing characteristics offered by nano-porous palladium functionalized microcantilevers.

2.1 INTRODUCTION

2.1.1 Background

Considerable effort has been expended in recent years to develop a hydrogen based transportation fuel economy. However, one of the critical issues that must be addressed if this technology is to be widely adopted is the perceived hazard from hydrogen gas leaks. As a consequence of this concern, comprehensive safety management of the storage, handling, and use of this gas is a necessity. In addition to safety-by-design and passive mitigation systems, a vital element of the safety management strategy must be the development of hydrogen sensing technologies that can sensitively detect hydrogen releases and provide valid alerts of system failures. The hydrogen sensors to be used in this application must possess a number of characteristics that ensure timely and appropriate responses to any hydrogen gas leaks or releases. Ideal requirements for a H₂ sensor for leak detection applications include high sensitivity, fast response, wide dynamic range, high specificity and immunity to common interferents. Additionally, the sensor must be very stable, operating for prolonged periods of time while giving acceptably low false positive responses. Operation at

near room temperatures (to minimize the risk of H₂ ignition) and easy incorporation in low power, low cost distributed sensor networks is essential for widespread commercial acceptance to occur.

2.1.2 Hydrogen Sensing Techniques

Many technologies have been explored and commercialized to sense low concentration hydrogen gas leaks. The more commonly used techniques include electrochemical,⁷¹ semiconductor metal oxide,⁵¹ thermal conductivity,^{72,73} catalytic,⁷⁴⁻⁷⁶ and optical sensors.⁷⁷⁻⁸⁴ A recent study of commercially available H₂ sensors came to the conclusion that although many of these sensors have a number of strengths, none could meet all the requirements for H₂ monitoring in both stationary and automotive vehicular environments.³⁹ Table 2.1 lists the most important sensor requirements in these applications, with the most demanding requirement being the fast response and recovery requirement for automotive applications.^{39,85} None of the commercially available sensors were found to adequately meet this requirement.

Numerous micro and nanostructure Pd based H₂ sensors have been proposed in recent years to improve the sensor H₂ sensitivity and temporal response characteristics. Thin palladium films catalyze the breakdown of H₂ into atomic hydrogen, which can be reversibly absorbed into the palladium film to form palladium hydride via equation (2.1).

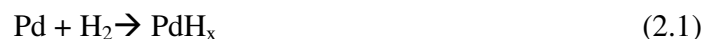


Table 2.1

Important performance requirements for H₂ Sensing

Performance requirement		np-Pd coated MC
Sensitivity range	<0.1 to >4%	0.01–4%
Survivability limit	100%	Linear response to 100%H ₂
Response time Automotive:	<3s	~4–5 s
Stationary:	<30s	
Recovery time Automotive:	<3s	~15 s
Stationary:	<30s	
Temperature range Automotive:	–40 °C to +125 °C	Yes
Stationary:	–20 °C to +50 °C	
Pressure range Automotive:	62–107 kPa	Yes
Stationary:	80–110kPa	
Ambient relative humidity range Automotive:	0–95%	0–100%
Stationary:	20–80%	
Interferent resistance	No false positive response	Excellent
Power consumption	<1W	0.5–1W
Lifetime Automotive:	6000h	
Stationary:	>5years	Demonstrated >2.5 years
Accuracy and Repeatability	Automotive: 5–10% Stationary: 10%	>±5

Under equilibrium conditions, the amount of H₂ absorbed into the Pd film is proportional to the square root of the H₂ partial pressure in the ambient air (known as Sievert's law).⁸⁶ The formation of palladium hydride alters the electrical, optical and mechanical properties of these films, and these changed properties can be exploited to create various types of H₂ sensors. Hydrogen sensors fabricated to measure changes in resistivity include thin film Pd based sensors⁸⁷⁻⁹⁰ and Pd nanostructured sensors.^{91,92} Optical techniques include Pd coated optical fibers with altered light transmission^{77,81,84} and surface plasmon electrical characteristics,⁷⁸ and Pd thin film coated surfaces also with varying optical transmission characteristics^{80,82,83} upon exposure to low concentrations of H₂ in air. Alternately, the atomic hydrogen can react exothermically with O₂ in air, and changes in film temperature due to this reaction can then be measured.^{93,94} Sensing platforms utilizing gasochromic transition metal oxides have also been reported.^{95,96} These reports provide limited information on selectivity and have shown short term fast response(<1s), degrading to nearly 4s in cyclic studies.

The current system involves a highly nano porous surface. Exploitation of this surface will result in an efficient means of H₂ exchange through adsorption and desorption within a sensing environment. The processes involved with a palladium based sensing device for H₂ include molecular adsorption, dissociation, and atomic absorption.^{86,93,96} During the process of dissociation hydride formation occurs and changes in the morphology/phases of the palladium result in lattice expansion. Other processes occurring in a gas phase environment involving palladium, hydrogen, and oxygen systems include an exothermic reaction related to the formation of water vapor. The use of the MC device described herein offers characteristics suited to monitor these processes including surface stress induced bending

upon adsorption, possible bi-metallic effect due to exothermic reactions, and rapid relaxation related to fast desorption from the nano porous palladium surface.

2.1.3 Microcantilever Based Hydrogen Sensors

Microcantilever (MC) based chemical sensors were first seriously explored as a trace gas sensing technology in 1990s^{12,97} with the first reported use of Pd coated MCs for sensing H₂ occurring in 2000.⁶³ Adsorption of a gas onto a thin film surface can cause large changes in stress and consequent bending of a thin cantilever structure.^{18,97,98} This bending response can be sensitively detected using piezoresistive, capacitive and optical techniques such that high sensitivities are achievable.^{18,98} In general, MC based chemical sensors have been shown to have high sensitivity, wide dynamic range and fast response times. Optically read cantilever sensors are particularly advantageous in the present application due the danger from H₂ ignition using heated or electrically operated sensors. Other advantages include very low power consumption, and their potential use in distributed wide area sensor networks allowing multiple low cost sensors to be located at H₂ storage or processing facilities, or on H₂ powered transportation vehicles.

The possibility of using Pd coated MC sensors to detect H₂ leaks has been examined in several previous studies.^{60-63,99,100} The issue with most previous thin film Pd sensors, and all of the previous Pd-based microcantilever sensors, is that the sensor response and recovery times are far longer than acceptable for most applications; response times for these microcantilever based H₂ sensor studies varied from 3-5 minutes^{62,100} up to 1 hour.^{60,61,99} The long response and recovery times observed in the previous studies were attributed to the long time for elemental hydrogen to diffuse into the palladium film.

In this Chapter the development and testing of a hydrogen sensor that utilizes new nanostructured Pd films, demonstrates that optically read MCs coated with this nanostructured Pd coating have near ideal fast response characteristics when monitoring low concentrations of H₂ gas. In particular, the response and recovery times measured with these sensors are far shorter (< 10 sec.) than those reported in all previous MC based H₂ sensor studies.

2.2 EXPERIMENTAL SECTION

2.2.1 Microcantilever Surface Modification

Microcantilevers used in this study were custom manufactured (MikroMasch, Sunnyvale, CA) rectangular free standing structures, fabricated from crystalline silicon wafers with the following dimensions; length – 400 μm, width – 100 μm and thickness – ~1 μm. The MC's, configured in 16-lever arrays with a 250μm pitch are used as received.

The first step in the deposition of the np-Pd sensing film was to vapor deposit a 2 nm chromium adhesion layer followed by a 20 nm layer of silver on one side of the MC. A saturated PdCl₂ solution sonicated and warmed to 100°C was prepared using deionized water (DI) obtained from a Barnstead E-pure water filtration system. The MC was then placed in the aqueous suspension for approximately 17 hours; this time interval was chosen for optimal analyte sensitivity, and will be discussed in more detail in a later chapter. The galvanic displacement reaction¹⁰¹⁻¹⁰⁴ occurs between silver metal on the MC surface and palladium ions in solution, resulting in the formation of an active granular Pd film. The consumption of Ag was followed using Inductively Coupled Plasma Optical Emission Spectrometry (ICP-

OES) using a Perkin-Elmer Optical Emission Spectrometer Optima 2100 DV. To promote homogeneity, the cantilevers were placed in a 10mL volumetric glass vial and sealed with a glass stopper fixed with parafilm. The vial was continually rotated for the duration of exposure and the MC's were subsequently rinsed in DI water and dried prior to testing. The created MC surfaces were inspected using scanning electron micrograph (SEM) imaging without applying a conductive coating to the surfaces. This technique allowed us to periodically examine the surfaces after H₂ gas exposure to see if the surfaces changed (i.e. delaminated, cracked or changed morphology) during the course of this study.

2.2.2 Testing Protocol

Testing was conducted in laboratories at both Oak Ridge National Laboratory (ORNL) and the University of Tennessee Knoxville (UTK). MCs were secured in a low volume flow cell (~150 μ L) and mounted at the end of a laser rail system. Changes in tip deflections of the MCs were measured using an optical readout technique. The read laser used was a 635 nm diode laser, which was aligned and focused on the tip of an individual MC at a distance of ~25 cm. A position sensitive detector (PSD – On-Track Photonics) positioned ~ 10 cm from the flow cell; was used to detect the reflected laser light and measure tip deflections; a schematic of this set-up is shown in Figure 2.1. Note that the flow cell is shown schematically in the figure for clarity and misrepresents the efficient washout characteristics of the actual design. Also the footprint of our device can be reduced substantially for portability. Calibration of the detector prior to data compilation was used to convert responses to tip deflection measurements. Gases used in this study were obtained from Airgas Inc. or Air Liquid Inc. Sample introduction was accomplished using a stainless

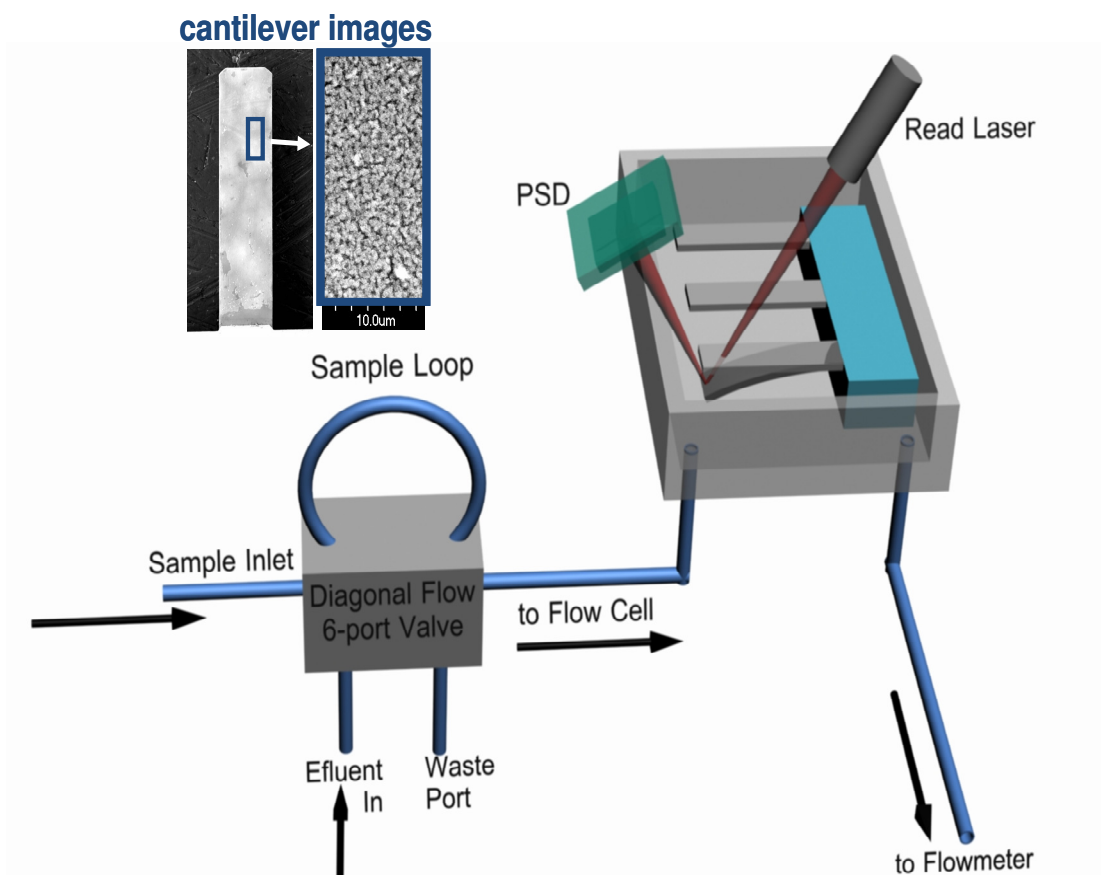


Figure 2.1 Experimental set-up illustrating static bending mode of detection and sample injection using a 6port valve. Inset: microcantilever and expanded surface image.

steel 6-port flow injector with a 5 mL stainless steel flow loop unless otherwise stated. Optimization of testing conditions was carried out to determine flow rate, carrier gas composition, and charging effects with respect to gas environment. This testing procedure will be further elucidated in the results and discussion section as a more complete response mechanism will be outlined in Chapter 3. The optimal carrier gas was composed of N₂/O₂ (80/20) delivered at flow rates ranging from 2-8 cc/min, with optimal conditions being achieved at ~ 6 cc/min. Stability and gas optimization studies were conducted at ORNL. Gas mixtures composed of 4% H₂/96% Ar were introduced into the flow injector and carried to the sampling device using carrier gases composed of either N₂, O₂, or a N₂/O₂ (80/20) mixture. Referring again to Figure 2.1, “effluent in” can be interfaced to a small cylinder of O₂ for gas phase regeneration. A vacuum apparatus could be connected to the exit port at “flowmeter”. With vacuum, ambient air with ~ 20% O₂ could be aspirated through the flow cell and serve to regenerate the system as well. Sensitivity and interference studies were conducted at UT. Carrier gases composed of O₂ were delivered via Princeton Instruments syringe pump. H₂ and interfering gases were collected in an SKC Inc sampling bag and diluted using N₂.

2.3 RESULTS AND DISCUSSION

The focus of this study was to explore novel means to create and use np-Pd films to detect hydrogen. Mechanistic considerations will be briefly addressed first as more detail will be presented in Chapter 3. A novel galvanic displacement process used to functionalize these sensors will be discussed and a system optimization and conditioning protocol will be

outlined. Next, results showing excellent analytical figures of merit compared to the required system parameters listed in Table 2.1 including selectivity, sensitivity, fast response, reproducibility, stability, and reusability using this platform for hydrogen sensing. Finally, possible future directions will be mentioned.

2.3.1 Mechanistic Considerations

The ability of palladium to selectively adsorb (surface effect) and absorb (bulk effect) molecular hydrogen offers a very attractive and selective means to sequester hydrogen from a complex sampling matrix. However, the absorption process is expected to be slow and may suffer from selectivity issues. Conversely, physical changes dominated by surface adsorptive effects are expected to be faster. Prior studies of palladium, hydrogen and oxygen environments¹⁰⁵ suggest that changes in surface composition, and possible charge related changes are occurring. Both of these descriptions may result in surface stresses which would be reflected in MC bending. However, the porosity of our system seems to be key to rapid responses. The nanoporous Pd layer created in our processing, as opposed to physical deposition, is a consequence of its formation. The current method involves a sacrificial galvanic displacement process which has been reported to form nanostructures that contain Bi, Te, Pb and noble metals.¹⁰²⁻¹⁰⁴ It appears that the slow reduction of the Pd²⁺ by Ag⁰, as well as pretreatment of the Pd coating with an O₂ purge influences performance (see below). It is further noted that a sacrificial galvanic displacement of a 20 nm thick layer of Ag gives rise to about a 100 nm layer which has been measured by profilometry and cross sectional HRSEM of np-Pd, which will be presented in Chapter 3.

2.3.2 Novel Wet Chemical Processing

The current study investigates a H₂ responsive np-Pd films. The appearance of the Pd film and the rapid response suggests that it is nano porous and, as such, the interaction is almost surface confined in nature. The wet chemical processing used in this study to our knowledge has not been reported for MC functionalization. During this process, a spontaneous exchange between Pd²⁺ and Ag⁰ occurs on the active side of this device. ICP-OES has also been conducted, testing the exchange of Pd and Ag. The processing procedure used in this study has shown that within 5 hours, less than 1 nm of the original 20 nm Ag film remains, and after 17 hours less than 0.5nm of the original 20nm Ag film remains. Structured surface features have been observed using SEM imaging, and these granular-nanoporous feature appear to facilitate the sorption/desorption of H₂ gas. The nature of this process resulted in a serendipitous sensing duality, which combines enhancement features related to both bulk and surface effects. Bulk features may influence sensing characteristics related to sensitivity, as this is reflected in our large sensor responses that obey Sievert's Law. However, the ability to respond and relax quickly may be indicative of a surface-like effect represented by fast sorption/desorption. More detail into the complex nature of this system, will be presented in Chapter 3.

2.3.3 Optimization/Gas Phase Composition

The differences in response characteristics were first evaluated with respect to choice of gas phase composition. Samples composed of 4% hydrogen diluted with argon or nitrogen gas were introduced into a low volume flow cell (~150μL) housing a np-Pd functionalized MC at a flow rate of approximately 6 cc/min. Using nitrogen as the carrier

gas resulted in responses that were both slow and broad (Figure 2.2a). Responses were then collected using oxygen as the carrier gas (a purge of at least 5 minutes). In Figure 2.2a, a faster response and recovery in the presence of oxygen compared to use of nitrogen was observed. A N₂/O₂ (80/20) purge and carrier gas (mimicking air) yields an even faster rise time, with highly reproducible response characteristics. When the carrier gas composition was changed back to nitrogen, the response is initially quite similar to that gathered using oxygen as the carrier gas. After extensive exposures, the responses were once again broadened and slow. Figure 2.2b shows this gradual change. This experiment suggests that an oxygen rich environment may favor a faster surface induced response and recovery, whereas nitrogen rich environments appear to be more influenced by the bulk absorption of hydrogen into the palladium. The faster rise and recovery in the presence of oxygen may be a consequence of the reaction exotherm due to water formation catalyzed by the presence of palladium. Removal of H₂ from the sensing environment due to reaction with O₂ may also assist in recovery of the device. Indeed, as discovered in later studies a longer O₂ conditioning protocol resulted in a long term stable response to H₂ these observations will be further addressed in the following chapter.

Flow rate studies were conducted to evaluate optimal sample delivery conditions. A comparative study in which the effects of flow rate with respect to gas composition was tested. These studies provided information not only on optimal conditions, but also possible mechanistic pathways that will be elaborated on in Chapter 3. Samples of 1.7%

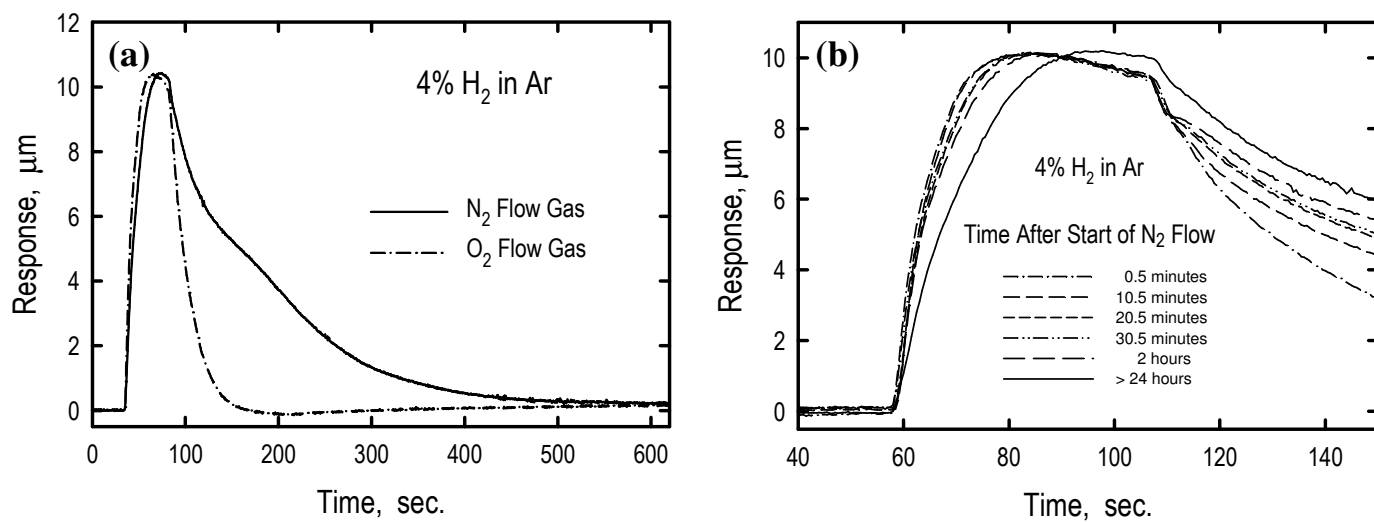


Figure 2.2 (a) Effects of response characteristics comparing N₂ versus O₂ environments. **(b)** Gradual changes in response characteristics upon return to a N₂ environment post O₂ flow.

hydrogen were prepared and introduced to the flow cell housing the np-Pd MC at flow rates ranging from 2 cc/min up to 8 cc/min. The use of nitrogen as the carrier gas resulted in slow response and recovery rates (tip deflection/time) at all flow rates Figure 2.3a shows the flow extremes conducted during this experiment. Conversely the rise time with oxygen as the carrier gas was fast but diminished slightly at the lowest flow rates; rate of recovery was reduced by 4 fold as flow rate was reduced by 4 fold, flow see Figure 2.3b. This observation points to possible differences in H₂ response depending on presence of O₂. Bulk absorptive effects, such as those possibly occurring in N₂ rich environments, would be less influenced by the rate of analyte exposure and removal. Bulk effects would be more dependent upon a diffusive mechanism, and thus may show similar response and recovery characteristics irrespective of flow rate. Other influences occurring during H₂ sensing may include morphological changes in the presence of an O₂ purge. The potential reaction of O₂ with H₂ to form water vapor may also be influencing this behavior, especially in terms of recovery as noted in Figure 2.3. These effects and observations will be further discussed in the following chapter.

2.3.4 Conditioning and Regeneration

Stability and long term use is vital for a successful sensing platform. Two methods have been evaluated in the current study; liquid phase regeneration and gas phase

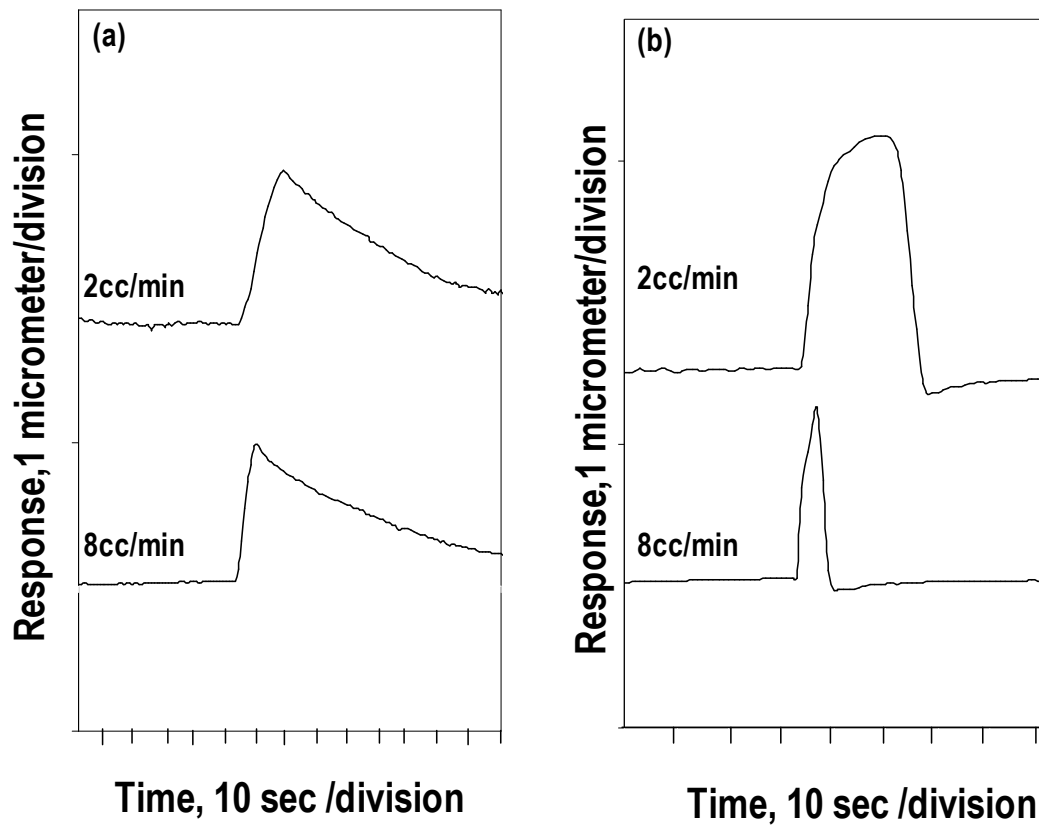


Figure 2.3 Effects of carrier gas and flow rate. **(a)** Increasing flow rate in N₂ rich environments results in no observable change in rise and recovery. **(b)** Increasing flow rate in O₂ environment results in observable response and recovery changes.

conditioning. Liquid phase regeneration was initially tested. Prior to discovering the criticality of O₂ purging to obtain large, rapid responses, sensor responses were found to diminish with continuous use, but could be regained to a large degree by rinsing with fresh PdCl₂ solution. It was demonstrated that a np-Pd MC could be tested, regenerated, and retested again in the same flow cell. This cumbersome affair required an overnight drying period, hence not conducive to rapid sensor turnaround.

Gas phase testing resulted in a better understanding of the processing conditions required for optimal results. The effect of gas phase composition on sensor performance was first examined at UTK using a freshly made np-Pd MC according to the chemical procedure described above. Initially, a new sensor shows poor response characteristics to H₂ gas. Continual use for approximately 1 hour results in a very fast and large response to samples composed of 4% H₂. The performance seems to be related to a cycling of O₂ followed by H₂ doses. This sampling/conditioning protocol has also been used for sensors that have been stored long term after use. The conditioning/re-conditioning protocol can be used to establish responsive calibration to a series of standards. The obvious advantages of this sensor regeneration/calibration method include a complete gas phase protocol that is field compatible, reduced sampling prep and sampling waste, and ability to regenerate or standardize new systems in less than 1 hour. This protocol has been adopted for our devices and has provided reliable results for over 2 years (see below). Typical comparisons between standards (4% H₂) and individual MCs deviate by ~ 3% relative standard deviations. Due to differences in preparation and optical alignment the cantilever to cantilever response factor variability is more like a factor of two, thus each cantilever must be individually calibrated.

2.3.5 Performance Evaluation

Paramount among the desired attributes of a H₂ sensor listed in Table 2.1 are rapid response and recovery time, suitable sensitivity range, and selectivity relative to potential interferences. In this regard, optimization of sensing needs with respect to processing conditions was evaluated early in this work by altering exposure times to the PdCl₂ solution. Short exposure times (~4.5 hours) resulted in slightly faster responses whereas longer exposure times (~17 hours) still yielded good response rates (response and recovery times of ~ 10 seconds), however sensitivity was improved at this longer exposure time. These early studies were conducted before realizing the benefits of a longer O₂ conditioning protocol. Specifically, the limit of detection limit approached 100ppm (Figure 2.4) with a linear dynamic range of 3 orders of magnitude. It is worth noting that the MC chip houses an array of cantilevers. Prior work demonstrated an ability to differentially modify the cantilevers in an array.^{35,106} Thus a single MC sensor array can provide both response redundancy (similarly processed MCs) and differentially prepared MCs (long versus short PdCl₂ exposure) that emphasize different response characteristics (e.g., response speed versus sensitivity). Arrayed MCs exploiting both np-Pd and other mixed metals using SGDR may provide a sensor capable of simultaneously detecting H₂, H₂S, CO; this is an area of current intellectual pursuit.

Selectivity is also an important attribute in terms of desirable sensing properties. Figure 2.5 shows excellent selectivity of the studied sensor comparing the normalized responses (all based on 4% v/v) to hydrogen and several common interfering agents including carbon dioxide, methane and water vapor. A common interfering agent in

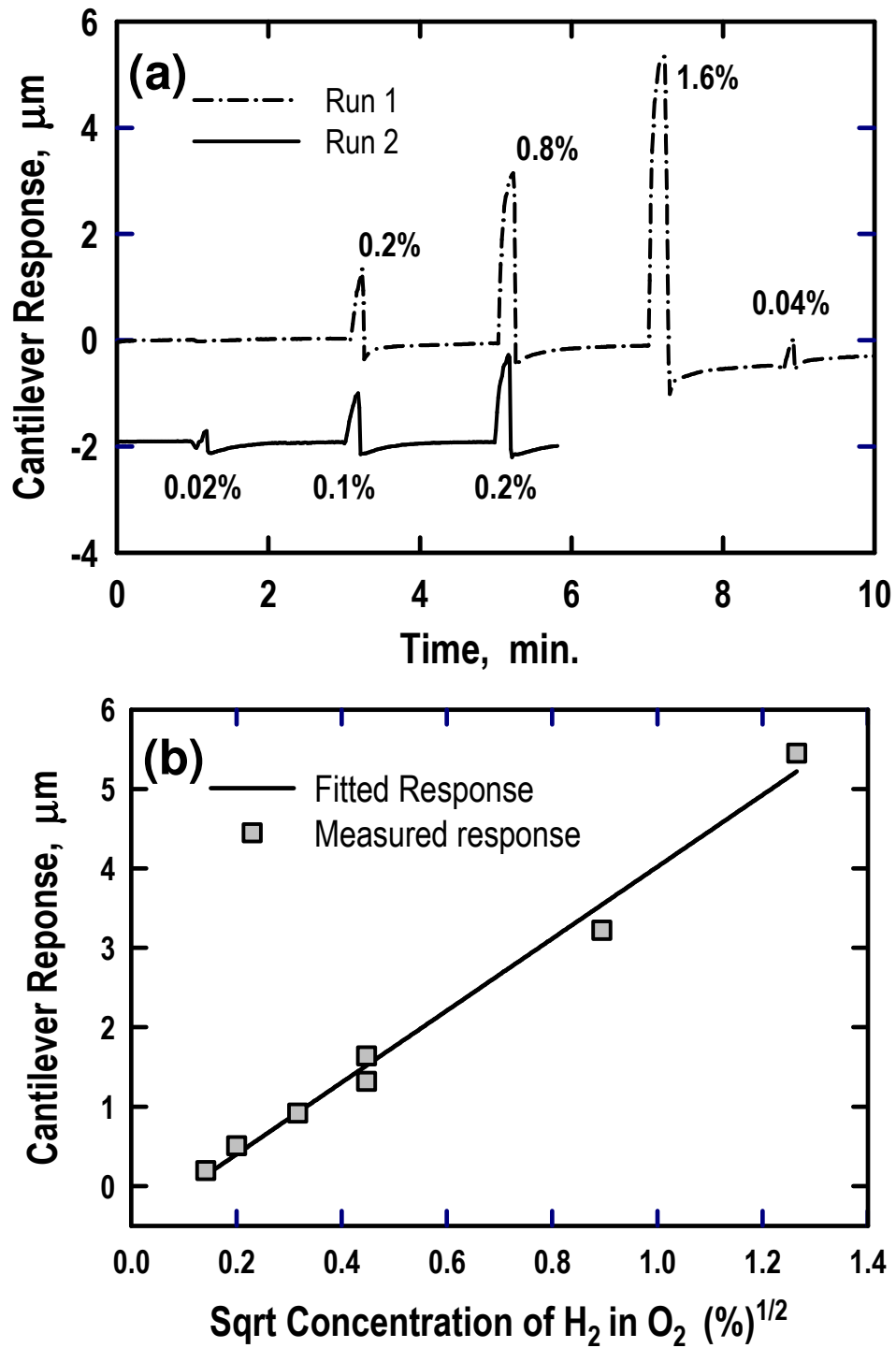


Figure 2.4 (a) Calibration data shown as responses to injections of H_2 over a large range of concentrations showing a limit of detection of approximately 100ppm. (b) Linear calibration plot showing the expected square root dependence as described by Sievert's Law and a regression constant of 0.992.

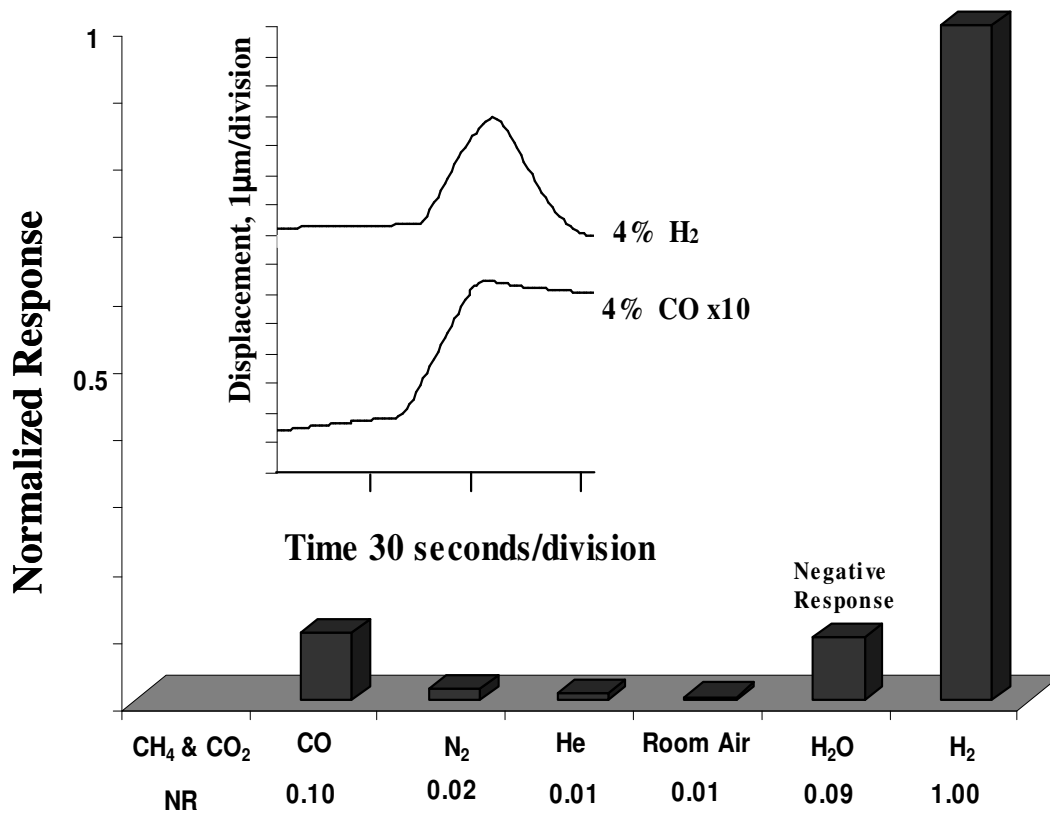


Figure 2.5 Normalized responses with respect to H₂ demonstrating good selectivity relative to potential interfering gases. Response profile is also shown comparing an injection of 4% H₂ in O₂ carrier gas and an injection of 4% CO that shows that carbon monoxide not only gives a 10-fold smaller response but it is also distinguishable in its profile.

vehicular fueling applications is carbon monoxide; hence, exposure to this compound was explored more in depth. The inset of Figure 2.5 compares response magnitude and signature response profiles of H₂ versus CO in which sampling was conducted using discrete injections of either H₂ or CO. The response magnitude of H₂ is not only an order of magnitude larger than CO, but distinguishing differences between the response profiles also bodes well for the discrimination of these gases as observed in prior gas phase MC sensing.^{32,107} In the following chapter, details regarding immunity will be emphasized more rigorously with respect to a mechanistic outline of the system. Testing similarly to the National Renewable Energy Laboratory (NREL) parameters have been conducted to evaluate a more extensive library of possible poisoning species, these results and the effects of surface chemistry/morphology will be presented in the following chapter.

Other important aspects of this sensing platform include a highly robust, reproducible and re-usable device. These sensors have been used for analysis for over 2 years. Figure 2.6 shows responses to 4% v/v H₂ of the same array over this time period. The appearance and response magnitudes of the profiles are quite similar with some differences due to evolving system optimization over this time interval as discussed previously. SEM images of the sensor coatings have also been evaluated and show no changes in appearance over a 2 year period. Requirements for external testing and real-world applications include testing at room temperature without the requirement for vacuum conditions in air. All testing conducted met these required specifications; for example Figure 2.2a shows that the best responses occurred in a N₂/O₂ (80/20) sample gas mixture. Five generations of chips have been created and continually improve. The latest improvement involves the use of an adhesive chromium

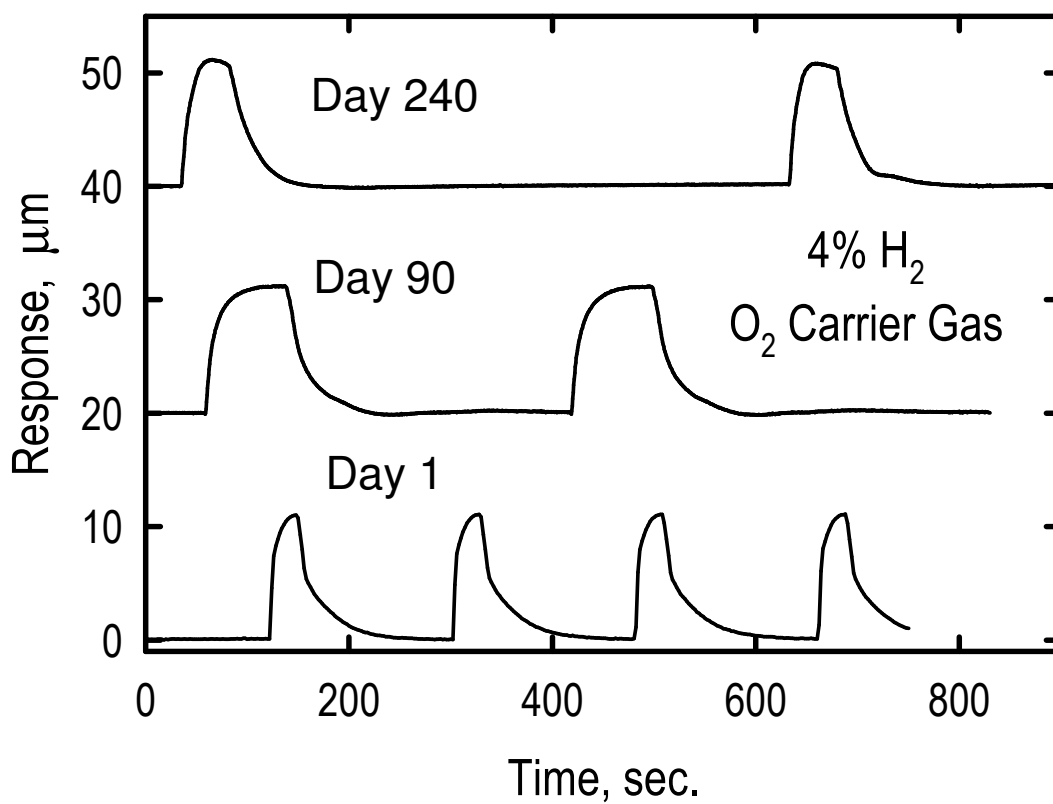


Figure 2.6 Long-term stability/reproducibility has been established over a 10-month period; although injection volumes and flow rates were not the same in these experiments, the responses on this particular cantilever (and others) have very similar profiles and magnitudes. SEM images revealed no discernable changes in appearance as well.

layer and a gold barrier layer below the surface of the silver layer to minimize coating delamination.

2.4. CONCLUSIONS

We have demonstrated in this paper that optically read MC sensors with nanostructured Pd coatings formed by sacrificial galvanic displacement have many of the attributes required for distributed sensing of hydrogen leaks in many applications. These include high sensitivity, wide dynamic range, fast response and recovery times and repeatable response. These sensors have been operating in a laboratory environment for over 2 years without noticeable changes in sensitivity, specificity, response time and appearance. Studies are currently being conducted to better understand the complex sensing environment, which includes exploring the use of thinner coatings, varying metal adhesive surfaces, and evaluation of surface morphology with respect to changing gaseous environments. Arrayed methods are also being evaluated in which various metals fashioned via SGDR may permit the ability to identify quickly H₂ leaks near the explosive limit of 4% in air along with other gases such as CO and H₂S.

CHAPTER 3: CHARACTERIZATION OF HYDROGEN RESPONSIVE NANOPOROUS PALLADIUM FILMS SYNTHESIZED VIA SPONTANEOUS GALVANIC DISPLACEMENT REACTION

Chapter 3 is an adaptation of a research article submitted to *Nanotechnology*. This article outlines a theoretical and experimentally supported mechanism for rapid H₂ interaction with nanoporous-palladium films synthesized using a novel spontaneous galvanic displacement reaction.

3.1 INTRODUCTION

3.1.1 Background

Palladium and palladium alloys interaction with hydrogen is of interest from both fundamental and practical standpoints. It is known that palladium selectively sorbs hydrogen reversibly. Molecular hydrogen dissociates at the metal surface and diffuses with a rate constant $\sim 10^{-7} \text{ cm}^2/\text{s}$ ^{55,108} into bulk as palladium hydride (PdH_x). Early studies have reported that the kinetics of hydrogen sorption for relatively thick palladium films (mm scale) is diffusion limited.^{64,65} To achieve faster kinetics work has involved thinner films (μm scale), wherein kinetic limitations shifts to dissociation of H₂ at the palladium surface and recombination of H₂ upon egress.^{109,110} Besides ill-defined models to describe kinetics, other limitations of Pd based films have included adverse effects of sulfides,^{111,112} carbon monoxide (CO),^{113,114} and hydrogen embrittlement.^{55,66,67,115,116} These limitations represent

obstacles for technological advances in storage, catalysis and detection of H₂ using palladium. In particular, H₂ detection using palladium based systems, which include; electro-chemical,⁵³ resistive,^{42,43,52-54,56} optical^{57,58,68} and micro electro mechanical systems (MEMS),⁵⁹⁻⁶¹ have suffered from slow response, contaminant poisoning and an inability to operate under certain ambient conditions.

The limitations addressed above including H₂ dissociation, recombination and effects of contaminants are influenced by surface-related phenomena. Nano-sized particle syntheses have been studied^{42-45,88,116-128} as a means to increase active surface area. This would increase the number of sites for H₂ dissociation and recombination ultimately leading to improved kinetics for H₂ sensing and detection applications. A novel means to create nano-sized particles is the use of a Spontaneous Galvanic Displacement Reaction (SGDR).^{69,70} Applications of SGDR strategies include the preparation of nano-needle covered palladium silver nanotubes,¹¹⁸ synthesis of hollow silver/palladium nanoparticles,¹¹⁹ palladium composite nanoboxes¹²⁸ and most recently as a method for functionalizing microcantilever (MC) sensing devices.¹⁷ The SGDR processing of nano-porous palladium (np-Pd) MCs offers fast, reversible, and sensitive response to H₂ with immunity to common interfering agents including CO and hydrogen sulfide (H₂S). The np-Pd MCs used for hydrogen sensing fashioned by SGDR show a unique relationship with oxygen in terms of response kinetics and selectivity,¹⁷ which will be elaborated upon herein.

The current work focuses on the following:

- Creating a better understanding of np-Pd particle interactions with H₂ and O₂ in terms of the effect of nanoscale grain structure on the reversibility, reaction rate and volumetric effects in the case of Pd-H₂ and Pd-O₂ systems.

- Expand on the details comparing response and recovery of np-Pd MCs upon exposure to H₂ in O₂ and O₂ free sampling environments. These studies will augment the differences that were briefly presented in Chapter 1.
- Addressing chemical and morphological effects on observed nanomechanical responses of np-Pd MCs.
- Exploring details of the SGDR processing conditions to better understand this pathway for nanostructuring. These include what processing conditions favor oxide formation, hence rapid H₂ interactions, and immunity to poisoning agents?
- Using MC nanomechanics as a unique diagnostic tool in parallel with more conventional characterization techniques.

Nanomechanical response profiles of np-Pd MCs are combined with Raman spectroscopy to study the chemical effects associated with exposure to oxygen. A signal response/recovery profile is presented which supports these observations. Morphological influences are then addressed with respect to processing conditions. Comparisons between np-Pd MC response profiles to H₂ and Pd-film composition using Inductively Coupled Plasma-Optical Emission Spectroscopy (ICP-OES) are discussed as well as the influence of oxide and nearly complete immunity to poisoning agents such as CO and H₂S. X-ray Diffraction (XRD), High Resolution Scanning Electron Microscopy (HRSEM) and visual appearance of color changes associated with surface exposure to H₂ are then presented. This exercise, along with MC response profiles to H₂, reveals the surprising necessity of the presence of palladium precipitate during SGDR processing in order to create desirable films. These studies offer insight regarding mechanistic pathways involved in the np-Pd material

created using SGDR and the influence of chemical and morphological effects on this system's ultimate interactions with H₂. MEMs sensing devices, specifically MCs, as a diagnostic tool are coupled with more traditional characterization methods to provide insights for work in H₂ catalysis, storage and improved detection applications, and may provide an impetus to expand SGDR strategies to other sensing platforms.

3.2 EXPERIMENTAL SECTION

3.2.1 Surface Preparation

SGDR preparation as an active surface on MCs has been described previously.¹⁷ Briefly, MC chips (Mikro-Masch) are delivered in 16 silicon lever arrays of the following dimensions - 400µm long, 100µm wide and 1µm thick. Chips are used as received. The MCs are coated by vapor deposition using a Cooke Vacuum Products Inc. physical vapor deposition (PVD) chamber with the following metal composite; an adhesion layer composed of 5-10 nm of chromium (Kurt J. Lesker), 40 nm gold (Gatewest Co.) barrier layer and 20 nm sacrificial silver (Ag 99.999% Alfa Aesar, MA) layer. Thickness of each metal layer are monitored using a quartz-crystal microbalance (QCM) positioned adjacent to the substrate. The chips are exposed for periods of up to 17 hours to a saturated warm PdCl₂ (Strem Chemicals) solution prepared in deionized water (Barnstead E-pure water filtration system). Palladium spontaneously displaces silver through a galvanic displacement reaction creating a porous palladium surface. Silicon slides (Wafer World) were processed in identical fashion to accommodate characterization techniques, which include Raman Spectroscopy, ICP-OES, HRSEM and XRD.

3.2.2 Instrumental

Microcantilever Analysis: MC testing was conducted at both Oak Ridge National Laboratory (ORNL) and the University of Tennessee Knoxville (UTK). The np-Pd MCs were placed in a low-volume flow cell (~150 μ l) and mounted at the end of a laser rail system housing a 632.8 nm red laser that was aligned on the tip of a single lever. An On-Trak Position Sensitive Detector (PSD) was calibrated to convert signal response (V) to tip displacement (μ m). Gases used in this study were obtained from Airgas Inc., or Air Liquid Inc. A Vici Instruments 6-port stainless steel flow injector was used to provide discrete H₂ injections through a 10.0 mL stainless steel flow loop (unless noted otherwise). A split “T” was used to introduce a constant flow of H₂ into the stream of carrier gas for steady state experiments. In this arrangement samples of H₂ were introduced by diluting 4% H₂ /96% Ar with carrier gas at a fraction of the total combined flow, optimal flow rate ~ 6 mL/min. Background gases were used prior to all experiments showing no artifact related to pressure drops through the “T”. Additional details regarding system optimization may be found in a prior report.¹⁷

In-situ Raman Testing: Raman testing was conducted on slides processed identically to MCs. Slides were placed in a low volume flow cell used for MC testing. The cell was secured to a JY-Horiba Labram Raman Spectrometer stage to allow spectra to be collected before and after gas phase cycling, mimicking the environment and conditions used for testing np-Pd MCs responses to H₂ gas. Carrier gas was composed of either Ar or N₂ (unless otherwise specified). Cycled O₂ or H₂ gases were delivered via Princeton Instruments Syringe Pump using a 60.0 mL syringe. The Raman Spectrometer uses an Olympus BX-40 microscope with a 50x (0.25 NA) objective that delivers up to 8.9 mW of the 632.8 nm radiation from an

electrically cooled He-Ne laser. The confocal hole and slit of the instrument were opened to 500 and 200 μm respectively. All spectra were acquired in 180° scattering geometry with a 2936 cm^{-1} spectral window. The scattered light was dispersed with a $600\text{ groove mm}^{-1}$ grating, imaged with a 1024×256 thermoelectrically cooled charge-coupled device camera, and processed with Labspec 4.03 software. A computer-controlled x-y-z stage facilitated focusing of the microscope objective and the positioning of the laser spot on the sample.

Inductively Coupled Plasma-Optical Emission Spectroscopy: ICP-OES was carried out using a Perkin Elmer ICP-OES Optima 2100DV, delivering 1500 Watts power, at a frequency of 40.68 MHz. The following parameters were used for the argon source; nebulizer flow 0.60 L/min, plasma flow 15 L/min, auxiliary flow 0.2 L/min at a pump rate of 2.0 mL/min. Data was collected using WinLab 32 software. Silicon slides were processed as described for np-Pd unless otherwise noted. Following SGDR preparation, slides were digested in 4 mL of an aqua-regia (AR) solution [(3)HCl:(1) HNO₃]. All samples were then diluted to a final volume of 10.0 mL using deionized water. Blanks composed of the diluted AR were run for background subtraction. Responses for silver and palladium using the 328.068 nm and 340.458 nm emission lines, respectively, are reported as signal intensity per slide area (mm^2).

High Resolution Scanning Electron Microscopy: A Zeiss Merlin VP SEM/STEM was used for high resolution sample imaging. Samples were mounted on aluminum stubs secured using adhesive carbon tape. Accelerating voltages used for individual SEM images are mentioned later but fall in the range of 1.0 to 15.0 kV.

X-Ray Diffraction Spectroscopy: XRD analysis was carried out in goniometer mode employing an Empyrean Panalytical X-Ray powder diffractometer. The anode material was composed of Cu K α with an excitation source wavelength of 0.15444 nm for surface characterization. Reference to ICDD PDF2/4 was used for peak identification using X'Pert High Score software.

3.3 RESULTS AND DISCUSSION

3.3.1 Chemical Effects: Oxide

The np-Pd MCs and slides were prepared according to the steps depicted in Figure 3.1, only four layers are shown for clarity. Chromium is used as an adhesive layer, followed by a gold barrier layer and finally a sacrificial silver surface is employed for the galvanic displacement with palladium ions. Details regarding galvanic displacement processes can be found in review discussions.^{69,70} The porous nature of the surface created by the SGDR processing is shown with a HRSEM (accelerating voltage of 3.00 kV) of a np-Pd MC that has been successfully used for H₂ sensing for over 2 years (Figure 3.1 e). Our earlier studies (Chapter 2) recognized the presence of O₂ was required to promote rapid nanomechanical response and recovery for H₂ detection; hence further testing was conducted to evaluate more thoroughly the critical role of O₂.

The use of Raman spectroscopy on silicon slides prepared under the same conditions used for np-Pd MCs showed a band assigned to PdO (650cm⁻¹).¹³⁰⁻¹³² To evaluate the effect of O₂ on this system, the PdO (650cm⁻¹) Raman band was monitored during gas phase

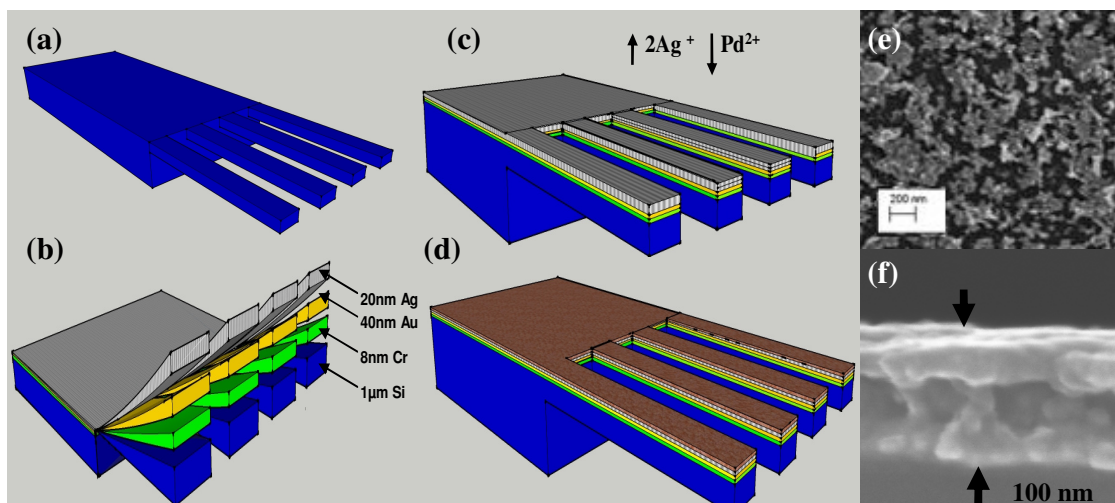


Figure 3.1 Processing of np-Pd MCs using an SGDR strategy. (a) Silicon MC chip is used as received, (b) deposition of supporting metal composite, (c) galvanic displacement of Ag with deposition of Pd, and (d) resulting nano-porous palladium active MC surface. HRSEM of (e) active np-Pd MC surface and (f) cross-section of silicon slide processed identically.

cycling between O₂ and H₂. A 150 μL flow cell used for MC studies was mounted on the Raman Labram spectrometer stage. The gases flowed through the cell using the same order and time intervals as that used for np-Pd MC measurements. Nanomechanical response profiles to H₂ were collected identically following gas cycling.

Prior to any exposure to non-ambient gases Raman spectra were collected showing a very weak band for PdO (Figure 3.2a). Response (MC tip displacement) rate of np-Pd MCs to 0.3% H₂ that have been only exposed to room air were less than 0.02 μm/sec (Figure 3.2a). Under this initial condition the only source of O₂ is that which exists in room air. A one hour continual O₂ conditioning exposure results in growth of Raman PdO band as the rate of tip deflection to steady-state response to 0.3% H₂ increased by a factor of 20 (Figure 3.2b). A one hour continual exposure to 0.3% H₂, mimicking long term effects, resulted in diminished PdO peak with reduction in the rate of MC tip displacement upon steady-state response to 0.3% H₂ following this simulated long term use (Figure 3.2c). Conditioning in a continual O₂ flow for one hour resulted once again in the growth of PdO band accompanied by a faster rate of MC tip deflection upon steady-state response to 0.3% H₂ (Figure 3.2d). Prior reports on np-Pd MCs¹⁷ used brief O₂ purges (~5 minutes) to encourage rapid response and recovery. However, the current study has evaluated more closely the effects of O₂ conditioning, and has adopted an initial one hour O₂ conditioning protocol based upon the findings established by the Raman/nanomechanics experiment. This protocol has furnished a sensing platform with more predictable behavior, optimizing response and recovery while

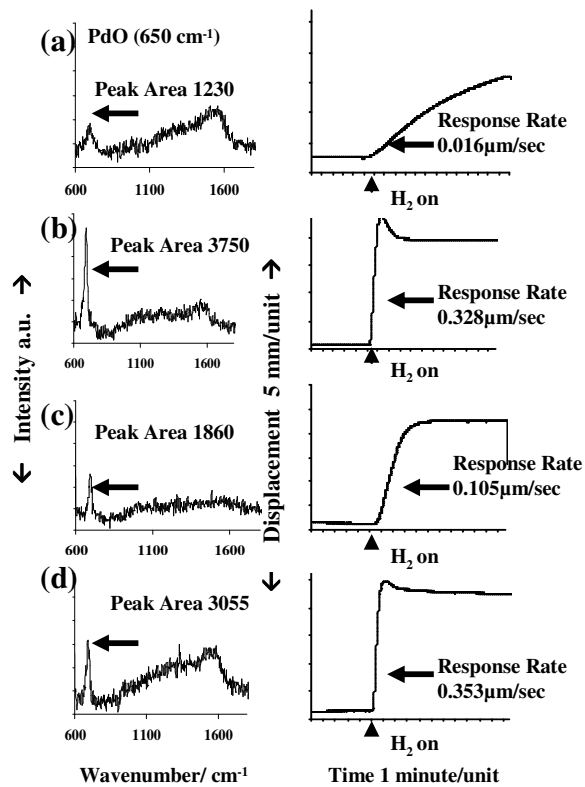


Figure 3.2 Progression of PdO band (left) and corresponding nanomechanical responses (right): **(a)** following preparation and storage in air, **(b)** after exposure to O₂ for 60 minutes, **(c)** after exposure to 0.3% H₂ in N₂ for 60 minutes, **(d)** after exposure to O₂ for 60 minutes. The responses correspond to steady state exposure of 0.3 % H₂ in N₂.

maintaining good sensitivity. Our studies have shown that environments with a constant source of O₂ (such as dry air) have provided good long-term performance characteristics.¹⁷ An advantage of independent multi-lever arrays would be to maintain active channels, quality control channels and conditioning channels thus permitting continual real time sensing. The independent nature required for each channel would fit a lab-on chip design, which is an active area of research. For the remainder of this report all MC responses are for np-Pd MCs processed using SGDR conditioned initially with O₂ for one hour unless otherwise stated.

The following exercise can be evaluated more closely considering the steps involved on a nano-scale. Figure 3.3 shows a representation of a single palladium nano- particle in the oxidized state and lists several events occurring in this environment. The sticking co-efficient of H₂ on palladium surfaces is greater than any other transition metal,⁴⁶ hence delivery of H₂ to the palladium surface should produce a favorable adsorption equilibrium. Because of the diminutive nature of the sampling environment (tubing, flow-cell, etc.) and fast wash-out, mass transfer of H₂ to the palladium film should not be an issue. Conversely, diffusion of dissociated hydrogen has been an area of debate concerning kinetic limitations of hydrogen/palladium systems.^{64,65,132,133} Reduction in the thickness of palladium films, membranes, and ultimately nano-particles have provided a path for hydrogen travel to test the limits imposed by a diffusive mechanism.^{17,109,110}

The Einstein expression (equation 3.1) for displacement (x) of a diffuser considers the movement of this diffuser from its initial position, as a function of time (t) and the relationship to the diffusion coefficient (D).⁵⁵

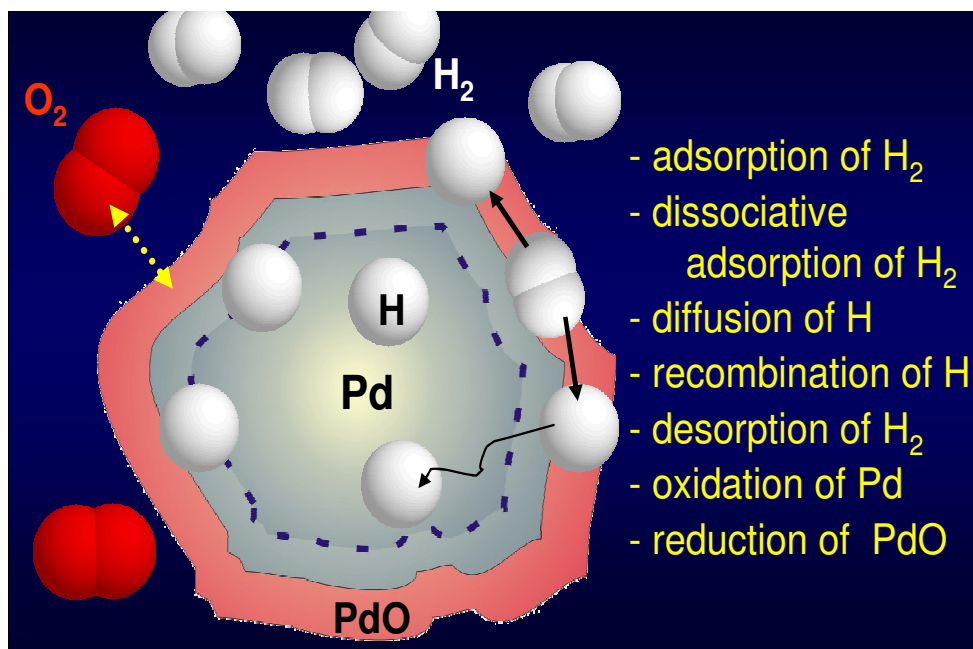


Figure 3.3 Depiction of Pd nanoparticle showing oxide layer and H₂/O₂ interaction processes.

$$x = \sqrt{2Dt} \quad (3.1)$$

A time factor for our thin Pd film system may then be calculated. A cross-sectional HRSEM (accelerating voltage 15.0 kV) shows that the thickness of the np-Pd is approximately 100 nm (Figure 3.1 f). Evaluating equation 1 with a diffusion coefficient (D) of 10^{-7} cm²/s, and displacement (x) 100 nm, would result in a time factor of less than 1 millisecond. Moreover, since the films are porous this treatment probably overestimates the time. The responses to H₂ of np-Pd MCs are typically measured on a second time scale so diffusion limitations to rates of tip deflection may be ruled out.

The rate of H₂ dissociation has also been reported to influence the kinetics of palladium/hydrogen based systems.^{109,110} However, the presence of oxide has been thought to accelerate dissociation of H₂.^{50,134} These prior studies and our experiments infer a signal response mechanism as listed in Figure 3.4(a) step I. The presence of oxide enhances hydrogen dissociation with rapid hydride induced swelling. As described above and depicted in Figure 3.2 nanomechanical response kinetics are improved upon conditioning in O₂ and influenced by formation of PdO

Recovery (removal of the hydride) is another issue which may be influenced by PdO. Figure 3.4(a) step III lists a recovery mechanism which is supported in the current study. A second MC test was conducted to evaluate the effect of O₂ on response and recovery of the np-Pd system in the conditioned state. Figure 3.4(b) shows duplicate np-Pd MC responses to discretely injected doses of 1% H₂. In an O₂ free (Ar only) environment recovery time (time

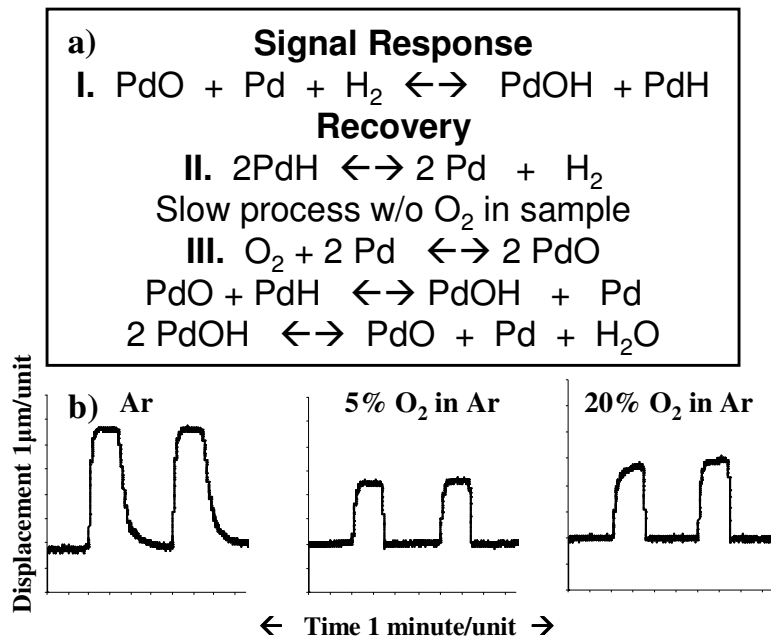
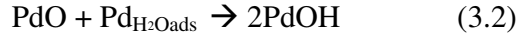


Figure 3.4 Effect of O_2 . (a) Proposed mechanistic scheme for chemical response and recovery. (b) Recovery of np-Pd in conditioned state to 1% H_2 with increasing O_2 in sensing environment

to recover to 10% maximum steady state deflection) is ~30 seconds. Adding a small concentration of O₂ (5%) in the Ar carrier gas the recovery time is ~7 seconds. By increasing O₂ (20%) in the Ar carrier gas improved recovery is recognized (~ 5 seconds). The recovery mechanism listed in Figure 3.4 (a) step II first considers a process in the absence of O₂, in this scenario recovery depends on hydrogen recombination. Introducing O₂ into the environment results in faster recovery as shown in Figure 3.4(a) recovery step III. A reasonable explanation for fast recovery of np-Pd MCs is due to removal of H₂ in the presence of PdO resulting in H₂O formation. This behavior has been supported by other studies^{55,59,100,135-138} which have reported that hydrogen desorption from palladium systems are augmented by O₂, with a resultant release of water vapor. Specifically, NMR studies conducted by Brady et. al.¹³⁹ of nanocrystalline palladium undergoing H₂/O₂ cycling support a mechanism involving H₂O formation and subsequent release. Additionally, Grasjo et. al.¹⁰⁹ claim that the steady state desorption rate of hydrogen recombination in vacuum is ten times less compared to steady state desorption rates measured in air. The difference in desorption rates attributed by Grasjo are due to combination of adsorbed hydrogen with oxygen in air and rapid release of H₂O vapor.

The response/recovery mechanism listed in Figure 3.4 showing H₂O as a final product also may be substantiated by equilibrium arguments. Considering Le-Châteliers principle the final step of recovery would not be favored if H₂O vapor is present. Our nanomechanical np-Pd MC testing of interfering agents has shown that water vapor does inhibit response and recovery. Experimental observations have included temporary slow responses with poor recovery. Considering the initial slow responses of Figure 3.2 it is possible that surface water vapor may be a source of contamination. A study conducted by

Nyberg et al¹⁴⁰ on palladium based systems and the dynamics involving H₂, O₂ and H₂O suggest that when PdO is exposed to adsorbed water vapor (Pd_{H₂Oads}) the oxide is converted to PdOH by equation (3.2).



In this case no oxide is available to assist in H₂ dissociation as pre-adsorbed oxygen is consumed, inhibiting Step I in Signal Response mechanism (Figure 3.4 a). The findings presented by Nyberg and the results of the current study suggest that H₂O contamination may inhibit PdO's ability to dissociate H₂.

3.3.2 Morphological Effects: SGDR Bath Composition and Processing Time

Nano-structuring using SGDR has been explored to increase the surface area of palladium, by introducing a dispersion of Pd nanoparticles in a silver matrix. The larger surface area combined with a one hour O₂ conditioning protocol results in a rapid oxide assisted H₂ response/recovery interaction with palladium. Two important processing parameters in creating np-Pd films include SGDR bath composition and bath exposure time. Considering that the SGDR medium is composed of sparingly soluble PdCl₂ it was anticipated that by filtering this suspension a more homogeneous film with improved adhesion could be attained. Hence a comparative study of filtered vs non-filtered SGDR bath processing conditions was conducted. Nanomechanical response to H₂ was compared with ICP-OES of remaining silver layer and active palladium layer on samples processed for 17 hours in an SGDR bath. The two conditions tested included sample set N-F (non-filtered) and sample set F (filtered). Sample N-F was exposed to the SGDR bath as prepared as set F was

exposed to a bath that had been passed through a 45 μ m mesh syringe filter prior to SGDR. In Figure 3.5(a-top) good nano-mechanical responses to H₂ are observed for processing without filtering, whereas poor responses are accompanied by filtering the SGDR bath. Figure 3.5(a-bottom) shows that silver is consumed by a greater extent, with formation of a greater amount palladium for non filtered.

A possible explanation for the important role of PdCl₂ precipitate is that Pd²⁺ is the limiting reagent in the SGDR, hence; the precipitate served the purpose of supplying a continual source of Pd²⁺ to exchange with Ag(s). To test this hypothesis the maximum number of moles of exchange species, i.e. silver versus palladium available for SGDR was determined. The processing conditions for np-Pd MCs would provide $\sim 2.5 \times 10^{-8}$ moles(Figure 3.6a) of silver (density $\sim 10\text{g/cm}^3$) available for exchange with palladium. ICP-OES was conducted to quantify the palladium available for SGDR processing. A series of palladium standards were generated and measurement of the intensity of the palladium 340.458 nm line was used to create a calibration plot (Figure 3.6b). An SGDR sample was prepared following the procedures used for np-Pd MC processing, an aliquot of this sample was tested using ICP-OES. The intensity of the 340.458nm palladium line for this SGDR aliquot was treated using the regression formula of the calibration plot. The results from this exercise show that $\sim 5.5 \times 10^{-5}$ moles of palladium are available for SGDR. Based upon these findings it appears that Pd²⁺ is not the limiting reagent. Therefore the presence of palladium precipitate does not serve the purpose of supplying a source of a limiting reagent. However, this study is based upon the bulk SGDR bath and may not reflect the situation within the nanopores of the developing palladium film. The continual consumption of silver

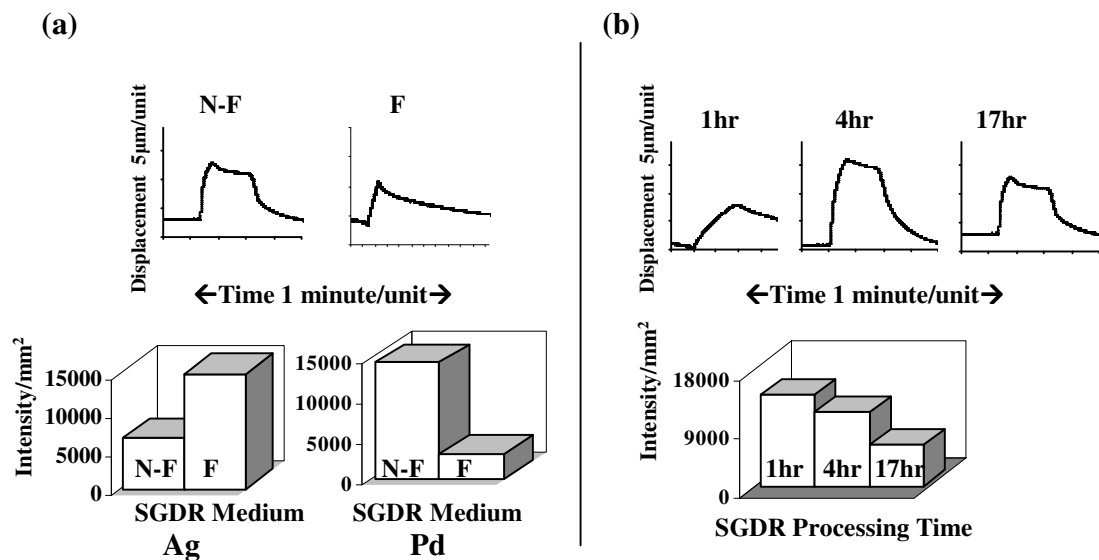


Figure 3.5 (a) Effects of filtering the SGDR Bath; (top) Responses of np-Pd MC to 4% H₂ and (bottom) ICP-OES of silver non-reacted and palladium formation for filtered (F) and non-filtered (N-F) cases. (b) Effects of processing time; (top) Responses of np-Pd MC to 4% H₂ and (bottom) ICP-OES non-reacted silver for these conditions.

a) Data

Silver data (MC)	Silver data (max slide)
Area 13mm ²	Area 90mm ²
Volume = 2.7x 10 ⁻⁷ cm ³	Volume= 1.8x10 ⁻⁶ cm ³
Mass silver= 2.7x10 ⁻⁶ g	Mass silver=1.8x10 ⁻⁵ g
Moles silver=2.5x10 ⁻⁸	Moles silver= 1.7x10 ⁻⁷
Ag/Pd (%) = 0.025	Ag/Pd (%) = 0.15

b) ICP-OES Calibration

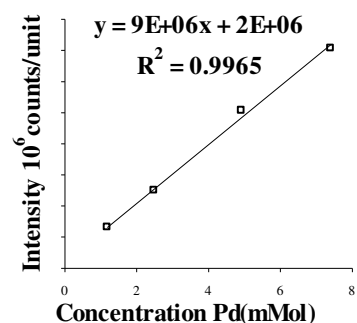


Figure 3.6 (a) Sacrificial silver data for MC chips and maximum size slide used for comparative characterization (b) Regression data of palladium standards used for measuring palladium solubility in SGDR bath.

for periods of time up to 17 hours suggests chloride precipitates in the local environment (pores etc.) may inhibit access to the Ag surface and reaction (SGDR processing) time.

Additional studies of SGDR processing were conducted to evaluate the effects of bath temperature with respect to PdCl₂ solubility. These studies showed that np-Pd MCs that were processed in a warm SGDR bath (~60°C, inhibited PdCl₂ solubility) experience better nano-mechanical response characteristics to H₂ compared to MCs that were processed in SGDR baths that were processed at lower temperatures (~5°C, enhanced PdCl₂ solubility). Based on thermodynamic data¹⁴¹ the spontaneity of the SGDR process is favored at elevated temperatures, which appears to dominate the reduction in solubility. Conditions which favor the presence of precipitate ie non-filtered and elevated temperatures encourage superior nano-mechanical response of np-Pd MCs to H₂. However, the temperature effect may also serve the role of hastening the SGDR rate as the spontaneity of the displacement reaction of palladium for silver is more thermodynamically favorable at the higher temperature.

The SGDR processing time interval is another important parameter. The processing time intervals for silicon slides and MCs was tested by comparing 1 hour, 4 hour and 17 hour (overnight) to a non-filtered SGDR bath. Figure 3.5b (top-bottom) shows nano-mechanical responses to 4% H₂ in the conditioned state and ICP-OES results for unreacted silver on similarly processed slides for the same time intervals, respectively. A 1 hour processing shows poor nano-mechanical response and recovery to H₂, accompanied by minimal silver consumption. After 4 hours processing the response magnitude to H₂ increases as kinetics improve along with an increase in silver consumption. After 17 hours of processing the response magnitude to H₂ decreases slightly but response kinetics improve by nearly 40% compared to the 4 hour interval, with further silver consumption. This experiment conveys

the expected necessity of silver consumption during the SGDR process to create a nano-structured palladium film. HRSEM (accelerating voltage 4.50 kV) of films created for 1hr and 17hr SGDR processing are shown in Figure 3.7(a-b), respectively. A 1 hour SGDR processing results in two-dimensional films, nearly void of any pore formation. np-Pd films undergoing 17 hours SGDR processing results in a more porous, three-dimensional film. The sponge-like nature of these films is expected to provide a greater surface area and a more extensive grain boundary.

The effects emphasized in the proposed mechanism (Figure 3.4a) are oxide assisted response/recovery and nanomechanical signal response due to swelling upon hydrogen absorption. This increased surface area supports a greater oxide contribution from the conditioning step, resulting in rapid response and recovery to H₂. The extended grain boundary created by nano-structuring also plays a vital role by improving hydrogen solubility in nano-sized palladium particles as discussed by Eastman et. al.¹³⁴ As silver is consumed extensive nano-structuring of the palladium continues giving rise to greater surface area.

The reduction in response magnitude to H₂ for the 17 hour processing relative to 4 hours Figure 3.5b (top) interval is additional evidence of the increasing contribution of an oxide surface due to an O₂ conditioned np-Pd film. This effect can be understood by considering the reduction in response magnitudes to H₂ presented in Figure 3.4b which compares nanomechanical response of 1% H₂ on the same np-Pd MC in O₂ free environment with environments richer in O₂. Similar observations of reduced response magnitude and accelerated recovery for resistive hydrogen sensing devices have been made by Yang et al⁵⁵. Yang claims that the presence of O₂ provides a new channel for removal of chemisorbed hydrogen. Our hypothesis based upon experimental observations considers that

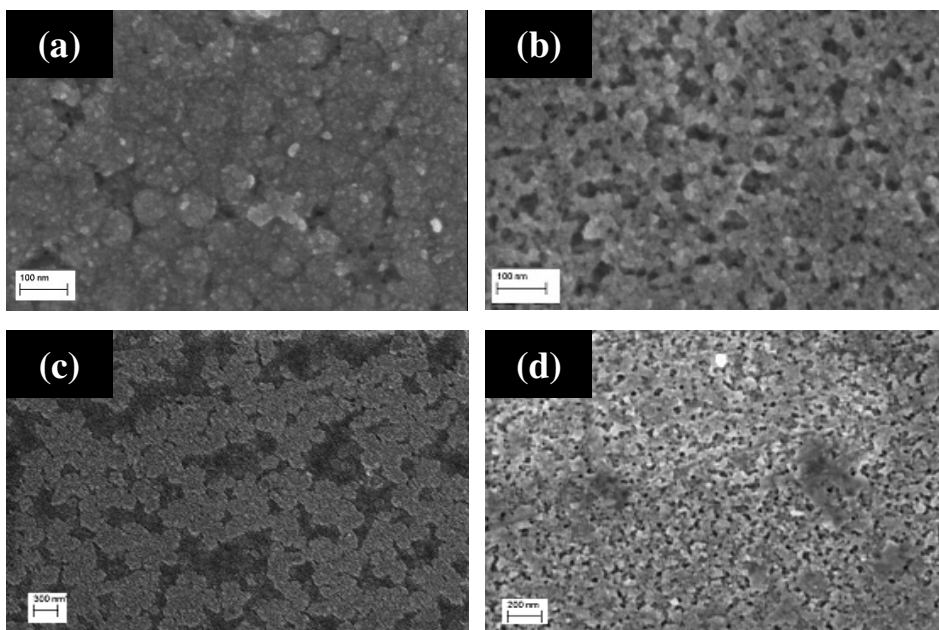


Figure 3.7 Nano-structure comparison of np-Pd films; comparing 1 hour (a) to 17 hours (b) SGDR and filtered (c) to non-filtered (d) SGDR baths.

the greater amount of surface oxide may reduce surface vacancies available for hydrogen sorption resulting in reduced response magnitude. Additionally, the increased availability of oxide promotes hydroxide formation competing with hydride formation (Figure 3.4 a Step III) for surface dissociated hydrogen. Therefore, our results suggest that in O₂ abundant environments there are both a reduction in surface vacancies available for palladium hydride formation plus a more efficient recovery path resulting in signal reduction accompanied by rapid recovery. The O₂ conditioning protocol has been tailored to minimize the effects on response magnitude reduction for sensing applications (sub 100ppm), while playing a key role in improving the kinetics and reducing the effects of surface contamination. Optimizing the steps involved in both processing and conditioning can be used for tailoring this material for desired application such as rapid response and recovery or greater sensitivity.

3.3.3 Effects of O₂ and H₂

Np-Pd films are influenced by the presence of O₂ and H₂ both chemically and morphologically. The kinetic effects in relationship to PdO have been discussed above, revealing a somewhat surprising requirement for the presence of precipitate for stable and rapid response and recovery to H₂ of np-Pd MCs. Additional Raman studies were conducted on films prepared with and without a PdCl₂ precipitate present yielding a strong oxide band at 650cm⁻¹ for the former but not the latter. This reinforces the requirement of PdO for optimal nanomechanical responses as depicted in Figure 3.5a (N-F). HRSEM images (accelerating voltages of 1.0 kV and 3.0 kV respectively) Figure 3.7(c-d) have been collected

comparing processed films in SGDR baths that are filtered versus non-filtered. Three-dimensional networks for non-filtered films show a greater extent of nano-structuring in comparison to the more two-dimensional appearance of the filtered case, quite comparable to the appearances of np-Pd films depicted in Figure 3.7(a-b).

Hydrogen also influences the appearance and chemical composition of np-Pd films. Surface appearance and XRD analysis Figure 3.8 was used qualitatively on slides processed in a warm non-filtered PdCl₂ bath for 17 hours. Prior to H₂ exposure the np-Pd slide surface appeared brown. XRD was then conducted on this slide secured in a sample holder which could be removed and replaced in an identical fashion within the confines of the instrument. XRD spectral results were fit to models using Panalytical X'Pert High Score Plus (PXHSP) and are consistent with the presence of PdCl₂ on the surface, with the most convincing feature assigned at a 2 Θ of 16.073°. The slide was then exposed 5 minutes to H₂, resulting in a darkened surface. The slide was placed identically in the sample holder used for pre-H₂ XRD analysis and spectra were collected again. The PXHSP results suggest that PdCl₂ was no longer present on the surface, with the models fitting most comparatively to palladium and palladium hydride, the features here are assigned to a 2 Θ of 40.107° and 38.126°, respectively. The color changes of np-Pd films after exposure to H₂ observed compare to reports describing darkened surfaces as those composed of metallic palladium.¹⁴² Processing of PdCl₂ in H₂ plasma has been reported by Koo et al¹⁴³ as a method to obtain palladium films. Indeed, XRD analysis conducted by Koo corroborates well with XRD collected in the current study.

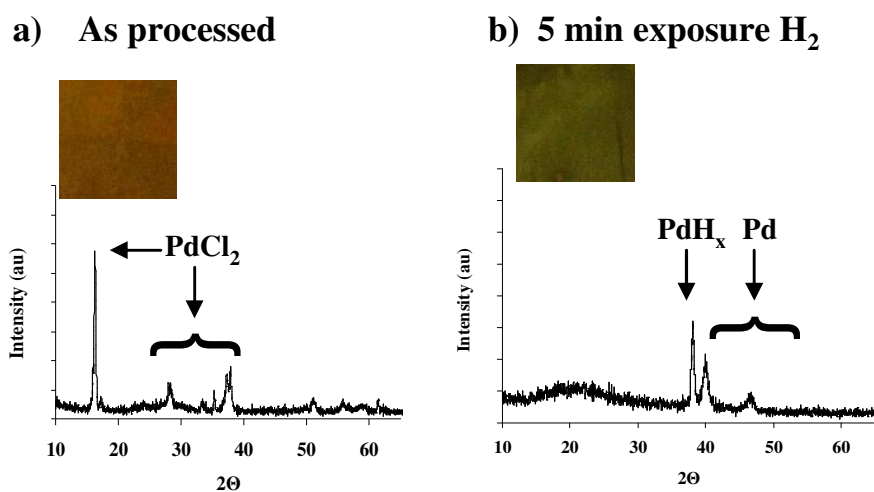


Figure 3.8 XRD of np-Pd surfaces (a) As processed (b) post 5 minute exposure to H₂. (Inset) Changes of surface color comparing surfaces “as-processed” and 5 minutes H₂ exposed.

The overall morphological influence appears to be related to changes in surface structure upon palladium reduction. Two processes influence the reduction of palladium and will be discussed chronologically. First surfaces composed of a sacrificial silver surface are exposed to a PdCl₂ bath undergoing SGDR resulting in a reduction of palladium ion in solution during exchange with silver. Palladium nanoparticles are created in the surface film, but in the non-filtered case there exists a precipitate composed of PdCl₂(s) throughout the film. In our earlier testing¹⁷ of np-Pd MCs during the conditioning procedure with O₂ periodic evaluation of H₂ response was collected and continual improvement in response/recovery kinetics were observed. The effect of H₂ during initial testing period appears to facilitate a second reduction process of palladium ion supplied by PdCl₂ precipitate. From ICP-OES studies it has been shown that not all of the sacrificial silver is consumed (Figure 3.5), therefore, it is possible that we have a morphologically complex system of palladium nanoparticles in the remaining silver layer (via SGDR reduction) intermixed with a surface of secondary palladium nanoparticles via PdCl₂ precipitate reduction in H₂. Conditioning in O₂ results in oxidation of the palladium giving a layer of PdO^{121,144,145} (see figure 3.3 depiction) that is important for rapid Pd-H₂ interaction. However it also appears that both sources of Pd nano-particles are beneficial, as the PdO layer assists in H₂ dissociation delivering free hydrogen to the sub-surface palladium particles via an extended grain boundary.

Finally, an important consequence of the O₂ conditioning protocol combined with nano-structuring is substantial immunity to poisoning agents such as CO and sulfur containing compounds. This additional advantage of np-Pd films again appears to be related

to a unique relationship with oxide formation. To evaluate the effects of interfering agents such as CO or H₂S on np-Pd MCs performance guidelines similar to those proposed by the National Renewable Energy Laboratory (NREL)^{146,147} were employed. Conditioned np-Pd MCs were secured in a low volume flow cell (~150 μ L) under a flow of O₂ at a flow rate of ~10 mL/min. Response profiles of these np-Pd MCs to 2 injections of 2% H₂ (1.0mL stainless steel flow loop) were obtained followed by 2 injections of 50 ppm H₂S in N₂ (Mesa Specialty Gases and Equipment) followed again by multiple injections of 2% H₂. Figure 3.9a shows that conditioned np-Pd MCs after 50 ppm H₂S exposure recover to nearly 85% initial response magnitude in ~ 7 minutes after H₂S exposure in an O₂ rich environment. Conversely, in environments lean in O₂ poor return to initial responsiveness is observed Figure 3.9b. These results suggest that O₂ may supply a surface oxide which hinders poisoning effects most commonly observed for palladium in the presence of compounds such as H₂S.

3.4 CONCLUSIONS

The foregoing studies have shown that np-Pd films used for H₂ responsive MC sensors show rapid response and recovery to H₂ under the influence of oxide formation. Nanomechanical responses are faster due to oxide assisted H₂ dissociation. Nanomechanical recovery is faster due to water formation and rapid release, which has been reported to be ten times faster than hydrogen recombination. The greater surface area

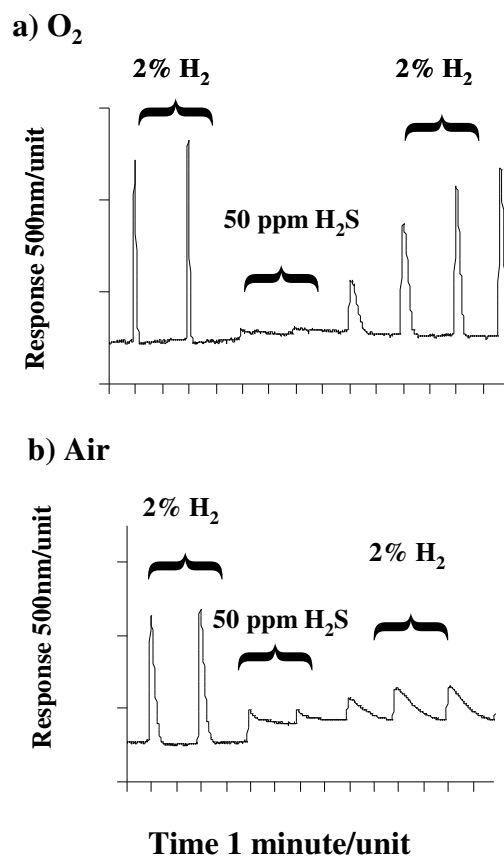


Figure 3.9 np-Pd MC nanomechanical response profiles showing immunity to H₂S with (a) no long term poisoning in O₂ versus (b) prolonged recovery in dry air.

of np-Pd provides a greater contribution of the PdO assisted effects for rapid response and recovery with minor loss in response magnitude. A morphological influence of this system is related to the presence of a PdCl₂ precipitate during SGDR surface preparation. The precipitate supports a greater contribution of surface oxide due to a larger surface area afforded by the presence of the precipitate. The precipitate itself undergoes a surface restructuring event in the presence of H₂. Our studies suggest that a segregated 3 dimensional matrix of palladium nano-particles are supported in a film of silver anchored via SGDR which may be protected by a shell of PdO due too conditioning in O₂ preceded by H₂ induced restructuring of precipitate. Besides encouraging rapid response and recovery of np-Pd MCs in response to H₂, PdO encourages immunity to poisoning agents such as CO and sulfur containing compounds.

CHAPTER4: EXPLORING NANOLAMINATE COMPOSITES AS MATERIALS FOR MICROCANTILEVER DESIGN

4.1 INTRODUCTION

A thorough discussion of microcantilever (MC) sensing devices has been presented in Chapter 1. The focus of this chapter addresses the requirements for MCs as a sensing platform; including advantages, limitations, and improvements through materials design and processing. A novel Nano-Laminate Composite (NLC) material has been developed to address these issues and will be discussed.

Micro-cantilevers as transducers for chemical, physical and biological sensing offer distinct advantages over other mass sensitive transducers such as the Surface Acoustic Wave and the Quartz Crystal Microbalance. The diminutive size of the MC offers excellent sensitivity and the possibility of external deployment providing the analyst with real-time information.¹⁸ MCs may also be operated in an arrayed fashion introducing a unique selectivity to targeted analytes adding to their utility for remote applications.

However several obstacles inhibit performance, for instance the use of metalized surfaces which are commonly used in functionalization strategies such as the gold/thiol pathway.³¹ Metals are also used for nano structuring surfaces, two examples include dealloying²⁹ and spontaneous galvanic displacement reactions.^{16,17} Metals are also used for improved reflectivity.¹⁴⁸ A major drawback of metallization is thermal drift, due to mismatch of thermal expansion coefficients of the metal and the substrate (silicon or silicon nitride). This limitation is a consequence of both laser probing and temperature fluctuations encountered under ambient testing conditions. Prolonged drift undermines the requirement of

fast turnover for real-time analysis. Other limitations include inefficient and poorly reproducible functionalization strategies, suffering from inadequate active surface adhesion leading to poor sensitivity.

Material design to mitigate the limitations discussed above is presented in the current study. A NLC material composed of alternating layers of SiN_x and SiO_2 has been tested for MC design and is shown to overcome some of the disadvantages encountered using metalized surfaces. The potential advantages of using a NLC material for MC design include:

- Maximum reflectance at the laser wavelength used.
- Better thermal stability in comparison to metalized surfaces.
- Asymmetric native structure offering more flexible surface functionalization strategies.
- A more elastic/sensitive cantilever beam in comparison to commercially available MCs.

The following report presents details of the processing and experimental conditions used to create and characterize NLC-MCs. Fabrication information will be limited due to confidentiality issues. This will be followed by a discussion of the advantages of these materials for sensing and detection. Applications of NLC-MCs will be presented, along with a summary of possible future directions.

4.2 EXPERIMENTAL

4.2.1 NLC-MC Processing

Fabrication of NLC-MCs has been conducted at Oak Ridge National Laboratories. (ORNL). Due to the confidential nature of this procedure limited details are presented. Figure 4.1 depicts a general process flow and SEM images involving MC fabrication. Briefly, the following steps are performed to fabricate NLC-MCs. First a structural silicon nitride layer followed by silicon dioxide layer is deposited on a silicon wafer with a pre-patterned sacrificial layer. This is followed by shaping of the cantilevers by patterning the silicon nitride film on the top surface using photolithography. A final potassium hydroxide etch removes the sacrificial layer resulting in MC release.

4.2.2 NLC-MC Testing

NLC-MCs were mounted at the end of a laser rail system secured in a low volume flow cell (~150 μ L). A 633 nm red laser, which will be used for all studies in this report unless otherwise noted, was focused on the tip of individual NLC-MCs. The laser spot was centered on an On-Trak Position Sensitive Detector (PSD), responses to specific analytes were collected and reported as electrical response (mV). Responses to analyte were conducted under a constant flow of N₂ for gas phase testing, or potassium phosphate buffered to pH 7 in aqueous phase experiments. Background was tested prior to data collection to account for any artifact introduced into the experimental protocol.

The measurement of fundamental resonance frequency has been conducted at the University of Tennessee using a Stanford Research Systems SRS 850 DSP Oscilloscope interfaced to the PSD. Chips were mounted on a laser rail system within flow cell, as

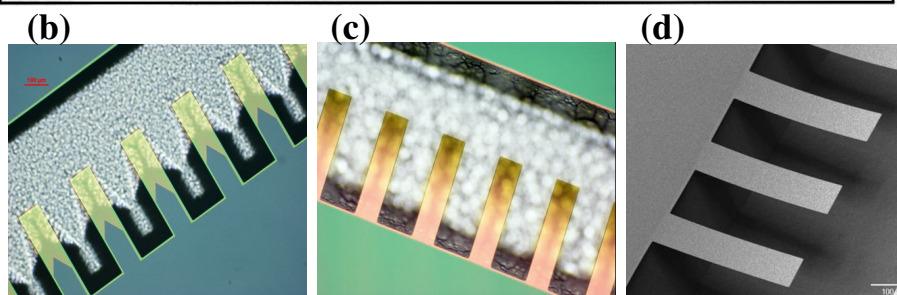
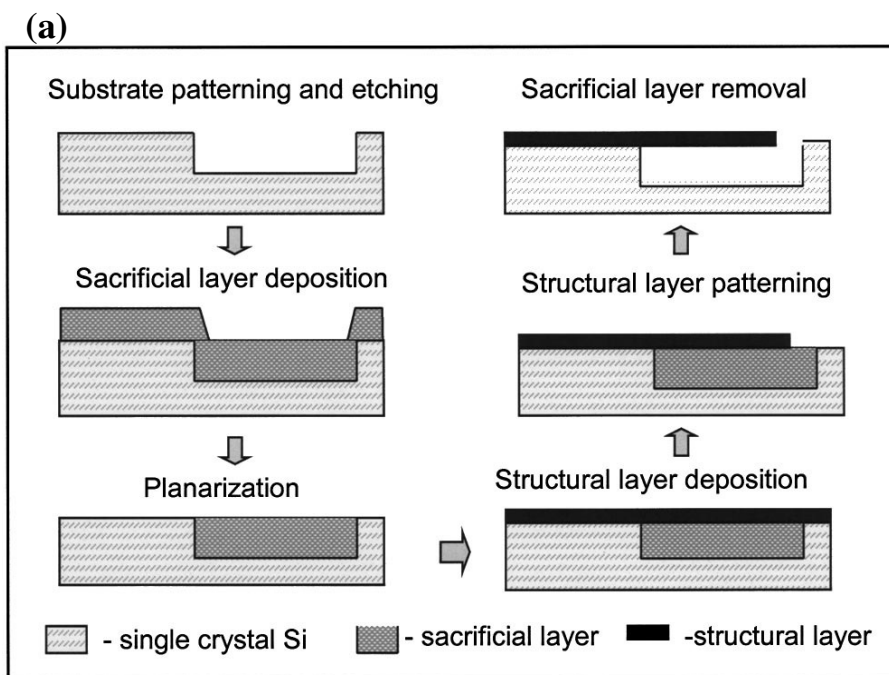


Figure 4.1. (a) Illustration of the steps in a process flow used for fabrication of silicon nitride, silicon dioxide micro-cantilevers. (b) Partially released MCs after 1 hour KOH etch. (c) Fully released MCs after 90 minute KOH etch. (d) SEM image of MCs as processed.

resonance frequency measurements are recorded under static conditions (no flow). Figures describing these instrumental features can be found in Chapter 1.

4.2.3 Instrumentation

X-ray photoelectron spectroscopy (ORNL)

Surface characterization was conducted using a Thermo Scientific K-Alpha X-Ray Photoelectron Spectrometer (XPS), equipped with a 180° double focusing hemispherical analyzer and a 128-channel detector. The X-ray source is an Al K- α micro-focused monochromator operating with a variable spot size (30-400 μ m in 5 μ m steps). The ion gun energy range is 100-4000eV, and is operated with a charge compensation dual beam source with an ultra-low energy electron beam. Sample handling is conducted with a 4 axis sample stage with a 60mm x 60mm sample area and a 20mm maximum sample thickness.

Fourier Transform Infra-Red Spectroscopy (UTK)

Fourier Transform Infra-Red (FT-IR) spectra were collected by performing specular reflectance with a Varian 4100 FT-IR spectrometer.

Contact Angle Measurements (UTK)

Contact angles were measured using a Rame-Hart NRL Contact Angle Goniometer (Model100).

4.3 RESULTS AND DISCUSSION

4.3.1 Characterization of NanoLaminate Composite Materials

Characterization was initially conducted to determine the chemical composition and physical attributes of the NLC material used in MC fabrication. X-ray photo-electron spectroscopy (XPS) was conducted on slides mimicking the top (SiN_x) and bottom (SiO_2) surfaces that would be created under the experimental conditions described previously. Figure 4.2 shows the XPS spectra collected depicting a nitrogen rich top surface and the nitrogen free bottom surface; notably oxygen is present on both surfaces likely due to room air exposure. The top surface (SiN_x) in comparison to the bottom surface (SiO_2) may be expected to experience different chemical and physical properties; hence experiments were initiated to explore these differences.

The contact angle measurement method is a common surface characterization technique used to evaluate wettability. The contact angle refers to the angle between the solid surface and the tangent line from a water droplet/solid surface interface. Surfaces with a small contact angle are more hydrophilic as water favorably disperses on the surface. Surfaces with larger contact angles are more hydrophobic as water retains a spherical droplet shape due to repulsive properties of this surface.¹⁴⁹

A comparative study of slides composed of 75nm SiN_x (top side surrogate) and 110nm SiO_2 (bottom side surrogate) deposited on silicon wafers were used for testing the affinity to H_2O of these surfaces using the contact angle measurement. As XPS results have shown (Figure 4.2) oxide exists on both top (SiN_x) and bottom (SiO_2) surfaces therefore etching

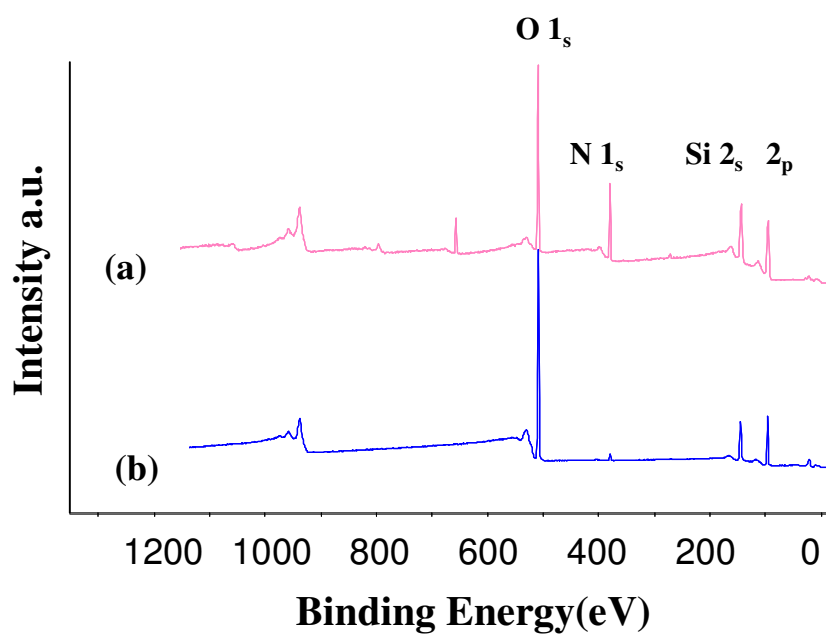


Figure 4.2. XPS survey spectrum of surfaces mimicking NLC-MCs. **(a)** SiN_x rich top surface. **(b)** SiO₂ rich bottom surface.

using a 5% hydrofluoric (HF) acid solution was conducted in conjunction with contact angle measurements. The time interval for etching along with contact angle measurements was recorded and is shown in Table 4.1. Initially the SiN_x surface shows a slightly more hydrophobic nature in comparison to SiO₂. This may be explained by a greater amount of surface silanol (SiOH) on the latter, resulting in a more hydrophilic surface. As samples are exposed to HF differences in the wettability of the surfaces become more pronounced. The SiN_x surface becomes more hydrophobic as the SiO₂ surface maintains a near constant contact angle (up to 1 minute). After 2 minutes the contact angle measured for both SiN_x and SiO₂ surfaces are nearly identical. A possible reason for this observation begins with a description of etching conditions made by Williams et al¹⁵⁰ reporting that 5% HF solutions preferentially etch silicon oxide, indeed SiN_x is typically used as an etch stop barrier in many processing applications. It is possible that the surface oxide, typically ~1nm,¹⁵¹ on the SiN_x is etched within 30 seconds resulting in a more hydrophobic surface (increased contact angle). The SiO₂ surface (110nm) may be etched completely by the 2 minute interval, exposing the hydrophobic support layer (silicon wafer).

NLC-MCs have been used as a characterization tool to evaluate the effects of etching these asymmetric surfaces. In this exercise NLC-MC response to HF vapor was collected. MC tip deflection resulting from the SiO₂ bottom surface being etched preferentially, compared to the top SiN_x, was anticipated. The NLC-MC was mounted in a low-volume flow cell and stabilized under N₂ flow. Headspace of buffered HF was introduced through a split “T” at a fraction of the total N₂ flow resulting in a series of HF exposures ranging from 2%HF-11%HF Figure 4.3 shows NLC-MC responses to HF at these various fractions. The positive deflection would suggest a tensile bottom side

Table 4.1 Effects of 5% HF etch and surface wettability of top (SiN_x) and bottom (SiO₂) NLC surfaces evaluated using contact angle measurements.

Etch Time (sec)	SiN_x Contact Angle(°)	SiO₂ Contact Angle(°)
0	48	37
30	61	37
60	67	41
120	67	70

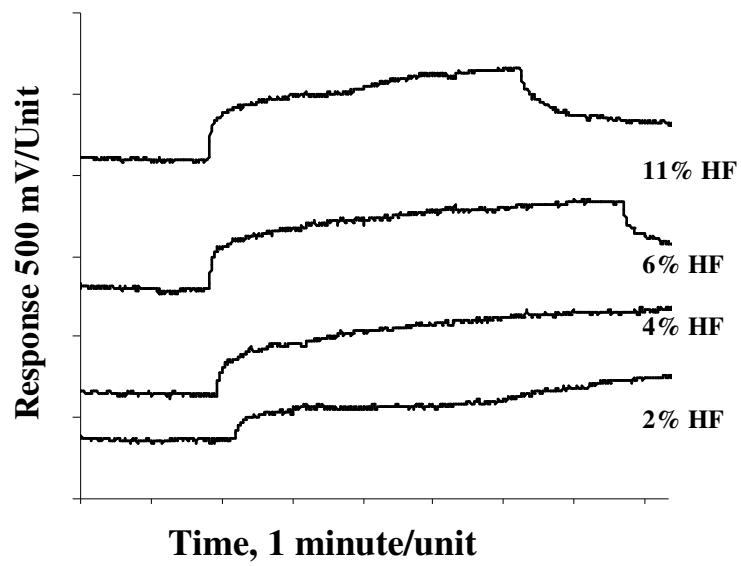


Figure 4.3. HF etch experiment demonstrating asymmetric nature of NLC-MCs via preferential HF etching of bottom SiO₂ surfaces.

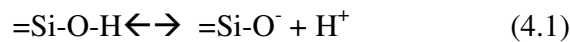
response; preferential etching (removal) of the bottom SiO₂ layer would support this observation.

The results of the NLC-MC diagnostic etching test are consistent with the measurements presented in the contact angle experiment. As hypothesized in the contact angle experiment, oxide may be present on the SiO₂ surface for nearly two minutes as the surface retains its hydrophilic nature, however after two minutes the silicon oxide may be consumed. The gas phase experiment (NLC-MC) suggests a more gradual loss of the thicker NLC-MC oxide (160nm), perhaps a consequence of an inefficient means of surface etching (gas phase), or may be due too a minute amount of HF in the fractions used from headspace testing. The asymmetric layering of these surfaces and the different chemical and physical attributes associated with these may be useful for analyte specific response of the native NLC-MCs.

A milder scenario to evaluate the differences in chemical composition is pH dependence. Surfaces composed of SiN_x and SiO₂ may experience different acidic and basic properties, hence it was hypothesized that MC deflection in response too changes in environmental pH may occur. Prior to testing brief etching in 5% HF solution was conducted to remove the effects of oxide on the SiN_x top surface. NLC-MCs were tested for pH response beginning with broad pH ranges, eventually the interval of pH 5 - 8 appeared to be optimal. The survey response information was used to design an experiment comparing native NLC-MCs deflection upon cycling between pH 5 - pH 8. NLC-MCs were secured in a low-volume flow cell and stabilized under a flow of pH 7 using a potassium phosphate

buffered solution. Results to cycling pH are shown in Figure 4.4 the following discussion outlines a possible explanation to the observed profiles.

The responses to pH for NLC-MCs may be due to a combination of effects which include interfacial surface stresses and charge related effects due to proton exchange with solvent. Upon increasing the pH (7 \rightarrow 8) surface SiOH is deprotonated, the deprotonation event may result in a surface experiencing negative charge as depicted below (4.1) (=Si represents a surface bound silicon).



Studies conducted by Dutta have outlined influences of surface charge effects and MC sensing environments. In this report¹⁵² details regarding the charge related effects of DA surfaces in comparison to smooth gold surfaces have been documented. DA surfaces experience a positive charge, whereas smooth gold surfaces experience a negative charge. Unmodified DA and smooth gold surfaces showed responses of opposite direction in terms of MC deflection upon exposure to metal ions in solution, attributed to the opposite charge state of the DA vs smooth gold surfaces. Indeed it has been described by Sepaniak et al¹⁹ that interfacial chemical reactions and modulation of electrical fields may serve to provide input for MC deflection. The SiN_x surface has less-well defined surface properties. It is possible that -NH groups present on the SiN_x surface may play a role in influencing the response of NLC-MCs under different pH environments tested in this study.

In summary these studies of characterizing surface asymmetry have shown that NLC-MCs in the native state respond (tip deflection) to variations in local environment. These responses may be initiated by either extreme conditions (etching) or milder cases such as pH

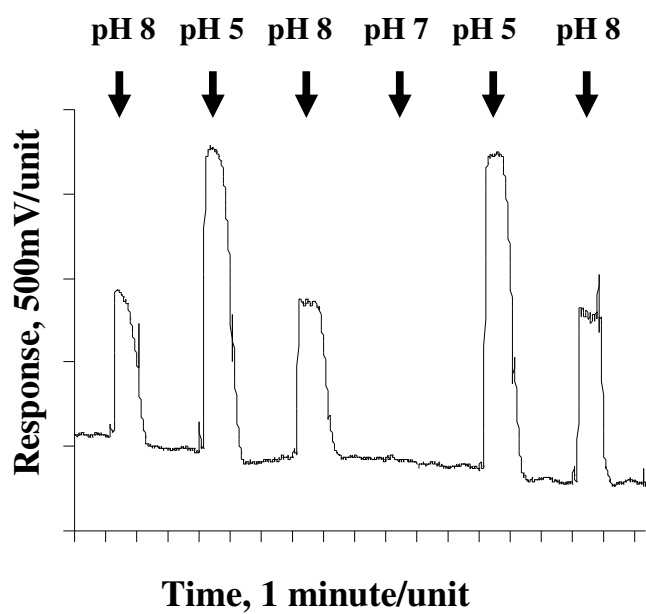


Figure 4.4. NLC-MC native state pH response.

control. The ability to induce response in the native state is an area which would require further testing to evaluate the full sensing potential of this unique situation.

An important parameter for characterizing MC performance is fundamental resonance frequency (f_0). Resonance is the tendency of a system, such as a suspended beam to oscillate at greater amplitude at certain frequencies. The f_0 of MCs can be used as a measurement tool in dynamic mode and as a quality assurance method for evaluating batch to batch reproducibility such as thickness and flexibility. Several batches of NLC-MCs have been characterized by measuring f_0 . The procedure was conducted by securing the NLC-MC within a flow cell and focusing a laser on the tip of individual levers. A Stanford Research System (SRS) 850 DSP Oscilloscope was interfaced to a PSD to convert the reflected signal to response. The average f_0 of NLC-MCs used in this study is ~ 5-6 kHz as shown in Figure 4.5. The f_0 of commercially available silicon MCs of the approximate same dimension are typically 9-10 kHz.

It is possible that the greater f_0 measured for silicon MCs are due to a more rigid structure perhaps due to material properties. Considering that the f_0 of free-standing devices is proportional to the square root of the Young's modulus (E)¹⁸ of a particular material a comparison can be made to describe the measured resonance frequencies. Silicon which is used for commercially available MCs has a reported E of 180 GPa.¹⁵³ NLC-MCs are composed of 80% SiO₂ ($E \sim 85$ GPa¹⁵³) and 20% SiN_x ($E \sim 290$ GPa¹⁵³). The overall greater thickness of SiO₂ may be the more influential factor for the reduction of f_0 observed for NLC-MCs in comparison to commercially available silicon MCs. The information gained by

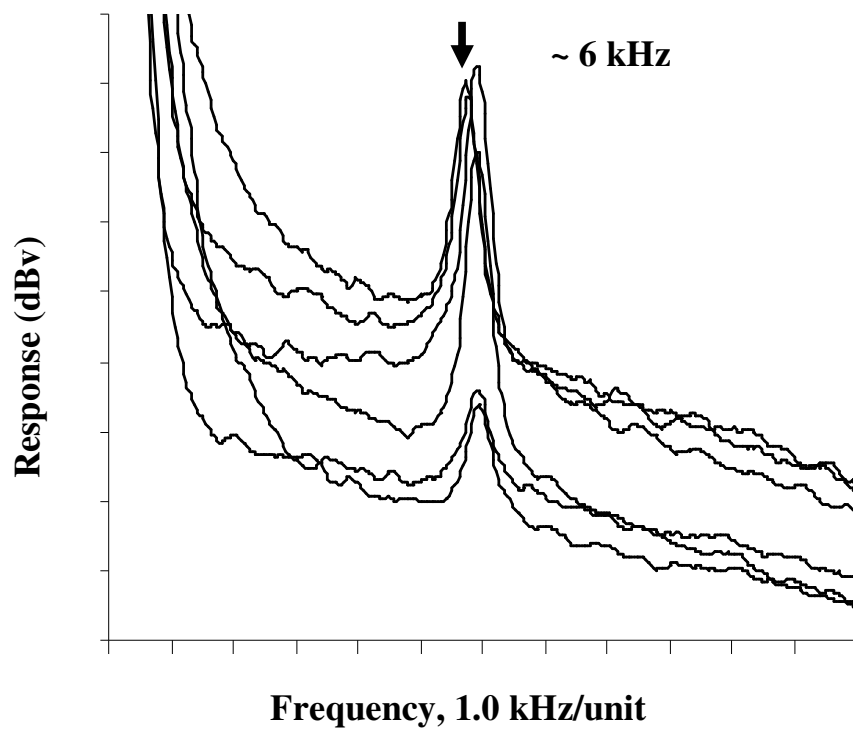


Figure 4.5. Resonance frequency profiles of NLC-MCs.

this exercise can be used for tailoring material properties such as thicknesses of individual layers for a desired application in terms of creating a more flexible MC device. It will be discussed later in this Chapter that tuning of layer thicknesses may also be advantageous for optimal reflectivity. Another possible reason for the differences in f_0 may be a consequence of processing. Slight differences in the thicknesses of silicon-MCs compared to NLC-MCs may be a result of the cantilever release step during the NLC-MC fabrication; ie., NLC-MCs may possibly be thinner in comparison to commercially available MCs. The lower f_0 of NLC-MCs suggest a more flexible beam which would yield a more sensitive nano mechanical sensing tool using the static mode of detection.

4.3.2 Advantages of Nano Laminate Composite MCs

Advantages of the NLC material presented in this study that will be illustrated include superior reflectivity, thermal stability, and flexible surface functionalization options. Reflectivity is an important attribute for MC sensing platforms since a reflective spot is required to measure sensor response using a beam bending technique. Introducing a material with ideal reflective properties would prevent the need for and disadvantages of metallization. In terms of reflectivity, the NLC material used in this study is a consequence of a clever design innovation using the concepts related to interference filter fabrication. An interference filter consists of multiple layers of dielectric materials composed of different refractive indexes. Maximum reflection of one or more spectral band or line can be achieved by choosing the proper thickness of these materials. Layering of SiN_x (40nm) followed by SiO_2 (160nm) results in maximum reflectivity of a 633 nm laser source (Figure 4.6). This demonstrates the ability to tune material properties, such as the thickness of individual layers;

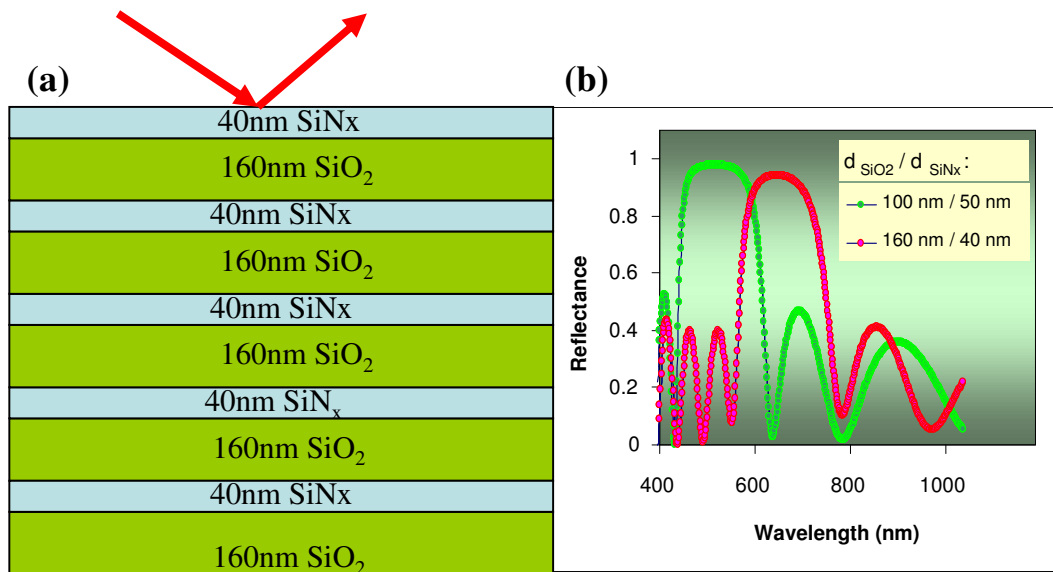


Figure 4.6. (a) Surface layering of SiN_x/ SiO₂. (b) Maximum reflectance of a 633 nm red laser for 160nm SiO₂/40nm SiN_x, in comparison to maximum reflectivity for 100nm SiO₂/50nm SiN_x composite.

to impart superior reflectivity of a laser operating at a specific wavelength. This effect is exemplified in Figure 4.6b, in which layering of SiN_x/SiO₂ in different proportions results in maximum reflectivity of radiation at a desired wavelength. This design parameter was explored experimentally.

Two NLC slides were processed NLC (633) and NLC (850). NLC (633) is designed to provide maximum reflectivity of a 633 nm laser. This has been accomplished by layering the SiN_x (40nm) followed by SiO₂ (160nm) as shown in Figure 4.6. NLC (850) was designed to provide maximum reflectivity of an 850nm laser. The 850nm wavelength was chosen since this is the wavelength of operation of a vertical cavity surface emitting laser (VCSEL), which is the source of radiation employed for MC arrays as described in Chapter 1. The VCSEL source was focused on each surface and the reflectivity was measured on a PSD as an overall output recorded in milli-volts. The surface reflectivity of the material tuned to 850 nm provided an output of 160 mV, as the surface reflectivity of the material tuned to 633 nm provided an output of 84 mV. The results of this study are shown in Figure 4.7 and have been magnified by a factor of 5 for scaling purposes.

The 633 nm laser was again used to compare the reflectivity of the NLC (633) with other materials commonly used in MC design including silicon and silicon nitride. A comparison of the relative reflectivity of these surfaces too that of a mirror are shown also in Figure 4.7. Indeed, layering of the SiN_x/SiO₂ composite shows better reflectivity of a 633 nm laser in comparison to individual surfaces of silicon or silicon nitride.

A stable baseline is vital for meaningful measurements made by any analytical device, thermal drift often undermines this requirement. Improved thermal stability of

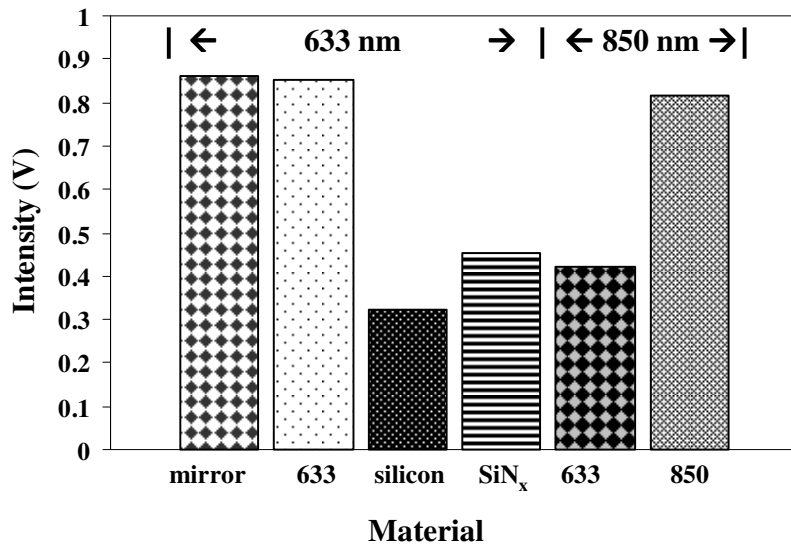


Figure 4.7 A comparison of the reflectivity of a 633 nm laser for a mirror, silicon, silicon nitride and a NLC surfaces. Tunability of material thickness to optimize reflectivity of an 850 nm laser. Shown here is a surface designed to reflect 633 nm in comparison to a surface designed to reflect 850nm (magnified x 5 for scaling).

NLC-MCs in comparison to metalized MCs has been demonstrated. A study to evaluate the effects of temperature fluctuations common to field analysis was conducted using two NLC-MCs, a native NLC-MC and a NLC-MC with a 30nm film of vapor deposited silver. The NLC-MC being tested was secured in a brass flow cell with a thermocouple attached externally. Under static conditions (no gas flow through the cell) a laser spot was focused on the tip of the lever to be tested as the spot was aligned on a PSD. Gradual tip-displacement (drift) of levers in this initial condition was observed possibly as a result of localized heating due too laser probing. The flow cell was then heated for 10 minutes with a heat gun resulting in a temperature increment of approximately 20 °C. The heat source was removed as drift profiles were again collected. These profiles showing initial state and heated state (20° C increase) for each NLC-MC (native and metalized) are presented in Figure 4.8. Metalized NLC-MCs experience a drift rate of ~ 1.0 mV/s to approach steady state as the temperature gradually returns to ambient conditions. However, native NLC-MCs drift by only ~ 0.2 mV/s during that experiment. In summary, thermal drift may undermine the interpretation of sensor response. NLC-MCs are shown to be less prone to drift due to temperature fluctuations which are prevalent in remote testing applications; hence NLC-MCs offer a distinct advantage to the use of metalized MC strategies.

Introduction of a MRP on a MC surface commonly employs a gold/thiol approach; the steps in this process include;

- 1) Physical vapor deposition of a chromium adhesion layer.
- 2) Physical vapor deposition of a gold active layer.
- 3) Exposure of the gold layer to a toxic thiol(commonly amine ethane thiol)

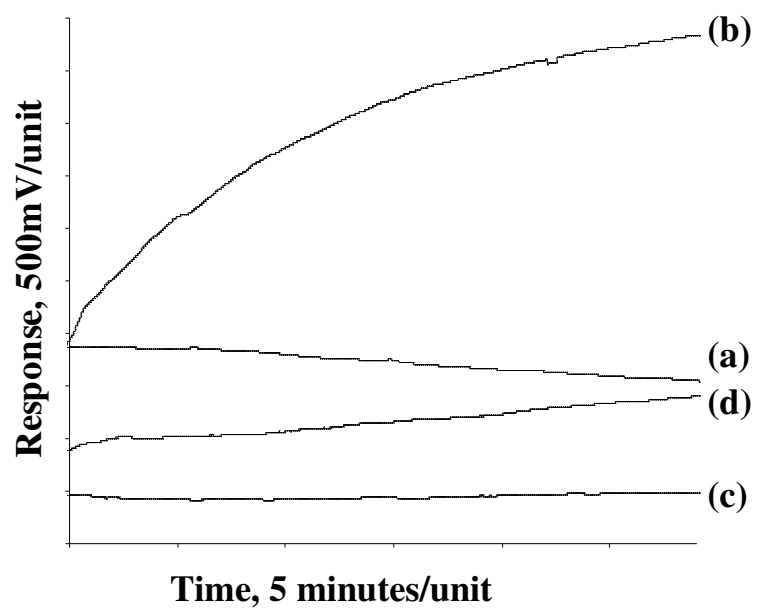
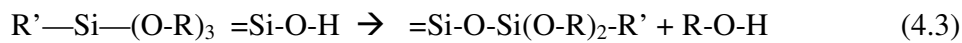


Figure 4.8. Thermal drift profiles for NLC-MCs. **(a)** With 30nm Ag. **(b)** With 30nm Ag upon 20°C increase in temperature. **(c)** Non-metalized surface. **(d)** Non-metalized surface upon 20°C increase in temperature

This multi-step strategy suffers not only from the obstacles imposed by metallization, but is also time consuming and requires the use of a toxic thiol. The native surface asymmetry of NLC-MCs may yield a flexible and simplified functionalization option offered by different chemical and physical pathways to introduce a MRP on the surface of choice. An alkylalkoxysilane route has been chosen in the current study to take advantage of this asymmetry. Kamisetty et al¹⁵⁴ have described a method to introduce alkyl species onto SiO₂ surfaces via silanol capping. Alkylalkoxysilanes are reacted with surface silanol groups which dominate the SiO₂ surface according to the following simplified reaction (4.3).



SiO₂ slides and SiN_x slides have been processed mimicking the bottom and top sides of the NLC-MCs, respectively. Following the procedure outlined by Kamisetty¹⁵⁴ all slides were rinsed with acetone, cleaned in piranha (70% H₂SO₄:30%H₂O₂), then exposed to ODTMS (octadecyltrimethoxysilane) in toluene for 3 hours. The slides were then rinsed in toluene followed by baking at 110° C for 1 hour. Characterization of the slides was conducted using Fourier Transform Infra-Red (FTIR) absorbance in reflectance mode. Figure 4.9 shows the FTIR spectra collected on slides identifying the vibrational fingerprint frequency range(2800 cm⁻¹-3000 cm⁻¹) typical of -CH_n groups, which includes -CH₃ (~2975 cm⁻¹), -CH₂ anti-symmetric (~2930 cm⁻¹) and -CH₂ symmetric (~2850 cm⁻¹). The broad features of the FTIR spectra may indicate the true complexity of the reaction (4.3) described above. These results suggest a successful grafting of ODTMS on the SiO₂ compared to the SiN_x surface. The grafting of a highly hydrophobic long chain hydro-carbon (ODTMS) is an example of a

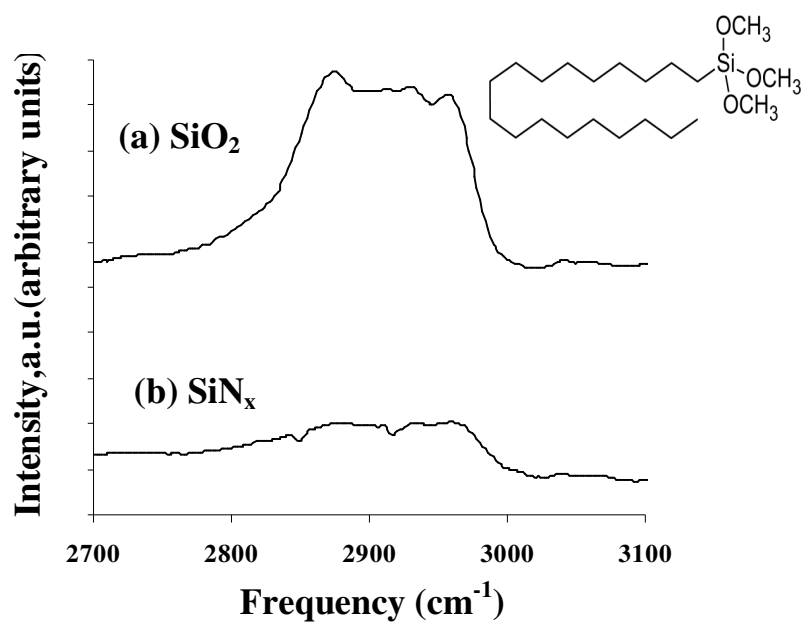


Figure 4.9. FTIR of ODTMS. (a) SiO₂ surface functionalized with ODTMS preferentially to (b) SiN_x surface. (inset) ODTMS

method which can be modified to prepare more exotic surface functionality depending upon the need of the desired application.

NLC-MCs have also been used for H₂ sensing experiments adding a rugged feature to the material properties offered by this platform. These studies explored the use of an SGDR process (see Chapters 2 & 3) to create a H₂ active np-Pd film on NLC-MCs. The sensing properties provided by the NLC-MCs showed excellent figures of merit and in some cases outperformed the commercially available np-Pd MCs, in terms of sensitivity and response time possibly due too the more flexible material properties of the NLC material as described above.

4.3.3 Future Directions

The nitrogen rich top surface (XPS) may provide a route of introducing proteins onto the NLC-MC surface avoiding the mutli-step process using a gold/thiol chemistry. Typically a self-assembled monolayer is created in which a gold surface is functionalized using an amine ethane thiol. The amine terminal group is then subjected to reaction with a glutaraldehyde (GA). The GA is then functionalized with a desired proteins free amine group by way of a carbinolamine bond. The native nitrogen rich NLC top surface may serve as a means for directly introducing the GA followed by protein attachment. This would reduce costs (no gold), toxic reagents (no thiol) and time (reduced number of steps including physical vapor deposition time) typically involved in protein surface functionalization strategies as described above. This metal-free route would overcome the limitations described previously providing thermal stability with improved adhesion as an active layer has been fabricated within the surface. Figure 4.10 compares models of the

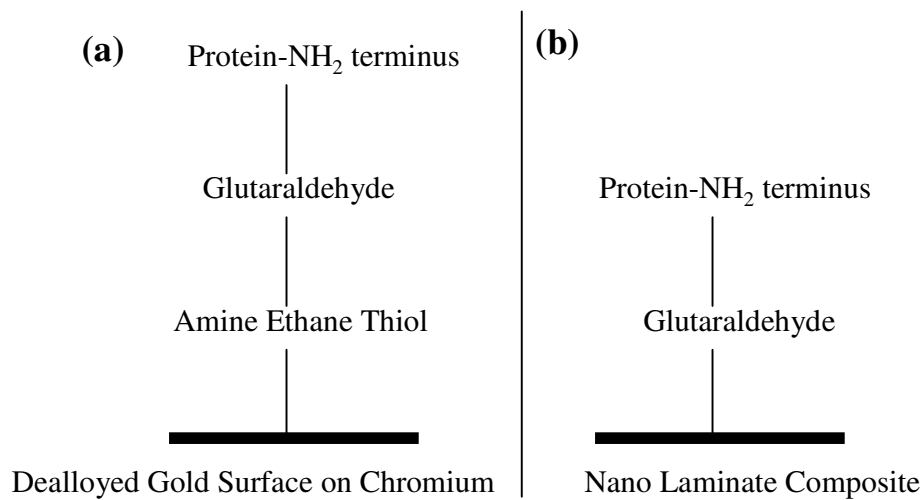


Figure 4.10. Protein chemical immobilization strategies using self-assembled monolayers. (a) Conventional.(b) NLC.

SAM formation of conventional gold-thiol strategy with the proposed methods possible structure. The differences in chain length between surface and analyte interaction point on the protein would need to be closely evaluated and optimized to fully take advantage of the NLC path.

4.4 CONCLUSIONS

A NLC material has been presented as a novel structure for MC design. XPS has been used to characterize the asymmetric chemical composition of the SiN_x top surface in comparison to a SiO₂ bottom surface. Contact angle measurements have provided information with respect to the differences in the hydrophobic/hydrophilic nature of this surface asymmetry. The use of NLC-MCs as a diagnostic tool to evaluate this surface asymmetry has been presented. The extreme conditions of HF etching and the more practical means of pH dependence suggest that surface asymmetry may be exploited in future studies for native state response to a specific analyte. The f_0 of NLC-MCs have been collected and compared to those of commercially available silicon MCs, with evidence suggesting a more sensitive analytical tool for the former. The advantages of the NLC-MCs include a superior reflective surface in comparison to other materials used for MC design. The non-metalized nature of these structures offer improved thermal stability in comparison too the metalized counterpart. This advantage may weigh favorably in producing a sensing platform better suited for real-time analysis. The asymmetric nature of the NLC-MC may be advantageous in exploring flexible surface funtionalization strategies as demonstrated for ODTMS using a traditional silanol capping technique. Future directions may include exploitation of possible top surface amines to create a more efficient protein functionalization strategy.

CHAPTER 5: CONCLUDING REMARKS

Research involving MC based sensing systems was both a rewarding and challenging task. A combination of both chemical and physical attributes of the MC must be met for the success of this sensing strategy for a desired analysis. The research presented in this work focused on innovations in surface modification strategies for advances in MCs as transducers for chemical sensing. Each of the preceding chapters has closed with a summary focusing on the agenda of the individual projects; some overall conclusions along with some comments on future directions of these projects will now be addressed.

Chapter 2 presented a chemical means to introduce a MRP onto a MC surface for H₂ related applications. The use of a SGDR created a np-Pd film that was successfully implemented for H₂ leak detection. These sensors met the most rigorous demands listed by the Department of Energy (DOE) for optimal performance, including fast response, low-cost, immunity to common interfering agents, and operable under ambient conditions. This early study provided a modest understanding of the potential of this protocol which was further explored in Chapter 3.

A more thorough treatment of the use of an SGDR pathway for designing a material such as np-Pd was outlined in Chapter 3. This study placed less emphasis on the use of this material in sensing applications and focused on treating this material as an interest for H₂ interactions which also has implications for H₂ storage and catalysis. Indeed, in this investigation a better understanding of the effects of both processing and conditioning were revealed. For instance during the early stages of development the success rate of np-Pd MCs

that performed optimally was less than 25%. By the end of collecting data and conducting experiments for the mechanistic studies involved with Chapter 3's development, the success rate was greater than 80% for optimal np-Pd MC preparation. Over 5 generations of successful batches have been processed, with the original np-Pd MC performing admirably after a two and a half year lifetime.

An interesting extension of this work may involve utilizing the SGDR strategy for different metals that show affinity for other gas phase analytes. For instance, work conducted by Liu et al¹⁵⁵ has reported that zinc oxide (ZnO) shows preferential interaction with H₂S. Hence introducing a zinc phase by use of an SGDR strategy could yield a MC sensor that shows response to H₂S. A more sophisticated design using the SGDR technique could take full advantage of creating a MC array. As an initial step designing a MC that demonstrates distributed selectivity to both H₂ and H₂S would offer the analyst a means to detect these analytes simultaneously.

Chapter 4 explores a physical means to improve MC design by introducing a novel NLC material for MC fabrication. The material created using this approach consists of alternating layers of SiN_x/SiO₂ and was made possible by the unique capabilities of the Center for Nanophase Materials Science at Oak Ridge National Laboratories. It was shown that these materials offer distinct advantages over conventional design processes which commonly employ a metalized surface. A major advantage of the NLC material is superior reflectivity in comparison to other materials commonly used for MC structures preventing the need for a reflective metal surface. Hence, NLC-MCs are more thermally stable in comparison to MCs which employ metallization. This advantage may be useful for remote sensing applications under temperature extremes in which thermally induced drift may

undermine interpretation of sensor response. The asymmetric surface layering has been shown to offer more flexible functionalization strategies. For instance an efficient silanol capping technique¹⁵⁴ has been demonstrated as a method to introduce a highly hydrophobic ODTMS preferentially on the SiO₂ surface

The work conducted using NLC materials may be further explored in terms of introducing more exotic surface functionalization architecture. The ODTMS that was successfully grafted using a silanol capping method opens up the potential to introduce a more useful surface functional group for sensing and detection applications. Another area of interest includes biologically inspired applications. The SiN_x surface may be evaluated as a pathway to introduce proteins more efficiently. This would reduce the number of steps, use of toxic thiols, and metallization typically involved for self-assembled monolayer formation. Finally the ability to mass produce NLC-MCs could be explored for lab on-chip electronic circuitry.

REFERENCES

1. Janata, J.; Bezegh, A. *Anal Chem* 1988, 60, 12, 62R-74R
2. Sauerbrey, G. *Z. Phys.* 1959, 155, 206-222
3. Jarrett, M.R.; Finklea, H.O.; *Analytical Chemistry*, 1999, 71,353-357
4. Kobayashi, T.; Murawaki, Y.; Reddy, P.S.; Abe, M.; Fuji, N.; *Analytica Chimica Acta*, 2001, 435, 141-149
5. Scheide, E.P.; and Taylor,J.K.; *Environmental Science and Technology*, 8, 1097, 1974
6. Scheide, E.P.; and Taylor,J.K.; *American Industrial Hygiene Association Journal*, 36,897, 1975
7. Scheide, E.P.; and Warner, R.J.; *American Industrial Hygiene Association Journal*, 39,745, 1978
8. Wohltjen, H.; Dessy, R. *Anal. Chem.* 1979, 51, 9, 1458-1464
9. Alexander, S.; Hellemans, L.; Marti, O.; Schneir, J.; Elings, V.; Hansma, P. K.; et al J. *Appl. Phys.* 1989, 65, 1, 164-167
10. Binnig, G.; Quate, C. F.; Gerber, C. *Phys. Rev. Lett.* 1986, 56, 930-933
11. Thundat, T; Warmack, R. J.; Chen, G.Y.; Allison, D. P. *Appl. Phys. Lett.* 1994, 64, 2894-2903
12. Barnes, J. R.; Stephenson, R. J.; Welland, M. E.; Gerber, C.; Gimzewski, J. K. *Nature* 1994, 372, 79
13. Itoh, T.; Suga,T.; *Applied Physics Letters*, 1994, 64(1), 37-39
14. Thundat,T.; Wachter, S.L.; Sharp, S.L.; and Warmack, R.J.; *Applied Physics Letters*, 66, 1995,1695
15. Chapman,P.,J.; Vogt, F.; Dutta, P.;Datskos, P.G. ; Devault, G.L. ; Sepaniak, M.J. ; *Analytical Chemistry*, 2007,79(1),364-370
16. Patton, J.F., Lavrik,N.V., Joy,D.C., Datskos,P.G. Smith, D.B.,Hunter,S.R., Sepaniak,M.J.; *Advanced Functional Materials*, 2012(submitted)
17. Patton, J. F.; Sepaniak, M. J.; Smith, D. B.; Datskos, P.G.; Hunter, S.R.; *Sensors and Actuators A*, 163, (2010),464-470
18. Lavrik, N. V.; Sepaniak, M. J.; Datskos, P. G. *Review of Scientific Instruments* 2004, Vol 75, No 7, 2229-2253
19. Sepaniak, M.; Datskos, P.; Lavrik, N.; Tipple, C. *Analytical Chemistry*, 2002, 568A-575A
20. Wang, Z.; Miao,J.;Tan,C.W.; Xu,T.; *Journal of Electroceramics*, 2010, 24;25-32
21. Yan, X.; Ji, H.; Thundat, T. *Current Analytical Chemistry* 2006, 2, 297-307
22. Ilic, B.; Czaplewski, D.; Zalatudinov, M.; Craighead, H.G.; Neuzil, P.; Campagnola, C.; and Batt, C.; *Journal Vacuum Science Technology*, B, 19, 2825,(2001)
23. Lavrik, N.V.; and Datskos, P.G.; *Applied Physics Letters*, 82, 2697, (2003)
24. Raiteri,R.; Grattarola, M.; Berger, R.; *Materials Today*, 2002, 22-29
25. Dareing, D. W.; Tian, F.; Thundat, T. *Ultramicroscopy* 2006, 106, 789-794
26. Tamayo, J.; Humphris, A.D.; Malloy,A.M.; Miles, M.J.; *Ultramicroscopy*, 2001, 86, 167-173
27. Stoney, G. G. *Proc. R. Soc. London, Ser. A*, 1909, 82, 172-177
28. Skoog, Holler, Nieman, *Principles of Instrumental Analysis*, 5th Edition

29. Lavrik, N. V.; Tipple, C. A.; Sepaniak, M. J.; Datskos, P. G. *Chemical Physics Letters* 2001, 336, 371-376
30. Dutta, P.; Tipple, C. A.; Lavrik, N. V.; Datskos, P. G.; Hofstetter, O.; Sepaniak, M. J. *Anal. Chem.* 2003, 75, 2342-2348
31. Dutta, P.; Hill, K.; Datskos, P. G.; Sepaniak, M. J. *Lab on a Chip* 2007, 7, 1184-1191
32. Senesac, L.R.; Dutta, P.; Datskos, P.G.; and Sepaniak, M.J.; *Analytica Chimica Acta*, 558, (2006) 94-101.
33. Fritz, J.; Baller, M.K.; Lang, H.P.; Rothuizen, P.; Vettiger, E.; Meyer, H.; Guntherodt, J.; Gerber, C.; and Gimzewski, J.K.; *Science*, 288, 316, (2000)
34. Wu, G.H.; Ji, H.F.; Hansen, K.; Thundat, T.; Datar, R.; Cote, R.; Hagan, M.F.; Chakraborty, A.K.; and Majumdar, A.; *Proceedings National Academy of Science, USA*, 98, 1560(2001)
35. Long, Z.; Storey, J.; Lewis, S.; Sepaniak, M.J.; *Anal. Chem.* 2009, 81, 2575-2580
36. Tipple, C. A.; Lavrik, N. V.; Culha, M.; Headrick, J.; Datskos, P.; Sepaniak, M. J. *Anal. Chem.* 2002, 74, 3118-3126
37. Headrick, J.; Lavrik, N.V.; Sepaniak, M.J.; Datskos, P.G.; *Ultramicroscopy*, 97, 417, 2003
38. Sandberg, R.; Molhave, K.; Boisen, A.; Svendsen, W.; *Journal of Micromechanics and Microengineering*, 15, 2005, 2249-2253
39. Boon-Brett, L.; Bousek, J.; Black, G.; Moretto, P.; Castello, P.; Hubert, T.; Banach, U.; *International Journal of Hydrogen Energy* 35 (2010) 373-384.
40. Graham, T.; *Philos. Trans. R. Soc London*, 156, 415 (1866)
41. Oriani, R.A.; *Fourth International Conference on Cold Fusion*, 1993
42. Yang, F.; Taggart, D. K.; Penner, R. M.; *Small*, 2010, 6, 13, 1422-1429
43. Jeon, K.J.; Jeun, M.; Lee, E.; Lee, J.M.; Lee, K.I.; von Allmen, P.; Lee, W.; *Nanotechnology*, 19, 2008, 495501(6pp)
44. Kobayashi, H.; Yamauchi, M.; Kitagawa, H.; Kubota, Y.; Kato, K.; Takata, M.; *Journal of American Chemical Society*, 2008, 130, 1828-1829
45. Oh, C.; Hong, K.S.; Lee, S.G.; Park, C.; Yu, I.; *Journal of Physics: Condensed Matter*; 18, 2006, 3335-3341
46. Lewis, F.A.; *Paltinum Metals Review*, 1960, 4, (4) 132-137
47. Nakatsuji, H.; Hada, M.; Yonezawa, T.; *Journal of American Chemical Society*, 1987, 109, 1902-1912
48. Messmer, R.; Salahub, D.; Johnson, K.; Yang, C.; *Chemical Physics Letters*, 1977, 51, 84
49. Louie, S.; *Physics Review Letters*; 1979, 42, 476
50. Hakanoglu, C.; Hawkins, J.; Asthagiri, A.; Weaver, J.; *Journal of Physical Chemistry C*, 2010, 114, 11485-11497
51. Aroutiounian, V.; *International Journal of Hydrogen Energy* 32 (2007) 1145-1158.
52. Favier, F.; Walter, E.C.; Zach, M.P.; Benter, T.; Penner, R.M.; *Science*, Vol 293, 21, September, 2001, 2227-2231
53. Martin, L.P.; Pham, A.Q.; Glass, R.S.; *Solid State Ionics* 175 (2004) 527-530
54. Ramanathan, M.; Skudlarek, G.; Wang, H.H.; Darling, S.B.; *Nanotechnology*, 21, (2010), 125501(6pp)

55. Yang, F.; Kung, S.C.; Cheng, M.; Hemminger, J.C.; Penner, R.M.; ACS Nano, Vol 4, No 9, 5233-5244, 2010
56. Lee, Y.T.; Lee, J.M.; Kim, Y.J.; Joe, J.H.; Lee, W.; Nanotechnology, 21, (2010), 165503(5pp)
57. Mohajeri, N.; Raissi, A.T.; Baik, J; Thermochemica Acta 518, 2011, 119-122
58. Ranjbar, M.; Fardindoost, S.; Mahdavi, S.M.; Irajizad, A.; Tahmasebi, N.G.; Solar Energy Materials & Solar Cells, 95, 2011, 2335-2340
59. Leervad Pedersen, T.P.; Liesch, C.; Salinga, C.; Eleftheriadis, H.; Wuttig, M.; Thin Solid Films, 458, (2004) 299-303
60. Baselt, D.R.; Fruhberger, B.; Klaassen, E.; Cemalovic, S.; Britton Jr, C.L.; Patel, S.V.; Mlsna, T.E; McCorkle, D.L.; Warmack, R.J.; Sensors and Actuators B, 88, 2003, 120-131
61. Chou, Y.I.; Chiang, H.C.; Wang, C.C.; Sensors and Actuators B, 129, 2008, 72-78
62. Hu, Z.; Thundat, T.; Warmack, R.J.; Journal of Applied Physics, 90 (2001) 427-431.
63. Britton Jr, C.L.; Jones, R.L.; Oden, P.I.; Hu, Z.; Warmack, R.J.; Smith, S.F.; Bryan, W.L.; Rochelle, J.M.; Ultramicroscopy 82 (2000) 17-21.
64. Kay, B.D.; Peden, C.H.F.; Goodman, D.W.; Physical Review B, Vol 34, No 2, 15, July 1986, 817-822
65. Ward, T.; Dao, T.; Journal of Membrane Science; 153, 1999, 211-231
66. Li, W.C.; Balk, T.J.; Materials, 2009, 2, 2496-2509
67. Pacheco Tanaka, D.A.; Llosa Tanco, M.A.; Nagase, T.; Okazaki, J.; Wakui, Y.; Mizukami, F.; Suzuki, T.M.; Advanced Materials, 2006, 18, 630-632
68. Liu, N.; Tang, M.L.; Hentschel, M.; Giessen, H.; Alivisatos, A.P.; Nature Materials, Vol 10, August 2011, 631-636
69. Carraro, C.; Maboudian, R.; Magagnin, L.; Surface Science Reports, 62, 2007, 499-525
70. Ali, H.; Christie, I.; Gold Bull.; 1984, 17(4), 118-127
71. Korotcenkov, G.; Han, S.D.; Stetter, J.R.; Chemical Reviews 109 (2009) 1402-1433.
72. Simon, I.; Arndt, M.; Sensors Actuators A, 97, (2002) 104-108
73. Yoshimura, K.; Nakano, S.; Uchinashi, S.; Yamaura, S.; Kimura, H.; Measurement Science Technology 18 (2007) 3335-3338.
74. Hana, C-H.; Hong, D-W.; Hana, S-D.; Gwak, J.; Singh, K.C; Sensors Actuators B 125 (2007) 224-228.
75. Park, S.C.; Yoon, S-I; Lee, C.; Kim, Y-J.; Song, S., Analyst 134 (2009) 236-242.
76. Nishibori, M.; Shin, W.; Izu, N.; Itoh, T.; Matsubara, I.; Yasuda, S.; Ohtani, S.; International Journal of Hydrogen Energy 34 (2009) 2834-2841.
77. Villatoro, J.; Diez, A.; Cruz, J.L.; Andres, M.V.; Electronic Letters 37 (2001) 1011-1012.
78. Bevenot, X.; Trouillet, A.; Veillas, C.; Gagnaire, H.; Clement, M.; Measurement Science Technology, 13 (2002) 118-124.
79. Sumida, S.; Okazaki, S.; Asakura, S.; Nakagawa, H.; Murayama, H.; Hasegawa, T.; Sensors Actuators B 108 (2005) 508-514.
80. Zhao, Z.; Carpenter, M.A.; Xia, H.; Welch, D.; Sensors Actuators B 113 (2006) 532-538.
81. Slamán, M.; Dam, B.; Pastural, M.; Borsa, D.M.; Schreuders, H.; Rector, J.H.; Griessen, R.; Sensors Actuators B 123 (2007) 538-545.
82. Nau, D.; Orzekowsky, R.B.; Seidel, A.; Meyrath, T.P.; and Giessen, H.; 2008 Conference on CLEO/QELS, IEEE 978-1-55752-859-9, pp. 3012-3013.

83. Lin, K.; Lu, Y.; Chen, J.; Zheng, R.; Wang, P.; Min H.; Optics Express 16 (2008) 18599-18604.
84. Monzón-Hernández, D.; Luna-Moreno, D.; Martínez-Escobar, D.; Sensors Actuators B 136 (2009) 562-566.
85. Hydrogen Sensor Workshop hosted by LANL and co-hosted by LLNL for the DOE hydrogen. Fuel cells & infrastructure technologies program, April 4th, 2007, Washington DC, USA. <http://www.lanl.gov/orgs/mpa/mpa11/sensors.html>.
86. Huang, T.C.; Wei, M.C.; Chen, H.I.; Separation Science And Technology, 36(2), (2001), 199-222.
87. Kiefer, T.; Favier, F.; Vasquez-Mena, O.; Villanueva, G.; Brugger, J.; Nanotechnology 19 (2008) 15502.
88. Khanuja, M.; Kala, S.; Metha, B.R.; Kruis, F.E.; Nanotechnology 20 (2009) 015502.
89. Kozłowski, M.; Diduszko, R.; Olszewska, K.; Wronka, H.; Czerwosz, E.; Vacuum 82 (2008) 965-961.
90. Goutam, D.; Kohn, R.; Xomeritakis, G.; Brinker, J.C.; Chemical Communications (2007) 1840-1842.
91. Yang, F.; Taggart, D.K.; Penner, R.M.; Nanoletters 9 (2009) 2177-2182
92. Wright, J.S.; Lim, W.; Gila, B.P.; Pearton, S.J.; Ren, F.; Lai, W.T.; Chen, L.C.; Hu, M.S.; Chen, K.H.; Journal of Vacuum Science Technology B 27 (2009) L8-L10.
93. Balducci, A.; D'Amico, A.; Di Natale, C.; Marinelli, M.; Milani, E.; Morgada, M.E.; Pucella, G.; Rodriguez, G.; Tucciarone, A.; Verona-Rinati, G.; Sensors Actuators B 111-112 (2005) 102-105
94. Park, S.-C.; Yoon, S.-I.; Lee, C.-I.; Song, S.; Kim, Y.J.; 2007 IEEE Sensors, 1-3 (2007) 197-200
95. Chan, C.C.; Hsu, W.C.; Chang, C.C.; Hsu, C.S.; Sensors and Actuators B, 145, 2010, 691-697
96. Shim, J.Y.; Lee, J.D.; Jin, J.M.; Cheong, H.; Lee, S.H.; Solar Energy Materials, Solar Cells, 93, 2009, 2133-2137
97. Wachter, E.A.; Thundat, Review Scientific Instruments; 66 (1995) 3662-3667
98. Datskos, P.G.; Lavrik, N.V.; Sepaniak, M.J.; in: S.Y. Yurish, M.T.S.R. Gomes, (Eds.), Smart Sensors and MEMS, Kluwer Academic Publishers, Netherlands, 2005, pp. 331-379
99. Fabrea, E.; Finota, J. Demoment, S.; Contreras, Ultramicroscopy 97 (2003) 425-432
100. Iannuzzi, D.; Deladi, S.; Slaman, M.; Rector, J.H.; Schreuders, H.; Elwenspoek, M.C.; Sensors Actuators B 121 (2007) 706-708
101. Simonet, J. Journal of Applied Electrochemistry 39 (2009) 1625-1632
102. Bravo-Vasquez, J. P.; and Fenniri, H.; Journal of Physical Chemistry C 113 (2009) 12897-12900
103. Chang, C.H.; Rheem, Y.; Electrochimica Acta 55 (2010) 743-752
104. Wang, C.Y.; Gong, N.W.; Advanced Mat_ 20 (2008) 4789
105. Dus, R.; Journal of Catalysis, 42 (1976), 334-343
106. Chapman, P.; Long, Z.; Datskos, P.; Archibald, R.; Sepaniak, M.; Analytical Chemistry, 79, 2007, 7062-7068
107. Archibald, R.; Datskos, P.; Devault, G.; Lamberti, V.; Lavrik, N.; Noid, D.; Sepaniak, M.J.; Analytica Chimica Acta, 584, 2007, 101-105

108. Baykura, S.; *International Journal of Hydrogen Energy*, 29, 2004, 1631-1636
109. Grasjo, L.; Hultquist, G.; Tan, K.; Seo, M.; *Applied Surface Science* 89,1995, 21-34
110. van Delft, Y.C.; Correia, L.A.; Overbeek, J.P.; Bongers, B.; Pex, P.P.A.C.;
Presented at the 9th International Conference on Inorganic Membranes-ICIM-9,25-29 June 2006, Lillehamer, Norway
111. Miller, J.; Alfonso,D.; Morreale, B.; Gellman, A.; *Hydrogen Dissociation on Palladium-Sulfide Surfaces*
112. Alfonso, D.; Cugini, A.; Sorescu, D.; *Catalysis Today*, 99, 2005, 322
113. Medlin, J.; Mcdaniel, A.; Allendorf, M.; Bastaz, R.; *Journal of Applied Physics*, Vol 93, No 4, 15, February 2003, 2267-2274
114. Zheng, G.; Altman, E.I.; *Journal of Physical Chemistry B*, 2002, 106, 1048-1057
115. Li, H.; Xu, H.; Li, W. *Journal Of Membrane Science*, 324, 2008, 44-49
116. Vogel, W.; He, W.; Huang, Q.; Zou, Z.; Zhang, X.; Yang, H.; *International Journal of Hydrogen Energy*,35, 2010, 8609-8620
117. Bhat, V.V.; Contescu, C.I.; Gallego, N.C.; *Nanotechnology*, 20,2009
118. Lu, Y.; Chen, W.; *Journal of Physical Chemistry C*, 2010, 114, 21190-21200
119. Lee, C.; Tseng, C.; Wu, R.; Wu, C.; Syu, S.; *Electrochimica Acta*, 54, 2009,5544-5547
120. Zhang, Z.; Wang, Y.; Qi,Z.; Zhang, W .; Qin, J.; Frenzel, J.; *Journal of Physical Chemistry C*, 2009 113,12629-12636
121. Kim, K.; Kim, K.L.; Shin, K.S.; *Journal of Physical Chemistry C*, 2011, 115,14844-14851
122. Li, W.; Balk, T.J.; *Scripta Materialia*, 61 (2009), 1125-1128
123. Gorodetskii, V.V.; Sametova, A.A.; Matveev, A.V.; Tapilin, V.M.; *Catalysis Today* 144 (2009), 219-234
124. Baca-Arroya, R.; Lopez Rodriguez, C.A.; Galvan-Arellano, M.; Romero-Paredes,G.; Pena-Sierra, R.; 2008, 5th International Conference on Electrical Engineering, Computing and Automatic Control (CCE2008)
125. Huang, C. J.; Pan, F.M.; Tzeng, T.C.; Chang, L.; Sheu, J.T.; *Journal of The Electrochemical Society*, 156(2), J28-J31,(2009)
126. Lu, W.; Wang, B.; Wang, K.; Wang, X.; Hou, J.G.; *Langmuir* 2003, 19, 5887-5891
127. Jose, D.; Jagirdar, B.R.; *International Journal of Hydrogen Energy* 35, (2010), 6804-6811
128. Chen, J.; Wiley, B.; McLellan, J.; Xiong, Y.; Li, Z.; Xia, Y.; *NanoLetters*, 2005, Vol5, No10, 2058-206
129. Otto,K.; Hubbard, C.; Weber, W.; Graham, G.; *Applied Catalysis B Environmental*, 1, 1992, 317-327
130. Garcia-Serrano, O.; Lopez-Rodriguez, C.; Andraca-Adame, J.; Romero-Paredes, G.; Pena-Sierra, R.; *Materials Science and Engineering Bne* , 174, 2010, 273-278
131. McBride, J.R.; Hass, K.C.; Weber, W.H.; *Physical Review B*, Volume 44, Number 10, 1 September 1991-II, 5016-5028
132. Mutschele, T.; Kircheim, R.; *Scripta Metallurgica*, Vol 21, pp 135-140, 1987
133. Elkina, I.; Meldon, J.; *Desalination*, 147, 2002, 445-448
134. Eastman, J.A.; Thompson, L.J.; Kestel, B.J.; *Physical Review B*, Volume 48, Number1, 1 July 1993-I,84-92

135. Petersson, L.G.; Dannetun, H.M.; Lundstrom, I.; Surface Science, 163, 1985, 273-284
136. Belousov, V.M.; Vasylyev, M.A.; Lyashenko, L.V.; Vilkova, N.Yu.; Nieuwenhuys, B.E.D.; Chemical Engineering Journal, 91, 2003, 143-150
137. Engel, T.; Kuipers, H.; Surface Science, 90, 1979, 181-196
138. Dus, R.; Lisowski, W.; Nowicka, E.; Wolfram, Z.; Surface Science, 332, 1995, 285-292
139. Brady, S.; Salazar, I.; Baker, D.; Browning, C.; Eastman, J.; Conrad, M.; Physical Review B 67, 054102, 2003
140. Nyberg, C.; Tengstal, C.; Journal of Chemical Physics, 80, 7, 1 April 1984, 3463-3468
141. Harris, D.C.; Quantitative Chemical Analysis, 8th Edition, W.H. Freeman and Company New York
142. Dissanayake, D.; Lunsford, J.; Journal of Catalysis, 214, 2003, 113-120
143. Koo, I.G.; Lee, M.S.; Lee, W.M.; Thin Solid Films 506-507, 2006, 350-354
144. Ingham, B.; Hendy, S.C.; Fong, D.D.; Fuoss, P.H.; Eastman, J.A.; Lassesson, A.; Tee, K.C.; Convers, P.Y.; Brown, S.A.; Ryan, M.P.; Toney, M.F.; Journal of Physics D: Applied Physics, 43, 2010, 075301(6pp)
145. Carbo, A.D.; Coronado, E.; Diaz, P.; Ribera, A.; Electroanalysis, 2010, 22, No. 3, 293-302
146. Buttner, W.J.; Post, M.B.; Burgess, R.; Rivkin, C.; International Journal Of Hydrogen Energy, 19 May 2010, 1-9
147. Buttner, W.J.; Burgess, R.; Post, M.B.; Rivkin, C.; The NREL Safety Sensor Testing Laboratory (SSTL)
148. Bhushon, B.; Springer Handbook of Nanotechnology, Volume 2, 445
149. Forch, R. Schonherr, H.; Tobias, A.; Jemkins, A.; Surface Design: Applications in Bioscience and Nanotechnology, Wiley-VCH, 471
150. Williams, K.R.; Gupta, K.; Wasilik, M.; Journal of Microelectro Mechanical Systems 12 ,6, 2003(761-778)
151. Chiang, J.N.; Ghanayem, S.G.; Hess, D.W.; Chemistry of Materials 1989, 1, 194-198
152. Dutta, P.; Chapman, P.J.; Datskos, P.G.; Sepaniak, M.J.; Analytical Chemistry, 2005, 77(20), 6601-6608
153. Boisen, A.; Dohn, S.; Keller, S, S.; Schmid, S.; and Tenje, M.; Reports on Progress in Physics, 74, (2011), 036101, (30pp)
154. Kamisetty, N.K.; Pack, S.P.; Nonogawa, M.; Devarayapalli, K.C.; Kodaki, T.; Makino, K.; Chemistry Letters, Vol 36, No2 (2007)(322-323)
155. Liu, Z.; Fan, X.; Zhang, D.; Gong, X.; Xu, J; Sensors and Actuators B, 136, 2009, 499-509

VITA

James Francis Patton was born in Pittsburgh, PA. He graduated from Bishop Boyle High School and received his BS in chemistry from University of Pittsburgh. After working in industry at PPG for several years James returned for post graduate work receiving his MS from the University of Tennessee. James taught at KCTCS for nearly two years before returning to finish his PhD from the University of Tennessee.